THESIS

SHEAR AND CONSOLIDATION BEHAVIOR OF SLURRY-DEPOSITED, DESICCATED TAILINGS AND COMPACTED FILTERED TAILINGS

Submitted by

Justin Michael Primus

Department of Civil & Environmental Engineering

In partial fulfillment of the requirements

For the Degree of Master of Science

Colorado State University

Fort Collins, Colorado

Summer 2024

Master's Committee:

Advisor: Christopher A. Bareither

Joseph Scalia IV
Lisa Stright

ABSTRACT

SHEAR AND CONSOLIDATION BEHAVIOR OF SLURRY-DEPOSITED, DESICCATED TAILINGS AND COMPACTED FILTERED TAILINGS

The objective of this study was to (i) evaluate and compare the undrained shear behavior and (ii) the consolidation behavior of slurry-deposited and desiccated tailings versus compacted filtered tailings. In general, the evaluation supports the hypothesis that desiccation and resaturation of a hard rock mine tailings yield higher peak undrained shear strengths relative to compacted filtered tailings when considering similar initial conditions (e.g., stress and density). The increase in undrained shear strength was attributed to the tailings fabric, which generated a stiffer response to loading and transitional behavior from contractive to dilative tendencies when sheared undrained. Consolidated undrained (CU) triaxial compression tests were conducted on 64-mm-diameter specimens that followed two different procedures. Slurry-deposited tailings were desiccated to a target void ratio and water content, resaturated, and tested in isotropic, consolidated, undrained axial compression. Filtered tailings specimens were prepared to similar initial void ratios as those measured on desiccated tailings specimens and tested in triaxial compression in the same manner. One-dimensional consolidation tests were also conducted on desiccated and filtered tailings specimens in a similar sequence.

The desiccated and filtered tailings exhibited contractive, strain-hardening behavior in the triaxial tests and yielded effective stress friction angles of 29.1° for the desiccated tailings and 27.7° for the filtered tailings. Desiccated tailings samples showed a stiffer initial peak deviatoric stress and slower decreasing rate of change in stress relative to the filtered tailings. There was no indication of a difference in stiffness or brittleness between tailings preparation methods. The higher shear strength of the desiccated tailings was attributed to (i) more pronounced inter-particle reinforcing effects and (ii) densification from stress-history of desiccation. One-dimensional consolidation tests yielded a trend of increasing preconsolidation pressure with decreasing initial

void ratio for both the desiccated and filtered tailings. There were slightly higher average compression and recompression indexes computed for the desiccated tailings relative to the filtered tailings, providing an indication of the different in the fabric behaviors.

ACKNOWLEDGMENTS

First, I would like to thank my advisor, Dr. Christopher Bareither. Chris and I spoke over zoom in the Fall of 2020 and that conversation led me to Fort Collins and CSU. The conversations we had, stories we shared, and hurdles we overcame together have helped me grow. I wish to extend my gratitude to Dr. Scalia and Dr. Stright for the guidance and direction they have offered and for serving on my graduate committee.

While at CSU, I had the opportunity to make memories with an incredible group of people. I have been humbled by the talent, intelligence, and dedication each one of them has displayed during the time we shared in grad school. I cherish every conversation and am honored to call you friends. Sam and Heath, you do far more than you realize and get far less credit than you deserve; the words thank you feel inadequate.

My family is the most important part of my life. My parents, Dan and Joni, have always picked me up, dusted me off, and sent me back out into the world, and I will always be grateful. My greatest teachers have been my sibling, Jayme, Jeremy, and Jenna. Having siblings who characterize the ideals of hard-work, resilience, and self-belief, has given me a standard to look to my entire life. I have only ever attempted to be seen in your eyes the way that you are seen in mine. I love all of you.

TABLE OF CONTENTS

LIST OF TABLES

LIST OF FIGURES

LIST OF SYMBOLS

A	Skempton's pore pressure parameter	w	water content
e	void ratio	$\Delta\sigma_d$ or q	deviator stress
e_i	initial void ratio (pre consolidation)	$\Delta\sigma_{d,max}$	maximum deviator stress
e_c	consolidated void ratio	ε_a	axial strain
e_f	final void ratio	ε_{af}	axial strain at failure
G_s	specific gravity	σ'_1	effective major principal stress
K_f Line	failure line in p'-q space	σ'_3	effective minor principal stress
SL	shrinkage limit	$(\sigma'_1/\sigma'_3)_{max}$	maximum principal stress ratio
LL	liquid limit	σ'_c	effective confining stress
PL	plastic limit	σ_v	vertical stress
PI	plasticity index	ϕ'	effective friction angle
p'	mean effective stress		
u_e	excess pore pressure		
$u_{e,max}$	maximum excess pore pressure		

CHAPTER 1: INTRODUCTION

1.1 Problem Statement

Modern mining involves sophisticated mineralogical extraction processes that aim to economically obtain a desired commodity (e.g., gold, copper, molybdenum, etc.). Target commodities exist at low mass percentages such that excavation and extraction processes yield a significant amount of tailings, which are a mixture of finely crushed rock, uneconomical minerals and metals, and process water. Mine tailings are generally sand-, silt-, or clay-sized particles with an angular shape due to mechanical crushing and grinding of ore. The addition of process water is essential to the separation of target commodities from the ore. The remaining tailings present engineering challenges for safe management without adverse effects to the environment and surrounding communities. Tailings are typically managed in tailings storage facilities (TSFs) and historically have been deposited as slurry materials with high water contents (Vick 1990).

A tailings management framework outlined in the Global Industry Standard on Tailings Management (GISTM, 2022) has placed increased emphasis on good engineering practices and safe management of TSFs. Increased prioritization of TSF stability and risk management has caused owners to reevaluate best available practices for tailings management. Tailings have long been considered an operational waste material and economical management strategies have previously limited capital spent on management. Conventional slurry-deposited tailings were the industry standard due to the low costs and status quo of the practice. However, promoting safe operations in tandem with evolving safety standards, technologies, and the increased emphasis on social implications of mining, methods of tailings management have continued to evolve (e.g., Morrison et al. 2022).

The diverse chemical and physical properties of mine tailings eliminate a universal approach to tailings management. Site specific tailing operations are developed around a framework for analyzing the risk of credible potential failure modes. An important failure mode

evaluated for all TSFs is tailings liquefaction (e.g., Jefferies & Been 2016), which integrates fundamental concepts of critical state soil mechanics to assess the state of tailings. Critical state soil mechanics is a framework used to understand, assess, and predict material behavior and is used to analyze the strength and stability of tailings (Schofield & Wroth 1968). A key consideration is identifying whether tailings have dilatant or contractive tendencies while undergoing shear deformation (Been & Li 2009).

Dilatant and contractive shear behavior of soils and tailings are linked to density and stress. Dense soils tend to dilate while undergoing shear deformation, whereas loose soils tend to contract. Critical state for a given material undergoing shear deformation is defined when the material reaches a constant shear stress, constant volume, and constant rate of shear (Schofield & Roth 1968). Tailings within a TSF that are dense of critical state are favorable compared to loose states because dilatant tendencies reduce the potential for liquefaction (Jefferies & Been 2019). Incidents involving liquefaction of tailings facilities have resulted in large economic and environmental consequences (Garino Libardi et al. 2021; Robertson et al. 2019; Morgenstern et al. 2016; Verdugo et al. 2012, Bray & Frost 2010).

Casagrande (1936, 1975) described liquefaction as “the post yield undrained behavior of contractive [soils]”. Although somewhat of an oversimplification, dilatant tailings are fundamental to reducing the potential for liquefaction via development of negative excess pore pressure during undrained shear deformation, which produces a temporary increase in effective stress and shear strength. Dense tailings are difficult to achieve via conventional slurry deposition due to high water contents and the tendency towards deposition in loose, contractive fabrics. The primary method of increasing the density of tailings in a TSF is through dewatering techniques (Vick 1990).

A wide variety of dewatering methods have been developed that consider varying economic constraints and operational demands of TSFs (Fitton & Roshdieh 2013). Slurry tailings involve limited dewatering, which is advantageous for pipeline transport, but often leads to saturated, loose tailings deposition that vary spatially in engineering properties. Dewatering slurry

tailings can yield different consistencies along the tailings continuum, which include thickened, paste, and filtered tailings. For example, filtered tailings are the most “soil-like” material and provide significant opportunities for water reclamation and mechanical compaction to increase as-placed density. However, capital expenditures and operational energy demands can make filtered tailings challenging for large tonnage applications.

Climatic conditions, such as high temperatures, low precipitation, and low humidity, can offer natural dewatering potential of tailings via evaporation. Environmental desiccation of tailings can enhance density via natural dewatering and the development of matric suction. Over the past decade, research has focused on the shear strength of both desiccated tailings and filtered tailings to support the use of these depositional methods in TSFs. Tailings in slurry, thickened, or paste consistency with subsequent desiccation has been researched by a few groups (e.g., Simms 2021, Simms et al. 2013, Simms et al. 2006, Reid et al. 2018, Reid et al. 2022a, Reid et al. 2022b, Reid et al. 2022c Reid et al. 2022d, Sonntag et al. 2022.) This research has revealed that when desiccated below certain water contents, which vary based on tailings characteristics, tailings tend to behave dilatant. Small degrees of desiccation can increase shear strength and density, and produce a phase change from contractive to dilative behavior (Daliri et al. 2012, 2014) that has been linked to increased matric suction (Rassam & Williams 1999). Although the effects of suction are negated once tailings are resaturated, the stress history from desiccation remains partially intact (Simms et al. 2013). Reid et al. (2022c) report that the strength of desiccated and resaturated thickened tailings lies somewhere between strength at full desiccation, unsaturated overconsolidation, and isotropic consolidation.

Desiccation produces an increase in tailings strength due to induced overconsolidation of the tailings. However, no specimen preparation technique directly represents the in situ fabric of tailings (Reid et al. 2021a; Hoeg et al. 2000; Chang et al. 2011). Furthermore, the beneficial density increase of desiccated tailings has not been compared to compacted tailings, whereby the latter represents an industry focus for creating dense, dilative tailings impoundment.

Research focused on the shear and deformation behavior of desiccated tailings and filtered tailings is needed to further assess the potential of achieving dense, dilative tailings fabrics via different techniques to support future TSF operations.

1.2 Research, Objectives, and Tasks

The objective of this study was to evaluate shear and consolidation behavior of desiccated tailings and compacted filtered tailings. Desiccated tailings were initially prepared as slurry and allowed to desiccate in the laboratory; filtered tailings were compacted at low moisture contents to void ratios similar to those measured on the desiccated tailings. The hypothesis was that desiccated and resaturated tailings yield a higher peak undrained shear strength and increased brittleness relative to compacted filtered tailings prepared to similar void ratios and consolidated under similar effective stress. The scope of work completed for this thesis included the following:

1. Characterized material properties of the tailings;
2. Created a laboratory specimen preparation technique for desiccated tailings that attempted to replicate in situ conditions for tailings undergoing desiccation in a TSF;
3. Evaluated strength and consolidation behavior of tailings desiccated to different void ratios based on shrinkage characteristics of the material and compared to filtered tailings prepared to similar void ratios; and
4. Compiled and compared data with literature to develop key findings and recommendations for future work.

Consolidated undrained (CU) triaxial compression and one-dimensional consolidation test were conducted on desiccated and filtered tailings. Different specimen preparation methods were used to suit the materials tested. Triaxial compression tests were conducted on 63.5-mm-diameter specimens using oversized, lubricated end platens coupled with end-of-test freezing. Triaxial compression tests were conducted at effective confining pressures (σ_c') targeting 50 and 100 kPa. One-dimensional consolidation tests were conducted on specimens with diameters of

64 or 70 mm, and were loaded at a consolidation loading ratio of approximately two from 5 to 2000 kPa.

CHAPTER 2: BACKGROUND

This study focused on the undrained shear behavior and consolidation of tailings prepared via different depositional methods. Information about the tailings continuum (slurry, paste, filtered tailings), depositional methods, and desiccation is provided for a better understanding of the comparative analysis in this study. Key concepts are provided to establish a baseline for evaluating the undrained shear and consolidation behavior.

2.1 Tailings

Tailings range in particle size distribution, plasticity, and clay content dependent on ore body geology and mineralogic processing. The majority of tailings derived from hard-rock mining are classified according to the Unified Soil Classification System as silty sands (SM) or non-plastic silts (ML) (Bussière 2007). Typical ranges and average tailings particle size distributions are presented in Fig. 2.1. Strength parameters are typically measured via undrained triaxial testing yielding effective stress friction angles (φ') generally between 30° to 42° due to the angularity of particles (Bussière 2007). Variable saturation is common in TSFs due to deposition (i.e. high water contents, loosely deposited, fine-grained) and commonly causes undrained conditions when subjected to shear. Deposition occurs on a continuum from slurry tailings to filtered tailings (high to low water contents).

The tailings continuum describes the range of tailings rheological properties as a function of solids content (i.e., ratio of dry solid mass to total mass) as shown in Fig. 2.2. Rheology is the science that deals with flow and deformation of matter. The yield stress of a non-Newtonian fluid (e.g., tailings) describes the ability of a material to resist flow. An increase in solids content coincides with progressive tailings dewatering and produces higher yield stress, which is proportional to an increased resistance to flow. A small increase in yield stress represents a change from slurry to paste tailings and a subsequent large increase in yield stress represents a

change from paste to filtered tailings (Boger 2009). Dewatering tailings (e.g., thickening or filtering) is most often used in operations for water recovery and also influences the strength and consolidation behavior of mine tailings.

2.1.1 Paste or Thickened Tailing Deposition

There has been considerable research dedicated to paste tailings in regards to the application of cemented-paste backfill for filling mine cavities (Fall et al. 2005, Belem & Benzaazoua 2008, Sheshpari 2018). Paste and thickened tailings represent tailings management the promotes water reclamation and densification of tailings prior to deposition. Thin-lift deposition of paste tailings is an operational technique that takes advantage of the higher tailings viscosity that allows for a smaller dam required for stability of the impoundment. Although some paste tailings contain additives or coagulants, the most common method of tailings thickening is by dewatering (Simms 2021). Thickening tanks that promote settling of solids are the most common method used by an operator to create a thickened or paste tailings. These materials are then pumped to a TSF and deposited (Vick 1990).

2.1.2 Filtered Tailings

Filtered tailings offer an alternative to thickened tailings deposition by creating a material that is more similar to a standard geotechnical earthwork material (e.g., soil). A filter press, for example, uses pressure to force water out of tailings through a filter or screen (Vick 1990). Filtered tailings must then be transported via conveyor or truck and mechanically compacted to create a stacked structure. Filtered tailings represent a final step in the tailings dewatering process and can be effective for water reclamation. In environments where water is scarce, costly, or requires desalination before use in mining operations, filtered tailings are considered an economic advantage (Fitton & Roshdieh 2013). Although filtered tailings are considered capable of creating

geotechnically stable TSFs and provide the most reclaimed water, the dewatering process is energy intensive and increases operating costs.

2.2 Desiccation

Desiccation is a natural process whereby water evaporates and capillary forces pull soil particles together. Higher rates of evaporation and/or longer deposition times between tailings lifts increase the rate of desiccation. As evaporation decreases the tailings water content, negative water pressure (i.e., matric suction) develops within the pore spaces that yield an increase in effective stress (Konrad & Ayad 1997). The pore size distribution of a given tailings determines the amount of desiccation cracking that occurs at the air-water interface. More pronounced tension cracking is generally observed in clayey materials.

The role desiccation plays in the dewatering process of tailings has led to increased complexity in TSF design and management. Facilities in arid regions with tailings exposed to high evaporation rates for long periods of time show high degrees of saturation within the tailings mass that were surrounded by dry, desiccated tailings (Oldecop et al. 2011). Laboratory studies have also indicated a connection between desiccation and cracking on the material behavior of tailings. Factors such as salt precipitation, desiccation cracking, resaturation, and evaporation have been found to contribute significantly to the compressibility and hydraulic properties of tailings (Fisseha et al. 2010; Daliri et al. 2016; Simms et al. 2017).

Many attempts have been made to formulate a model that predicts the rate of desiccation cracking in unsaturated tailings (e.g. Konrad & Ayad 1997, Saleh-Mbemba et al. 2010a, Barrios et al. 2012, Simms et al. 2013). Allowing desiccation to occur can be a strategic tool for tailings operation by providing additional dewatering (Simms 2017). Desiccation increases effective stress due to matric suction and simultaneously increases tailings density, which imparts a stress history on the tailings (Simms 2021). Although desiccation can increase the dilatative tendency during shearing, the strength gained due to matric suction is reduced after resaturation. However,

Simms (2021) reports that the effects of desiccation after resaturation remain within the stress history and densification of the tailings.

2.3 Undrained Shear Behavior

Tailings impoundments span hundreds of meters in height. These large scales, along with high water contents, mean the potential for undrained shear failure in the TSF may develop due to lower hydraulic conductivity of the fine-grained material. Understanding the undrained shear behavior is paramount in tailings management because an undrained failure of loose, contractive tailings can lead to flow failures (e.g., Morgenstern et al. 2016; Robertson et al. 2019). Laboratory analysis is a predominate tool used to define the undrained shear behavior of a material. The role of excess pore water pressure when undergoing undrained shear is a major component that controls the shear resistance of a saturated material.

During undrained loading, excess pore pressure within tailings changes the effective stress. Three general types of undrained behavior for soils under monotonic compression are (i) flow, (ii) non-flow, and (iii) limited-flow, as illustrated in Fig. 2.3 (e.g., Macedo & Veragay 2022). The effective stress paths are shown in a MIT notation, where $p' = (\sigma_1' + \sigma_3')/2$, $q = (\sigma_1' - \sigma_3')/2$, and σ_1' and σ_3' are the major and minor principal effective stresses, respectively. Flow is defined for a material that can lose strength and “flow” like a liquid during undrained shear due to a tendency for the material to contract that leads to positive excess pore pressures. This phenomenon represents a worst-case scenario for most tailings impoundments. The tendency for a material to dilate during undrained shear yields a strain-hardening, no-flow behavior. Limited-flow behavior represents an intermediate response between flow and non-flow conditions resulting in a slight increase or decrease in shear strength depending on the magnitude of excess pore pressure.

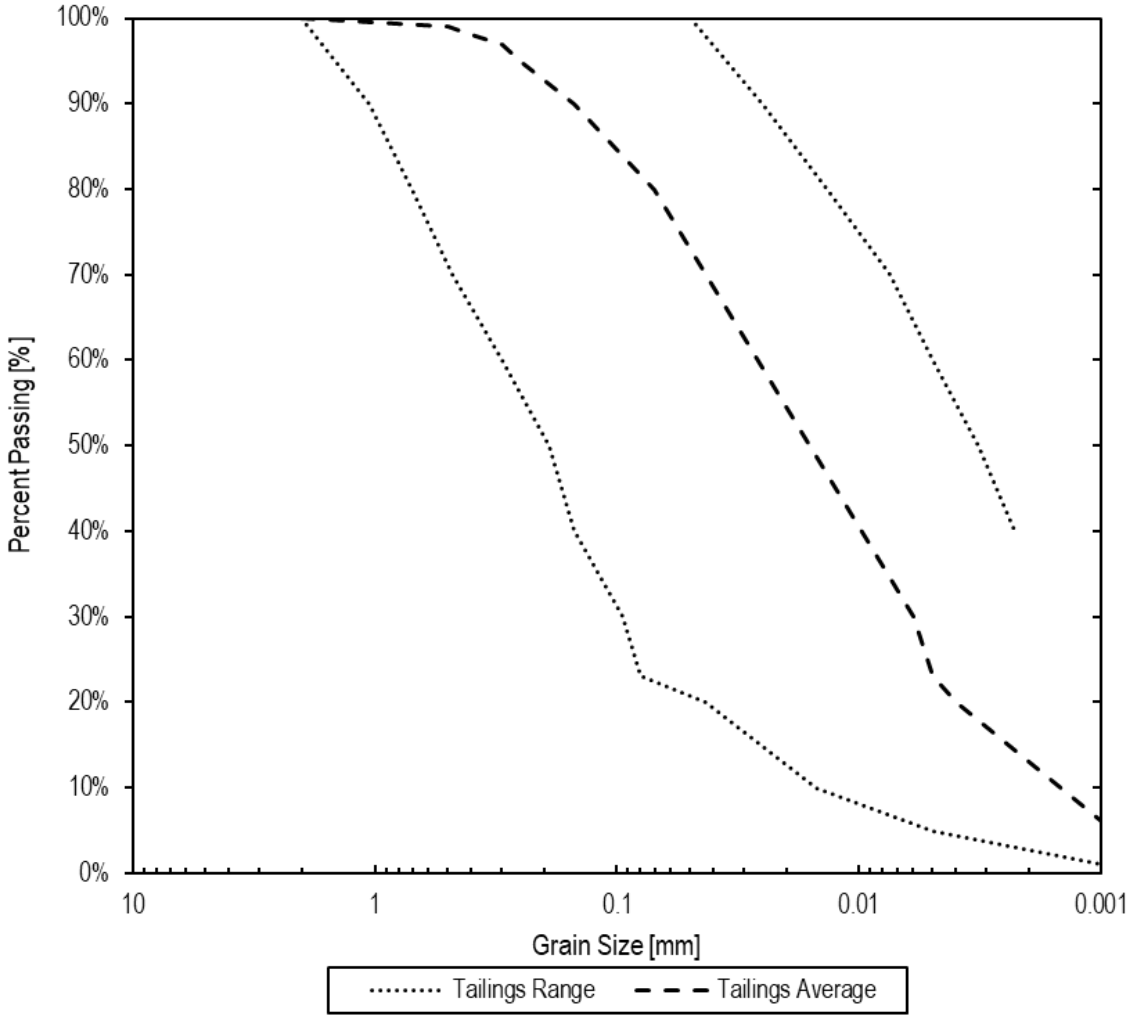

Fig. 2.1. Range and average particle-size distributions for mine tailings compiled from Qiu and Sego (2001) and Bussière (2007).

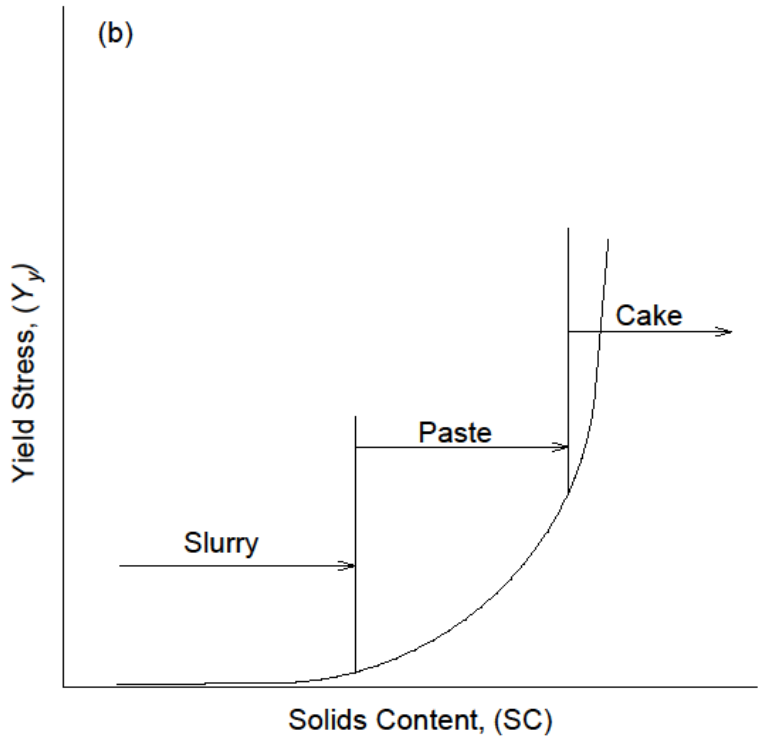

Fig. 2.2. Typical yield stress behavior for the tailings continuum based on solids content. Adapted from Boger 2009.

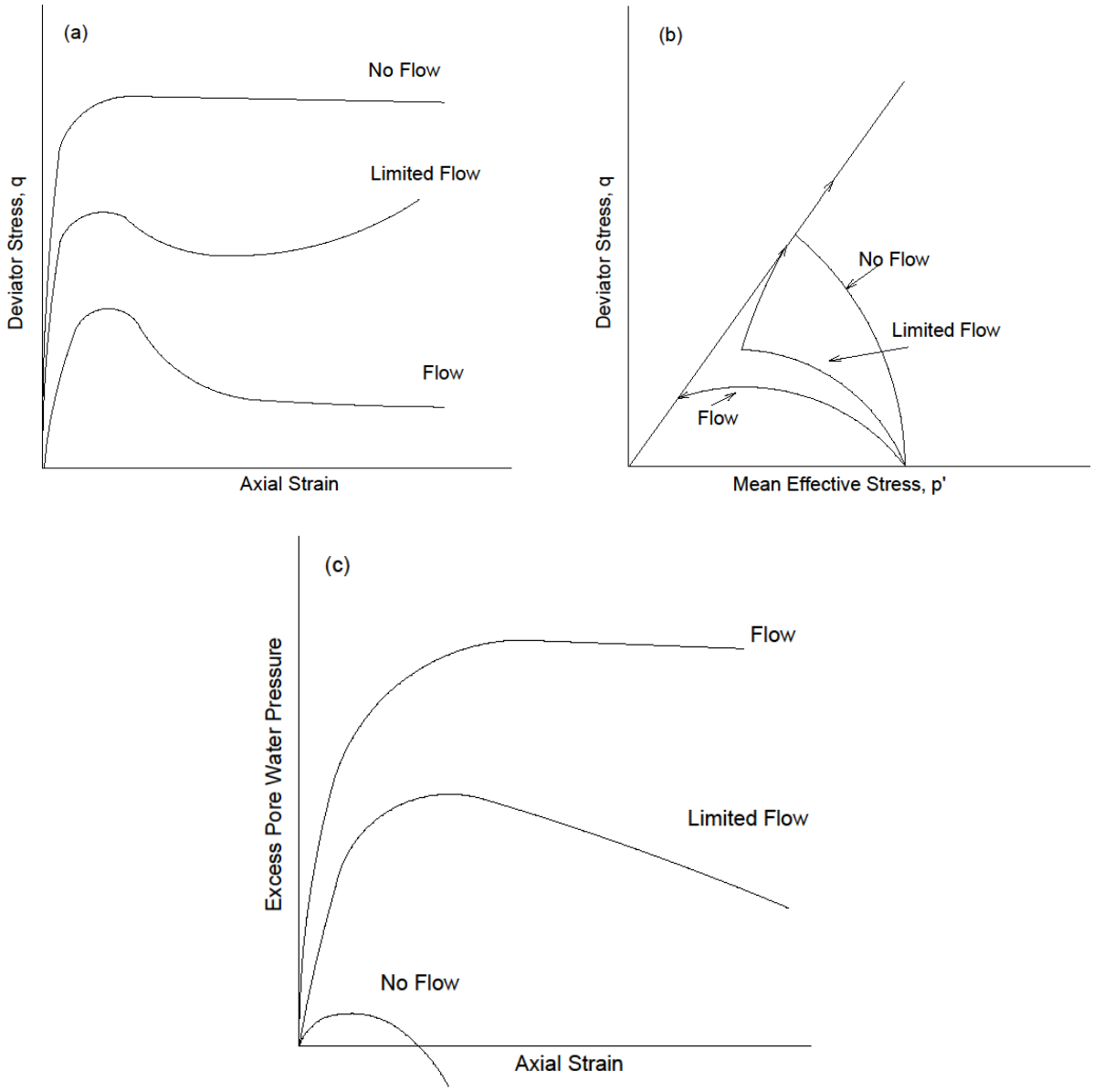

Fig. 2.3. Schematics of three distinct undrained shear flow behaviors for (a) deviator stress ($\Delta\sigma$) versus axial strain (ε_a), (b) effective stress paths, and (c) excess pore water pressure (u_e) versus axial strain (ε_a). Modified from Bobei et al. (2009).

CHAPTER 3: MATERIALS AND METHODS

3.1 Materials

Mine tailings from a gold mine in Central America were used for this study. All tailings samples were sterilized via oven drying upon receipt at Colorado State University. Prior to testing, all oven dried tailings were passed through a No. 4 sieve (4.75 mm) and homogenized to create a uniform material. All test specimens were prepared from a single homogenized material.

3.1.1 Tailings

Geotechnical characterization of tailings included mechanical sieve and laser hydrometer (ASTM D422), Atterberg limits (ASTM D4318), and specific gravity (ASTM D854). The particle size distribution of the tailings is shown in Fig. 3.1. The tailings were predominantly fine-grained (> 93%) and contained approximately 17% clay-sized particles (< 0.002 mm). Tailings classified as low plasticity silt (ML) in accordance with the USCS (ASTM D2487) and had a liquid limit of 34, plastic limit of 24, and plasticity index of 10. In general, tailings used in this study were comparable to common hard rock mine tailings (e.g., Bussiere 2007). The G_s of the tailings was 2.76, which was measured using the water pycnometer method described in ASTM D854.

3.2 Sample Desiccation

3.2.1 Solids Content Determination and Shrinkage Tests

A target solids content for the slurry tailings was necessary to prepare the initial tailings prior to desiccation. Selection of a solids content was determined based on yield stress (Boger 2009). Miniature-vane shear tests (ASTM D4648) were conducted on slurry tailings to determine yield stress as a function of solids content, as shown in Fig. 3.2. A solids content of 55% was estimated to coincide with a yield stress of approximately 100 Pa, which was a reasonable target solids content for tailings leaving a thickener. Settling tests conducted in 1000-mL beakers on

tailings at a solids content of 55% revealed minor solid-liquid separation and a final settled void ratio of 1.95 that corresponds to a void ratio at near zero effective stress (Tian et al. 2019).

Shrinkage tests were conducted on tailings prepared to a solids content of 55% to understand the shrinkage behavior during desiccation (ASTM D4943, Saleh-Mbemba et al. 2010b). Three shrinkage tests were run simultaneously until no change in volume was observed. Samples were then oven-dried to obtain final solids mass of each specimen to back calculate all water contents and void ratios from mass and volume measurements of the shrinkage specimens. Relationships of void ratio versus gravimetric moisture content from the three shrinkage tests are shown in Fig. 3.3. The shrinkage curves displayed generally linear behavior between void ratio and water content down to the estimated shrinkage limit of 21%. The slight non-linearity in the shrinkage curves was attributed to the manual measurement process in the wetter portion of the curve when specimens were too wet to remove from the confining ring without disturbance. A linear relationship from the initial as-prepared specimens to the shrinkage limit was assumed and verified in subsequent large-scale desiccation testing.

The shrinkage curve in Fig. 3.3 was used to determine five target void ratio zones and associated water contents for bucket desiccation tests. These five zones were chosen at water contents below 45%. The upper water content limit was selected because tailings at this water content were workable, and the integrity of exhumed samples above a water content of 45% was not sufficient to create repeatable test specimens. The five void ratio zones were selected to capture a range of strength and consolidation behavior in the lower end of the shrinkage curve where the effects of desiccation are more impactful to TSF stability.

3.2.2 Bucket Desiccation

Conventional 20-L plastic buckets with a plastic liner were used to create desiccated laboratory test specimens via air-drying. Procedures were similar to Reid et al. (2022d) who noted that this desiccation method created realistic conditions for tailings desiccation relative to the field.

Oven-dried tailings passing the No. 40 sieve were homogeneously mixed with deionized water to a solids content of 55% (gravimetric water content of 82%) and evenly distributed into five buckets. Buckets were labeled B-1 through B-5 with increasing number associated with increasing desiccation. The initial and final characteristics of each bucket are in Table 3.1. All five bucket samples were allowed to dry naturally under ambient laboratory conditions; however, towards the end of the drying process, a fan was positioned atop the final two buckets (B-4 and B-5) after they had reached the shrinkage limit to accelerate desiccation to their target void ratio zones.

Shrinkage curves for the five buckets are shown in Fig. 3.4. Incremental measurements of total tailings mass and volume were made on each bucket to determine the void ratio versus water content relationships. Assumptions of complete initial tailings saturation and all mass loss attributed to water were incorporated into the mass-volume calculations. Each bucket was allowed to air-dry to a target void ratio, whereupon reaching the target void ratios, tailings in the buckets were exhumed for triaxial, consolidation, moisture, and density testing.

Observations indicated that the drying process at the outer edges and surfaces of the bucket samples was more accelerated than the inner tailings volume. Radial shrinkage of the sample from the sides of the bucket occurred with increased loss of water mass. Over extended drying times, salt precipitation appeared on the surfaces until an almost uniform crust developed, which was consistent with observations in Libardi et al. (2022). Specific times and measurements of the salt precipitation and crust formation were not recorded because evaporative conditions were not held constant. Mass and volume measurements were made at non-uniform increments over the entirety of the drying period to create the shrinkage curves shown in Fig. 3.4.

The estimated volume of tailings in each bucket during desiccation was computed via Eq. 3.1 to determine if a given bucket had reached the targeted zones:

$$V_{dessicated\ tailings} = \frac{\pi}{3} y\left[\left\{\frac{y\left(\frac{D}{2}-\frac{d}{2}\right)}{H}+\frac{d}{2}\right\}^2+\left\{\frac{y\left(\frac{D}{2}+\frac{d}{2}\right)}{4H}+\frac{d}{2}\right\}\frac{d}{2}+\left(\frac{d}{2}\right)^2\right] \quad (3.1)$$

where y is the current height of the desiccated tailings, D is the diameter of the top of the bucket, d is the diameter of the bottom of the bucket, and H is the fixed height of the bucket. The equation was necessary because the sides of the buckets were at an angle, with different top and bottom diameters. Once radial shrinkage occurred and the sample separated from the outer edges of the bucket (i.e., at approximately 40-45% water content), Eq. 3.1 equation was abandoned and estimates of the volume were made on an average measured sample height and diameter.

3.2.3 Bucket Sampling

Target sampling locations and sample IDs for the triaxial, consolidation, moisture, and density specimens obtained from each bucket are shown in Fig. 3.5. Procedures for sampling were chosen to obtain quality specimens with sufficient duplicates in case of necessity for retesting. In Buckets B-1 and B-2, triaxial specimens were extracted via pushing four, 300-mm-tall by 63.5-mm-diameter plastic tubes into the center of the buckets. The plastic tubes were precut and taped along their vertical axis to minimize sample disturbance upon extraction from the tubes and transfer to the triaxial cells (described subsequently). The tubes had a wall thickness of approximately 1.9 mm, and the penetrating edge of the tubes was sharpened to facilitate cutting. After insertion of the plastic tubes, the bucket liners, with the desiccated tailings intact, were removed from the bucket and cut to expose the final full desiccated block of tailings. Final height and diameter measurements were made prior to the removal of any tailings specimens. Consolidation samples were then taken radially outside of the triaxial specimen tubes, with moisture and density samples taken near the edge of the bucket (Fig. 3.5).

Additional samples were sealed in plastic wrap to preserve moisture and placed aside in case of retesting needs. The plastic tubes were then carefully removed from the remaining tailings sample, with the two additional plastic tube samples sealed with plastic and tape to preserve the moisture and placed aside. The selected test specimens were then prepared for subsequent testing procedures.

In Buckets B-3, B-4, and B-5, triaxial and consolidation samples were taken from the same locations but were obtained by exhuming intact blocks and carving specimens with a surgical scalpel to the target dimensions. Specimen preparation for the respective test procedures immediately after removal from the buckets are outlined in proceeding sections.

3.2.4 Moisture and Density Testing

Moisture and density samples were exhumed from each bucket during sampling (Fig. 3.5). Samples were taken at near equal intervals in the vertical profile from top to bottom. The density samples were coated in wax (ASTM D7263) and used in conjunction with moisture samples to estimate the approximate final void ratio of each bucket. Results of the three samples used to measure moisture content and two used to measure density via wax-coating and water displacement are tabulated in Table 3.2. Moisture contents were measured via oven-drying at 105 °C for at least 24 h. These samples provided a water content profile of each bucket, and the average water content was used to compute void ratios of the two density samples. Although the overall void ratio of a given bucket was similar to the target void ratios, water contents and densities varied horizontally and vertically within a given bucket as observed in Table 3.2.

3.3 Triaxial Compression Testing

3.3.1 Consolidated Undrained Compression

Consolidated undrained (CU) triaxial compression tests were conducted in accordance with ASTM D4767. Specimens were back-pressure saturated to achieve a B-value ≥ 0.95. Saturation consisted of incrementally increasing cell and back pressures while keeping a constant effective stress of approximately 7 kPa until the target B-value was achieved. Specimens were then isotropically consolidated for at least 24 h under target effective stresses of either 50 or 100 kPa. Complete consolidation was verified by observing no change in the outflow water level during a period of at least 8 h.

Compression loading was conducted at an axial strain rate of 1.0 %/h to a target axial strain of 30%. Maximum axial strains were limited by machine capabilities, with test values typically ranging between 25% and 30%. The strain rate was determined via ASTM D4767 to promote pore pressure equilibration throughout the specimens during shear. Measurements of axial load, axial displacement, cell pressure, and pore pressure within the tailings specimens were made during triaxial testing. Axial load was measured using a load cell (Artech Industries, Inc., 8900 ± 0.4 N) and axial displacement was measured with a linear potentiometer (Novotechnik, 50 ± 0.003 mm). Cell and pore pressure were monitored with pressure transducers (GeoTac, 1378 ± 0.07 kPa; ELE International, Ltd., 700 ± 0.07 kPa), and pore water pressure was measured at the base of a specimen during shear. All data were collected by a data acquisition system (CU Triaxial Mode, GeoTac).

All desiccated and filtered tailings specimens had diameters of 63.5 mm and included oversized (72-mm diameter), lubricated end platens. The target height-to-diameter ratio of all specimens was two. Test specimens included a 0.25-mm-thick latex membrane and were inundated / back-pressure saturated with deionized, de-aired water. The end-of-test specimen freezing technique was used to determine specimen void ratios (e.g., Reid et al. 2020). After shearing was completed, the cylinder containing the cell water was removed, the test specimen remained in-place with all valves closed to prevent water loss from the specimen. The specimen and triaxial base stand were placed in the freezer for up to 24 hours (Reid et al. 2020). The specimen was then removed from the freezer and the O-rings, top platen, and bottom platen were removed. The membrane was removed by placing the sample vertically on a plastic cylinder and pulling the membrane downwards, allowing the membrane to separate from a still-frozen specimen. After successfully removing the membrane, porous stones and filter paper were removed and the mass of the frozen specimen was recorded. The specimens were then oven-dried at 105 °C for at least 24 h to determine dry mass of tailings solids.

The void ratio (e) of all tailings specimens was determined after shearing via Eq. 3.2:

$$S \cdot e = w \cdot G_s \tag{3.2}$$

where S is the degree of saturation and w is water content. The final void ratio was computed based on the total specimen water content, G_s = 2.76, and assuming S = 100%.

3.3.2 Specimen Preparation

3.3.2.1 Desiccated Tailings Specimens

Desiccated tailings specimens were prepared for triaxial testing via two methods depending on the average water content of the tailings in the desiccated bucket. All tailings specimens with water contents > 30% (Buckets B-1 and B-2) were transferred into an over-sized, 76-mm-diameter, membrane-lined split mold via the plastic sampling tubes. Vacuum was applied to the split-mold to pull the membrane flush to the mold walls and then a tailings specimen and one-half of the plastic tube, separated in half vertically, were inserted into the split-mold. A given specimen was carefully extruded from the separated half of the plastic tube and placed sideways in the membraned-lined, oversized split mold to avoid the specimen sliding off the mold. Vacuum was then removed such that the membrane closed-in on the side walls of the specimen within the split-mold. The specimen was placed vertically on an oversized, lubricated end platen, the split mold was then removed, and top platen added. The triaxial cell was then arranged and water added under low pressure (< 7 kPa) to fill the triaxial cell and support the specimen in place.

Desiccated tailings specimens with water contents < 30% (Buckets B-3, B-4, and B-5) were prepared by carving specimens to the target height and diameter. These lower water content specimens were all self-supporting such that oversized desiccated tailings blocks were cut from the whole desiccated tailings bucket sample. Subsequently, triaxial specimens were trimmed on a specimen-trimmer to the target diameter of 63.5 mm and then to target heights of 127 mm. These intact desiccated tailings specimens also were transferred sideways into the oversized, membraned-lined, split-mold. Vacuum on the membrane was removed to hold the specimen within the membrane in the mold. Finally, the specimen was placed between oversized, lubricated

end platens, the mold removed, and water was added to the triaxial cell to apply the confining pressure.

3.3.2.2 Filtered Tailings Specimens

Filtered tailings specimens were created using oven-dried tailings that were moisture conditioned to 5% water content, mixed thoroughly, and left in a sealed container overnight to equilibrate. Triaxial test specimens were prepared to target void ratios using mass-volume relationships and compacted via moist tamping to achieve similar initial void ratios as the desiccated tailings specimens. Target densities were achieved via compacting in 10 lifts of equal mass as outlined by Reid et al. (2022a). An undercompaction ratio of 5% was used as outlined in the specimen preparation procedure in Ladd (1978). The undercompaction corresponds to lower compacted lift densities progressing from the bottom to the top of the specimen. All filtered tailings specimens were prepared in a 63.5-mm-diameter split mold with oversized, lubricated end platens.

The filtered tailings specimens (FT-1, FT-2, FT-3, and FT-4) created to produce similar void ratios as the least desiccated tailings samples, were quite loose and prone to slumping if not supported laterally. A paper-mold technique, described in Jehring and Bareither (2016), was used for these loose, filtered tailings specimens to support initial specimen dimensions. Tracing paper cut to appropriate dimensions was wrapped around the outside of the membrane and secured with low-adhesive tape prior to compacting the specimens within the split mold. The tracing paper prevented the loosely compacted tailings from sloughing between split-mold removal and application of cell pressure. Water within the triaxial cell removed the adhesion of the tape on the tracing paper, which separated the tracing paper from around the membrane prior to shearing (Jerhing and Bareither 2015; Borja et al. 2020).

3.4 One-Dimensional Consolidation Testing

One-dimensional consolidation tests were performed in conventional fixed-ring consolidation cells on both desiccated and filtered tailings in accordance with ASTM D2435 (ASTM 2014). Desiccated tailings specimens were prepared in a similar manner to the procedures previously described for triaxial specimens. Specimens with high water contents (> 30%) were prepared using a thin-walled plastic tube to place the specimen inside a consolidation ring. Specimens with lower water contents (< 30%) were carved using surgical blades to fit within a consolidation ring. Filtered tailings specimens were prepared with an initial moisture content of 5%, moisture equilibrated in a sealed container overnight, and compacted in three lifts to a target density.

All desiccated tailings were tested in consolidation rings with an inside diameter of 63.5 mm and height of 25.4 mm. Measurements of axial load and axial displacement were measured during consolidation testing. Axial load was measured using a load cell (Artech Industries, Inc., 8900 ± 0.4 N) and axial displacement was measured with a linear potentiometer (Novotechnik, 50 ± 0.003 mm). All data were collected by a data acquisition system (SIGMA 1D, GeoJac).

Filtered specimens were prepared in two different size rings depending on the consolidation apparatus: one had an inside diameter of 70.0 mm and height of 19.0 mm and the other had an inside diameter of 63.5 mm and height of 25.4 mm. Filtered tailings specimens were placed in oedometers and vertical deformation was recorded for all specimens. Vertical loads for all filtered specimens were applied via dead weights incrementally increased every 24 h following Method A in ASTM D2435 (ASTM 2014).

A seating stress of 5 kPa was applied vertically to all consolidation test specimens following setup and specimens were immediately inundated. The vertical stress was increased every 24 h to the following target stresses: 10, 25, 50, 100, 250, 500, 1000, and 2000 kPa. After reaching the final target stress of 2000 kPa, all specimens were unloaded to 1000, 100, and 10 kPa, with each unload stress maintained for 24 h. Test conditions between specimens were

similar during loading, and temperature and humidity of the laboratory were approximately constant. At the end of each consolidation test, the final specimen dimensions were measured, and the entire specimens were weighed and then oven dried to determine final water content and void ratio.

Table 3.1. Summary of initial and final characteristics of the desiccated tailings bucket samples based on preparation data and mass-volume relationships.

Specimen	Target Initial Solids Content [%]	Initial Mass [kg]	Final Mass [kg]	Initial Volume [cm^3]	Estimated Final Volume [cm^3]	Estimated Initial Void Ratio	Estimated Final Void Ratio	Estimated Final Water Content [%]
Bucket 1	55	25.905	19.697	16,589	10,866	2.21	1.10	38.2
Bucket 2	55	25.636	18.162	16,619	9,476	2.25	0.85	28.8
Bucket 3	55	26.277	17.682	16,660	9,068	2.18	0.73	22.3
Bucket 4	55	26.631	17.012	16,666	8,592	2.14	0.65	16.1
Bucket 5	55	25.651	15.137	16,714	8,371	2.27	0.64	7.2

Table 3.2. Moisture and density measurements on exhumed samples from for desiccated tailings buckets after estimated target zones were reached through evaporative drying.

Bucket 1		Bucket 2		Bucket 3		Bucket 4		Bucket 5	
Sample	Void Ratio	Sample	Void Ratio	Sample	Void Ratio	Sample	Void Ratio	Sample	Void Ratio
WX-1	1.14	WX-3	1.00	WX-5	0.88	WX-7	0.75	WX-9	0.61
WX-2	1.18	WX-4	1.02	WX-6	0.91	WX-8	0.74	WX-10	0.68
Average	1.16	Average	1.01	Average	0.89	Average	0.75	Average	0.64
Sample	Water Content [%]	Sample	Water Content [%]	Sample	Water Content [%]	Sample	Water Content [%]	Sample	Water Content [%]
MD-1	40.4	MD-4	31.5	MD-7	24.8	MD-10	17.5	MD-13	6.6
MD-2	41.3	MD-5	32.0	MD-8	25.4	MD-11	17.8	MD-14	6.8
MD-3	41.8	MD-6	32.6	MD-9	24.4	MD-12	14.9	MD-15	8.9
Average	41.2	Average	32.0	Average	24.9	Average	16.7	Average	7.4

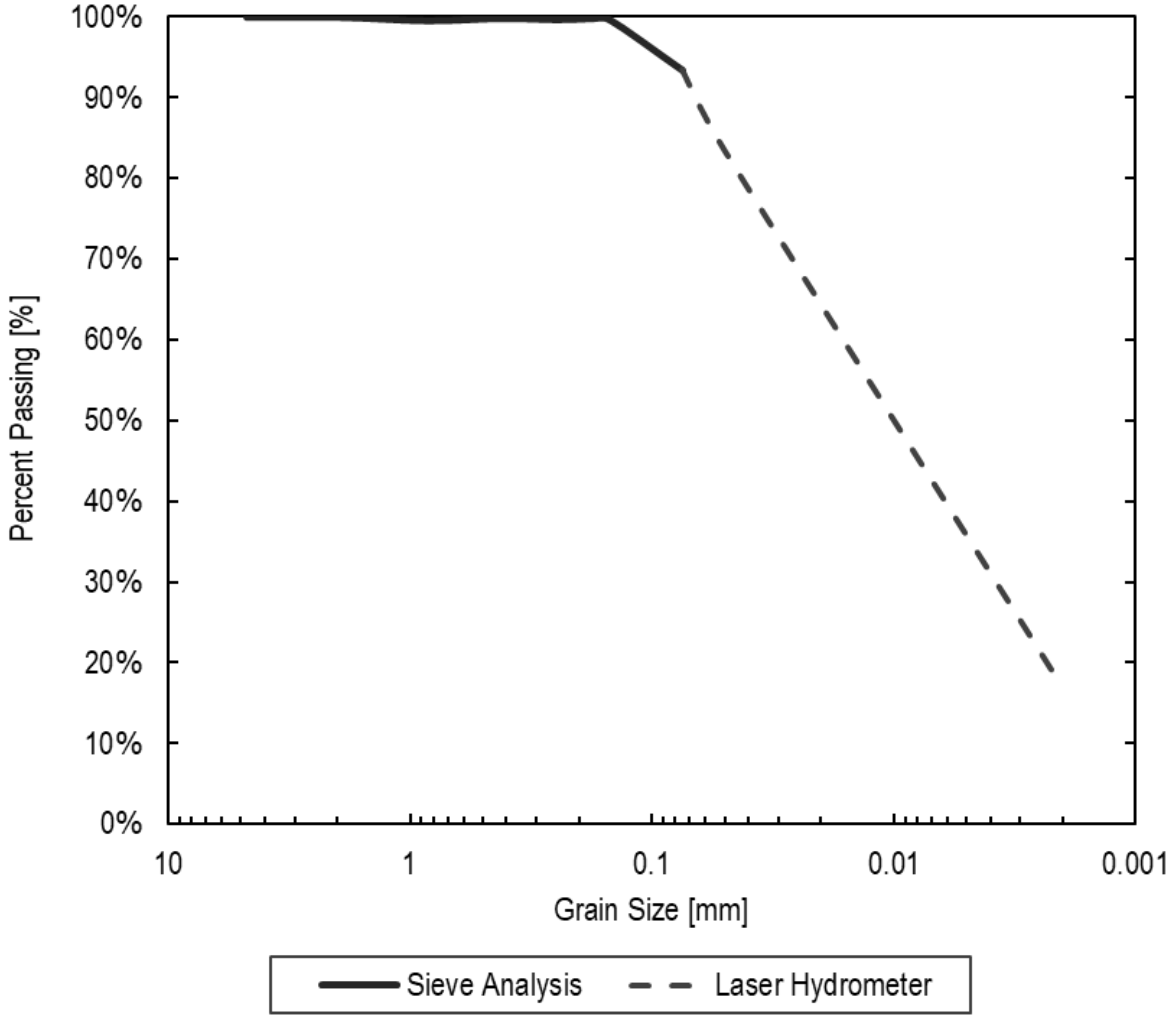

Fig. 3.1. Particle-size distribution for the mine tailings by sieve and laser hydrometer analysis.

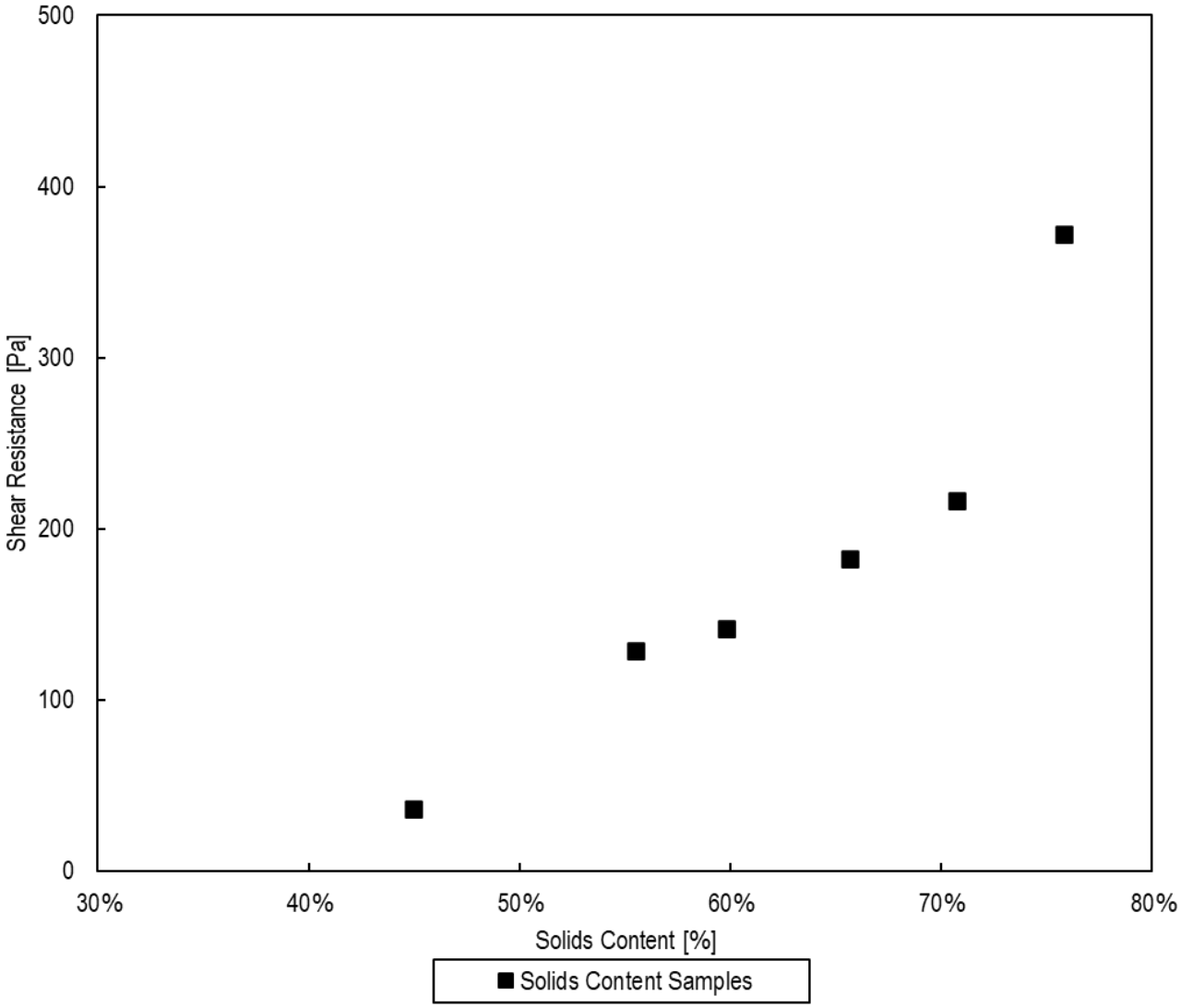

Fig. 3.2. Relationship between peak shear resistance (i.e., yield stress) measured in miniature vane shear and tailings solids content.

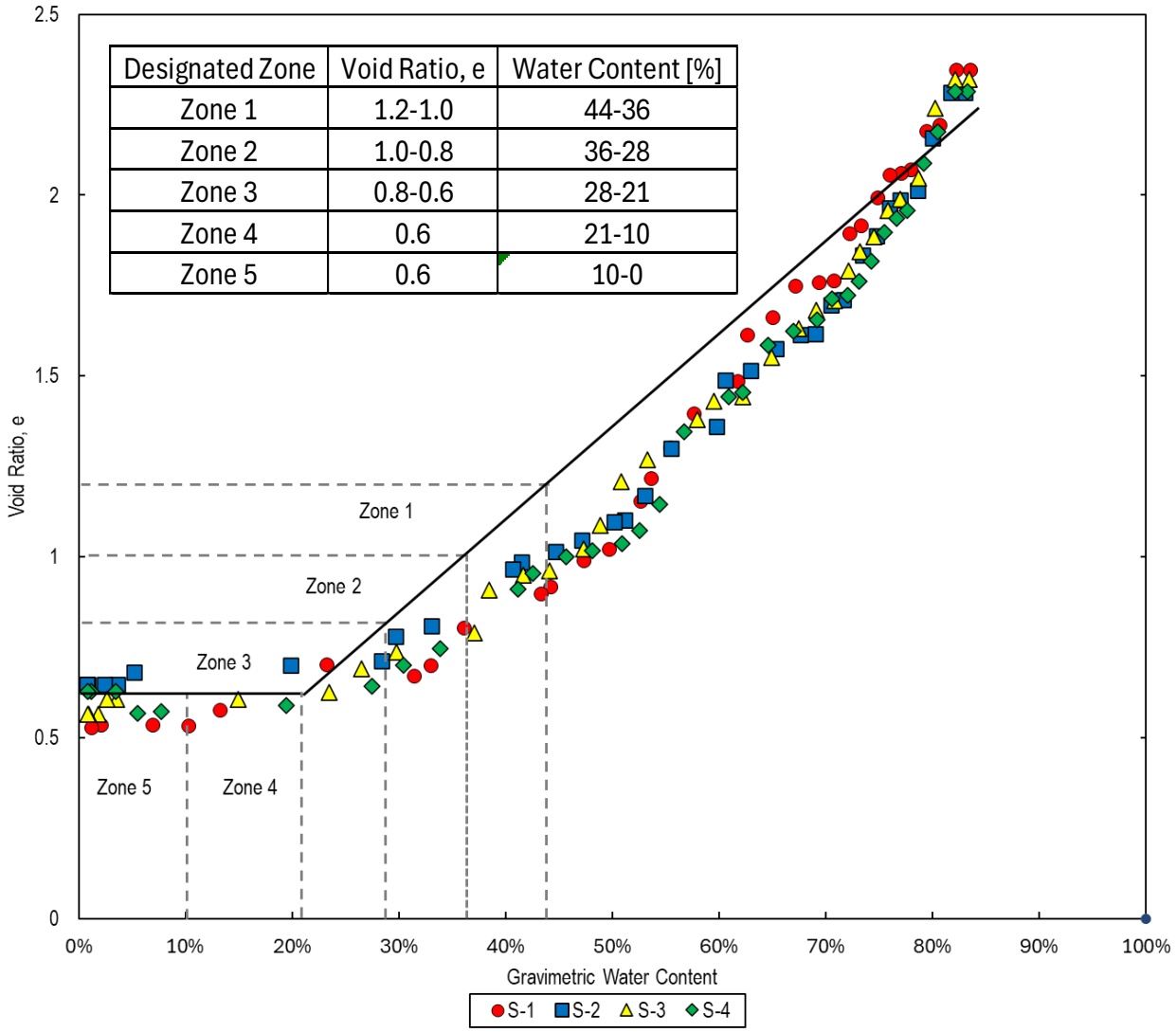

Fig. 3.3. Shrinkage curves from four samples of mine tailings that were used to develop target zones for void ratios and water contents for subsequent testing procedures.

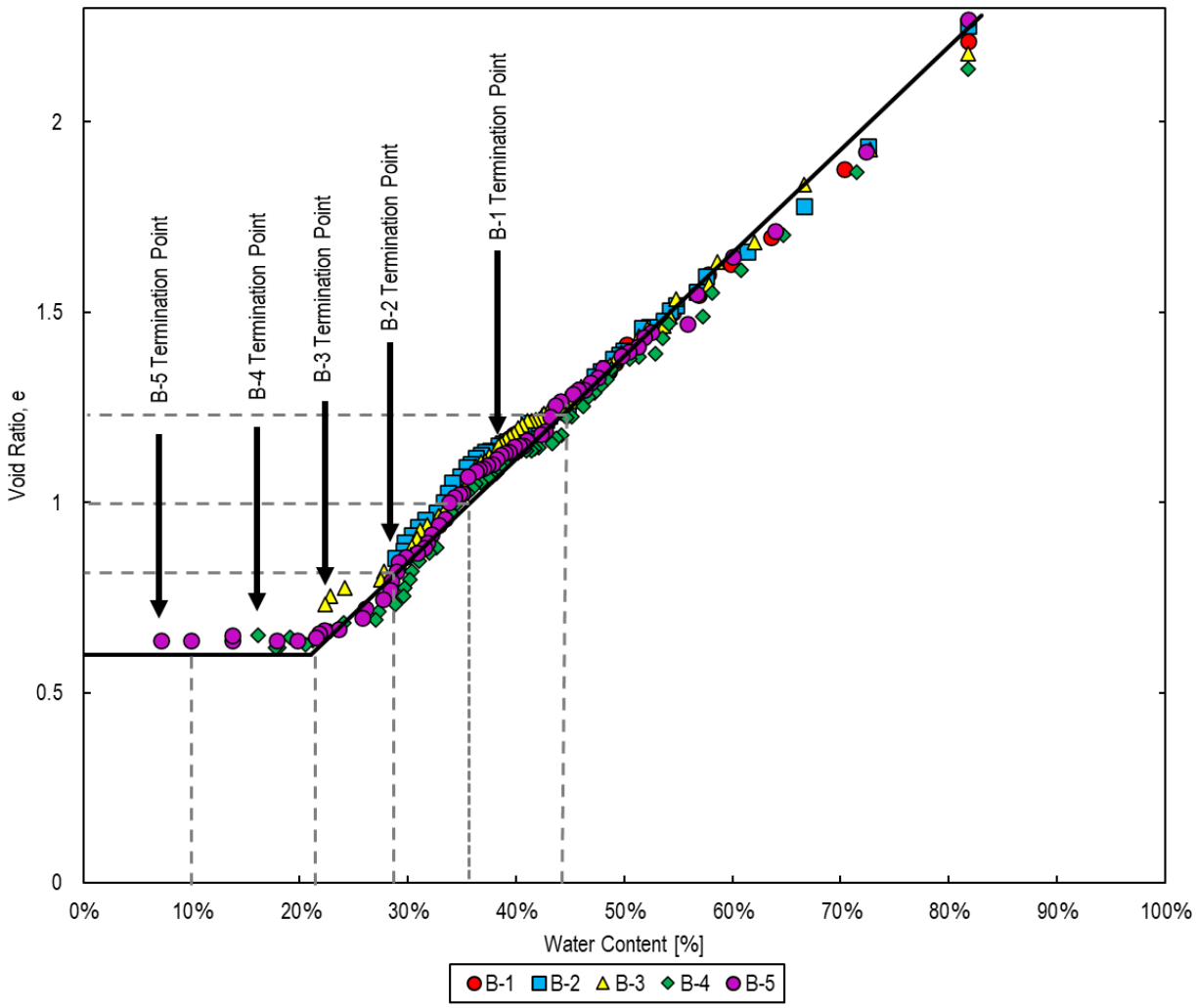

Fig. 3.4. Shrinkage curves for the five desiccation buckets plotted with the target void ratio – water content zones determined from shrinkage limit testing.

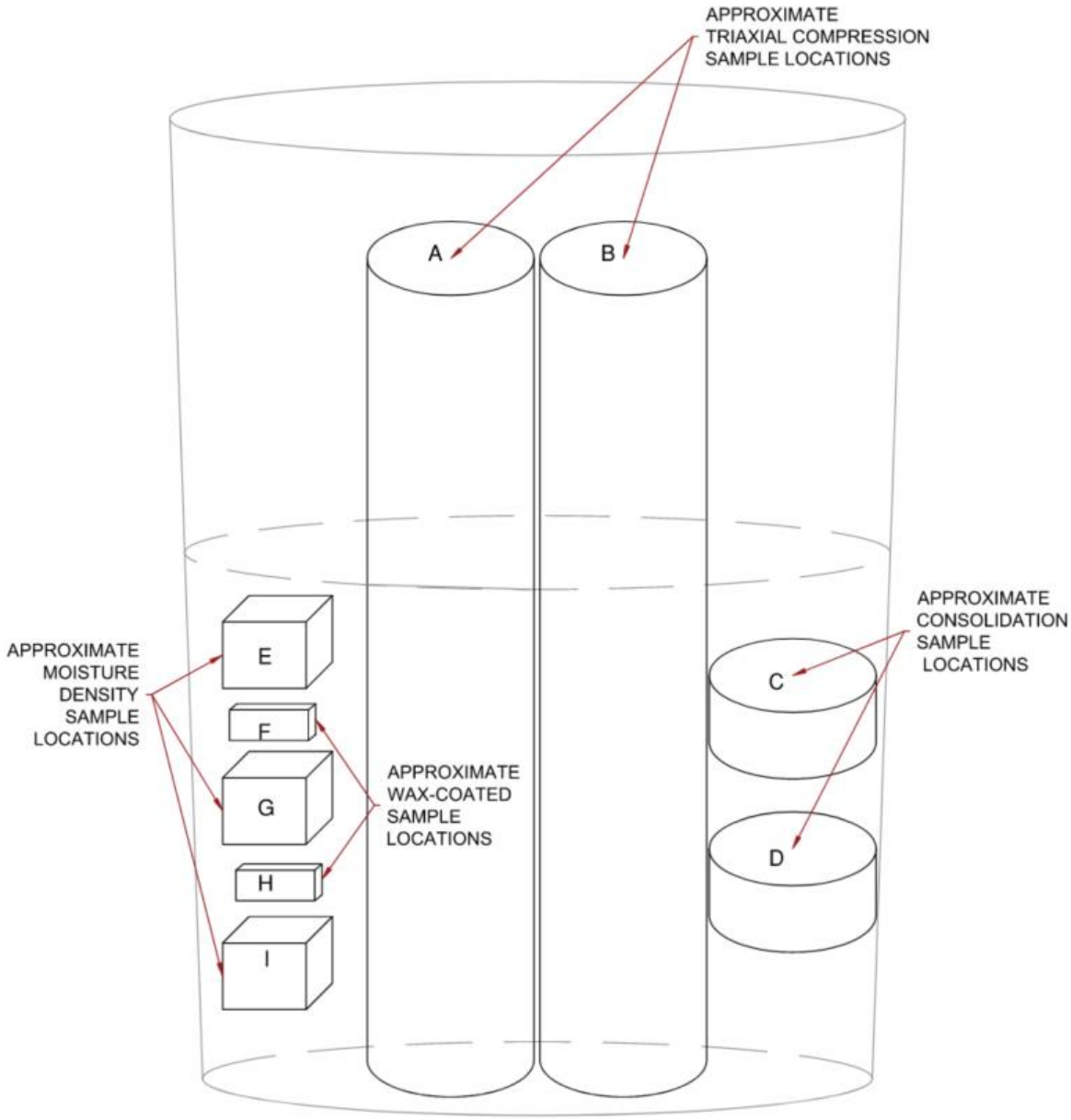

Sample Location	B-1	B-2	B-3	B-4	B-5
A	PT-1	PT-3	PT-5	PT-7	PT-9
B	PT-2	PT-4	PT-6	PT-8	PT-10
C	PC-1	PC-3	PC-5	PC-7	PC-9
D	PC-2	PC-4	PC-6	PC-8	PC-10
E	MD-1	MD-4	MD-7	MD-10	MD-13
F	WX-1	WX-3	WX-5	WX-7	WX-9
G	MD-2	MD-5	MD-8	MD-11	MD-14
H	WX-2	WX-4	WX-6	WX-8	WX-10
I	MD-3	MD-6	MD-9	MD-12	MD-15

Fig. 3.5. Sampling locations for the desiccation buckets after reaching target void ratio - water content zones and a list of samples collected that were used in the test program.

CHAPTER 4: RESULTS AND DISCUSSION

A summary of the consolidated undrained (CU) triaxial tests conducted on the desiccated and filtered tailings is in Table 4.1. The data compilation includes the following: target and actual effective confining stress (σ'_c), axial strain at failure ($\varepsilon_{a,f}$), deviator stress at failure ($\Delta\sigma_{d,f}$), effective major (σ'_{1f}) and effective minor (σ'_{3f}) principal stresses at failure, secant friction angle (φ'_{sc}), undrained shear strength ratio (Su/σ'_C), and other parameters described subsequently. Triaxial test results were analyzed to determine how void ratio and stress states at failure change depending on the initial method of densification (desiccation vs. mechanical compaction) prior to undrained shear testing. Triaxial tests were conducted at target effective confining stresses of 50 and 100 kPa on desiccated tailings and filtered tailings, whereby the filtered tailings specimens were prepared to similar initial void ratios measured in the desiccated tailings specimens. A compilation of the CU triaxial compression test results is in Appendix A.

A summary of results from one dimensional consolidation tests conducted on the desiccated and filtered tailings is in Table 4.2. The data compilation includes the following: initial void ratio (e_i), final void ratio (e_f), initial and final water contents, preconsolidation stress, compression index (C_c), and recompression index (C_r). Consolidation tests were conducted on two desiccated tailings specimens from each bucket and on two filtered tailings specimens that were prepared to similar initial void ratios as those measured on the desiccated specimens. Equipment between the tests varied, which resulted in slight variations of consolidation behavior via the monitoring equipment during loading. These differences (e.g., mechanical versus dead-weight loading; swell pressure vs. swell volume change) produced some scatter of data recorded during the initial loading stages. Although specimens were intended to be compared based on initial void ratio, a more informative comparison was developed via comparing the general consolidation behavior between the desiccated and filtered tailings. A compilation of consolidation test results is in Appendix B.

4.1 Shear Behavior

4.1.1 Tailings

Relationships of deviator stress ($\Delta\sigma$), excess pore water pressure (u_e) and q/p' ratio versus axial strain (ε_a) for the CU triaxial tests conducted on desiccated and filtered tailings at target effective consolidation stresses of 50 and 100 kPa are shown in Fig. 4.1 and Fig. 4.2, respectively. In general, undrained shear behavior for all specimens reached peak excess pore pressure between 3% to 6% axial strain, peak deviator stress between 16% to 24% axial strain, and then excess pore pressure and deviator stress remained relatively constant through the end of shearing at $\varepsilon_a \approx 25\%$ (Fig. 4.1a, Fig. 4.2a). Specimens targeted for testing at either $\sigma'_c = 50$ kPa or $\sigma'_c = 100$ kPa exhibited contractive tendencies as observed in the generation of positive excess pore pressure, which reached maximums between $\varepsilon_a = 3\%$ and 10% (Fig. 4.1b, Fig. 4.2b). All specimens exhibited modest transitional behavior (i.e., transition from contractive to dilative tendency) as observed by a slight reduction in excess pore pressure following the maximum, which produced modest strain-hardening behavior and an increase in deviator stress.

The relationships of q/p' versus ε_a (Fig. 4.1c, Fig. 4.2c) indicate that a maximum ratio was achieved in nearly all tests near $\varepsilon_a \approx 5\%$. Furthermore, the q/p' ratio for all specimens reached a uniform ratio between 0.4 and 0.5 and remained nearly constant for the duration of shearing. Effective stress friction angles for all test specimens ranged between 27° and 32°, which is consistent with other reported values for mine tailings (e.g., Macedo and Veragay 2022).

4.1.2 Desiccated and Filtered Tailings Comparison

Comparisons of undrained shear behavior were made between the desiccated tailings and filtered tailings prepared to target void ratios. In all triaxial specimens, consolidation occurred during application of an effective confining stress such that the final void ratio always was less than the initially prepared void ratio (Table 4.1). Initial void ratios of desiccated specimens decreased with increasing desiccation, and thus, the prepared filtered tailings specimens also

decreased to create similar void ratios. There were no initial tailings densities that were sufficiently dense to mitigate subsequent consolidation with application of cell pressure to the target effective stress levels of 50 or 100 kPa.

Relationships of the principal effective stress ratio (σ'_1/σ'_3) and Skempton's A parameter ($u_e/\Delta\sigma$) versus ε_a for the desiccated and filtered tailings triaxial tests conducted at target effective confining stresses of 50 kPa and 100 kPa are shown in Fig. 4.3 and Fig. 4.4, respectively. The trend in σ'_1/σ'_3 between the desiccated and filtered tailings was comparable, which was expected considering the similarity in q/p' ratios and effective stress friction angles determined for all individual test specimens (Table 4.10). The *A* parameters for all tailings were positive and indicative of overall contractive behavior; however, the A parameter for the desiccated tailings generally showed a stiff initial peak followed by a sharp decrease with increasing strain. This behavior is indicative of a stiffer initial fabric and more pronounced tendency for transitional behavior that shifts from contractive to dilative tendencies. This is consistent with research (Daliri et al. 2014) showing "desiccated tailings exhibit a much small increase in peak strength at [phase transition] but show a higher degree of strain hardening past the PT point." The filtered tailings exhibited similar behavior with a less prominent decrease with increasing strain. Additional discussions on shear behavior are included in Section 4.2 that pair with the discussion of shear strength.

4.1.3 Brittleness and Stiffness

The hypothesis of this research incorporated the presumption that desiccated and resaturated tailings would exhibit stiffer and stronger responses relative to filtered tailings when undergoing undrained axial compression. A compilation of brittleness and stiffness of the desiccated and filtered tailings is in Table 4.3. The brittleness index was calculated as follows (Bishop 1967, 1973; Robertson 2017):

$$Brittleness\ Index = \frac{Su_f - Su_r}{Su_r} \cdot 100\% \quad (4.1)$$

where Su_f was the undrained shear strength at the point of maximum deviatoric stress ($\Delta\sigma_{max}$) and Su_r was the residual undrained shear strength at the end of testing (ε_a = 25%). The brittleness index for desiccated tailings ranged between 0.2 and 5.3 percent. The range for filtered tailings is 1.3 to 3.9 percent. Data for both tailings preparation methods contained a significant amount of scatter. While desiccated tailings have a more variability in indices than filtered tailings, there was no discernible trend.

Further analysis was done to assess tailing stiffness. Tailings stiffness was quantified as Young's Modulus (E), which was computed as the slope (i.e., axial stress vs. axial strain) of the initial linear portion of the stress-strain curve. All tailings samples reached non-linear stress-strain behavior prior to 1 percent axial strain. The limitations of instrumentation sensitivity and the reading schedule during triaxial test cause significant variation in the computed E due to the limited data recorded prior to non-linear portion of the stress-strain curve. Quantitively, there is not a distinguishable pattern indicating a difference between the initial stiffness between preparation type in the elastic zone. The similarities in general shear behavior provide no indication in differences in stiffness or brittleness between tailings preparation methods. Rather, the higher shear strength of the desiccated tailings was attributed to more pronounced inter-particle reinforcing effects and densification from stress-history of desiccation.

4.1.4 Relative Compaction: Desiccation vs. Mechanical Compaction

Relative compaction describes the relationship between the dry density of a sample and the maximum dry density achievable based on standard laboratory compaction testing. Relative compaction, water contents, and dry density of both the desiccated and filtered tailings triaxial samples prior to shear testing are tabulated in Table 4.3. The maximum dry density of the filtered tailings in this study is 1.69 g/cm^3 (Hale 2022). To verify that densification due to desiccation of

tailings is a feasible alternative to mechanical compaction of filtered tailings, relative compaction of the filtered tailings samples and the desiccated tailings was compared. Based on the shrinkage limit and the zero effective stress void ratio determined in this study, the relative compaction values for the desiccated tailings ranges from 54.2 to 100%. Through desiccation, the thickened tailings samples were able to achieve a similar amount of relative compaction and a higher dry density than the filtered tailings samples. This relationship shows that through desiccation it is feasible to achieve similar relative compaction for thickened tailings as for mechanically compacted filtered tailings.

4.2 Shear Strength

4.2.1 Evaluation and Definition of Failure

A definition of failure is necessary to develop a comparison of shear strength parameters obtained from laboratory analysis. Brandon et al. (2006) evaluated the undrained shear behavior and shear strength of silty soils and identified six different failure criteria: (1) maximum deviator stress, $\Delta\sigma_{d,max}$; (2) maximum principal stress ratio, $(\sigma'_1/\sigma'_3)_{max}$; (3) maximum excess pore pressure, $u_{e,max}$; (4) limiting value of Skempton's pore pressure parameter A (e.g., $A = 0$); (5) stress path reaches the failure line (K_f Line) in p'-q space; and (6) limiting axial strain (e.g., $\varepsilon_a = 5$ or 10 %). These failure criteria were subsequently evaluated in in Wang and Luna (2012) and Jehring and Bareither (2016). The latter considered all interpretations for tailings and reported that maximum deviator stress, maximum excess pore pressure, and limiting axial strain were applicable to CU triaxial compression testing and yielded the smallest bias in determining shear strength parameters for mine tailings. In regard to recommendations in Brandon et al. (2006) and Jehring and Bareither (2016), failure was defined by $\Delta\sigma_{max}$, $u_{e,max}$, and $\varepsilon_a = 25\%$ (Table 4.1).

Effective stress paths in q-p' space reach failure and theoretically maintain a constant q/p' ratio for the remainder of axial deformation in a CU triaxial test. In this study, all tailings specimens were normally consolidated to slightly over consolidated materials, which was supported by the

predominately strain softening behavior, generation of positive excess pore pressure, and Skempton's A parameter at failure ranging between 0.5 to 1.0 (Skempton 1954). Thus, all strength enveloped (i.e., K_f Lines) were assumed to pass through the origin ($p' = 0$ and $q = 0$). The *q-p'* data from each CU test specimen were evaluated, and all chosen failure criteria yielded approximately the same *q/p'* ratio for a given specimen (Table 4.1).

The first failure criterion evaluated for each test was peak excess pore pressure, which occurred at small initial axial strains. The second evaluated failure criterion was peak deviatoric stress, which occurred at much larger axial strains than the peak excess pore pressure, which was attributed to the ductile nature of the contractive material. The last evaluated failure criterion was the limiting strain of 25%. This was chosen due to the ductile nature of the material while undergoing shear such that at an axial strain of 25% the critical state more than likely would be achieved. These selected failure criteria were evaluated in in *q-p'* space and the slope of a given K_f Line was used to compute effective stress friction angles (ϕ') for each material (Table 4.1).

4.2.2 Shear Strength of Tailings

Effective stress paths in *q-p'* space for desiccated tailings and filtered tailings at a target consolidation stress of $\sigma'_c = 50$ kPa are shown in Fig. 4.5 and for $\sigma'_c = 100$ kPa are shown in Fig. 4.6. All effective stress paths (Figs. 4.5 and 4.6) are non-linear and exhibit undrained behavior associated with positive generation of excess pore pressure. The arrangement of the five plots in each of Figs. 4.5 and 4.6 is such that desiccation increases from plot (a) to plot (e), which is from top to bottom in the figures. In both Figs. 4.5 and 4.6 there is an observable change in the shear behavior and shear strength of the desiccated tailings with higher amounts of desiccation. For example, in Fig. 4.5a that CU tests on PT-1 and FT-1 exhibit similar effective stress paths yielded comparable shear strength when peak excess pore pressure was reached (i.e., $\Delta\sigma_d = 37$ kPa for PT-1 at $\varepsilon_a = 4\%$, and $\Delta\sigma_d = 32$ kPa for FT-1 at $\varepsilon_a = 8\%$). The higher shear strength of PT-1 could be attributed to the slightly higher effective confining stress relative to PT- 1 (Table 4.1).

However, the difference in shear strength for the most desiccated specimen (PT-9) relative to the comparable filtered tailings specimen (FT-9) can be seen in Fig. 4.5e. In this comparison the shear strength of PT-9 was higher for all shear strength criteria (Table 4.1), and in particular at peak excess pore pressure for PT-9, $\Delta\sigma_d$ = 54 kPa at ε_a = 2% and $\Delta\sigma_d$ = 36 kPa for FT-9 at a comparable level of axial strain. Tailings desiccation yielded a 50% increase in shear strength for the comparison of PT-9 to FT-9, which supports the main hypothesis of this study.

The effective stress paths for the desiccated tailings specimens at σ'_c = 50 kPa, coupled with the trends of the A parameter (Fig. 4.3), suggest that the fabric created from slurry deposition and desiccation was uniquely different from the fabric created via compacting filtered tailings. Desiccation appears to create a stiffer and more dilative fabric relative to compacting filtered tailings. This behavior can also be observed in the effective stress paths (Fig. 4.6) and A parameter (Fig. 4.4) for desiccated and filtered tailings tested at σ'_c = 100 kPa. The peak of the A parameter at low axial strain and subsequent reduction is less pronounced at σ'_c = 100 kPa relative to σ'_c = 50 kPa. In addition, the effective stress paths appear more similar between the desiccated and filtered tailings at σ'_c = 100 kPa, except for the PT-10 and FT-10, which compares the most desiccated specimen. In this case, shear strength defined at peak excess pore pressure was $\Delta\sigma_d$ = 97 kPa for PT-10 at ε_a = 6% and $\Delta\sigma_d$ = 66 kPa for FT-10 at ε_a = 8%. Again, there is a quantifiable increase in shear strength of nearly 50% due to desiccation relative to compacting filtered tailings. In general, the suppression of the pronounced A parameter and more similar stress paths at σ'_c = 100 kPa was attributed to the higher effective confining stress, which most likely nullified additional effects of desiccation-induced overconsolidation.

Due to the creep of air pressure in the laboratory controls for cell pressure, the actual σ'_c was not always in agreement with the targeted σ'_c. Fig 4.7a-d displays the deviatoric stress normalized by the effective confining stress ($\Delta\sigma_d/\sigma'_c$) and compared to the axial strain for each sample method and target stress to showing the effects of desiccation. There is observable increase in $\Delta\sigma_d/\sigma'_c$ ratio for increased levels of desiccation at lower initial confining stresses.

Additional testing is needed to further investigate the coupled effects of increasing desiccation and consolidation to higher confining stresses to evaluate strength gain from desiccation.

A compilation of all effective stress paths for desiccated tailings is shown in Fig. 4.8a and for filtered tailings in Fig. 4.8b. Stress states at failure for the three failure criteria and the composite K_f Line in q-p' for desiccated tailings is shown in Fig. 4.9a and for filtered tailings in Fig. 4.9b. The effective stress paths for the desiccated tailings appear to form a unique strength envelope, which is supported by the small amount of scatter in shear strength points that plot around the single K_f Line in Fig. 4.9a. The composite K_f Line for the desiccated tailings yielded an effective stress friction angle of 29.1°. Although there is slightly more scatter in the shear strengths for the filtered tailings determined from the three failure criteria in Fig. 4.9b, a single K_f Line effectively captures the strength data and yielded an effective stress friction angle of 27.7°. The effective stress paths in q-p' space for the filtered tailings (Fig. 4.8b) all show similar nonlinear behavior that is representative of a soft, contractive material.

Undrained shear strength was calculated for all three failure criteria. The selection of undrained shear strength at maximum excess pore pressure and peak deviator stress were chosen to represent the maximum undrained strength achieved during testing prior to the phase transition and at maximum strength. Relationships of undrained shear strength versus effective confining stress prior to shear (σ'_C) for desiccated tailings and filtered tailings are shown in Fig. 4.10 based on strength identified at maximum excess pore pressure and peak deviator stress. The relationships are linear and exhibit an increase in undrained shear strength with an increase in effective confining stress prior to shear, which was expected and is well developed in literature (e.g., Ladd 1991). In general, the undrained shear strength for a given effective confining stress is larger for desiccated tailings relative to filtered tailings, which further supports the main hypothesis for this study. Interestingly, the range of undrained strengths in the data sets increase for both desiccated and filtered tailings when considering undrained strength defined at maximum deviator stress, and more so for the desiccated tailings. The variation in undrained shear strength

for the desiccated tailings at σ'_C = 50 kPa can be attributed to the effects of desiccation, which can produce an overconsolidated material. Any amount of overconsolidation for a given material would increase the undrained shear strength for a given level of effective confining stress (Ladd 1991).

Undrained shear strengths were normalized by the effective confining stress prior to shearing (Su/σ'_C) to compare shear behavior among test specimens, and these ratios are plotted in Fig. 4.11 with respect to the specimen ID. Undrained shear strength based on peak excess pore pressure and maximum deviator stress were used in the normalizations to represent strength at the phase change and maximum strength conditions, respectively. The undrained strength ratios for the desiccated tailings (0.37 to 0.53 for peak excess pore pressure and 0.45 to 0.74 for maximum deviator stress) were consistently greater than the filtered tailings (0.29 to 0.39 for peak excess pore pressure and 0.32 to 0.48 maximum deviator stress); the one exception was PT-1 and FT-1 for undrained strength defined at peak excess pore pressure. In general, there is an increase in Su/σ'_C for desiccated tailings that experience higher amounts of desiccation, and also that were tested at lower effective confining stress. These trends suggest that increasing desiccation led to higher undrained strength under a given level of effective stress. In addition, the increase in effective confining stress from σ'_C = 50 kPa to σ'_C = 100 kPa reduced the undrained strength ratio for a given level of desiccation, which agrees with past research that observed a diminishing effect of desiccation-induced overconsolidation with increasing effective stress (Daliri et al. 2014).

An additional analysis of the undrained strength ratios was completed with a comparison to the initial specimen void ratio and end-of-consolidation void ratio. Relationships of the undrained shear strength ratio versus (a) the initial, pre-consolidation void ratio (b) and final, post-testing void ratio are shown in Fig. 4.12 for S_u defined at peak excess pore pressure and in Fig. 4.13 for S_u defined at maximum deviator stress. The paired desiccated and filtered tailings specimens (e.g., PT-1 and FT-1) were prepared to similar initial void ratios and yielded similar

final end-state void ratios for each pair (Table 4.1). Although there is a slight trend of decreasing undrained strength ratio for higher initial void ratios in Figs. 4.12a and 4.13a, there is no observable trend when the undrained shear strength ratio is plotted as a function of void ratio at the end-of-consolidation (i.e., post-shear void ratio). The lack of any trend between the undrained shear strength ratio and end-of-consolidation void ratio was attributed to confounding factors of enhanced desiccation and varying effective stress, that likely led to unique tailings specimens for each level of desiccation and stress. These confounding factors limit the ability to isolate the influence of any variable on the relationship between undrained shear strength and void ratio.

4.3 Consolidation Behavior

A summary of the one-dimensional consolidation tests conducted on all desiccated tailings and filtered tailings, included void ratios, water contents, compression indices, and preconsolidation pressures, is in Table 4.2. Duplicated consolidation tests were conducted for each desiccated bucket; for example specimens PC-1 and PC-2 were exhumed from Bucket 1 (see Fig. 3.5). A compilation of the desiccated tailings consolidation curves is in Fig. 4.14 and a compilation of the filtered tailings consolidation curves is in Fig. 4.15. An increase in desiccation decreased initial void ratio of the consolidation test specimen (Table 4.3) and yielded more curvature in the consolidation curves at low stress, which is indicative of the desiccation-induced overconsolidation. Less curvature was observed in the consolidation curves for the filtered tailings, and a decrease in the initial void ratio, related to increased specimen compaction, appeared to have modest influence on inducing overconsolidation within the test specimens. Consolidation curves for samples methods were originally intended to be compared based on initial void ratio, however, due to the differences in test equipment, the overall consolidation behavior for the two sample preparation methods was compared.

The relationship between initial specimen void ratio and preconsolidation stress for all desiccated and filtered tailings specimens is shown in Fig. 4.16. Preconsolidation stress were

determined graphically using Casagrande procedures. In general, preconsolidation stress increased with decreasing initial void ratio for both the desiccated and filtered tailings. Linear regression of the desiccated tailings data yielded an R^2 of 0.57 and of the filtered tailings data yielded an R^2 of 0.77. The linearity of the data sets supports that a decrease in initial void ratio, via either desiccation or compaction, corresponded to an increase in preconsolidation stress. The preconsolidation stress in the desiccated tailings was attributed to suction stress that increased the effective stress as the material became unsaturated. The preconsolidation stress in the filtered tailings was attributed to compaction. A higher preconsolidation stress was observed for the desiccated tailings relative to the filtered tailings towards the lower end of the initial void ratios, which coincided with the most desiccated tailings specimens.

Relationships comparing initial void ratio to compression index and recompression index for consolidation tests on all desiccated and filtered tailings specimens are shown in Fig. 4.17. Although there is scatter in the data sets, there is a slight linear trend of increased compression indexes with higher initial void ratios. Desiccated tailings tended to have a steeper response in compression indexes with each increase in initial void ratio than filtered tailings. The data for recompression index also exhibits a large amount of scatter; however, there is a slight increasing linear trend for the filtered tailings and decreasing linear trend for the desiccated tailings (Fig. 4.17b). Overall, the compression and recompression indices found in the desiccated tailings were slightly higher, on average, relative to the filtered tailings.

4.4 Practical Implications

The objective of this study was to evaluate and compare the undrained shear behavior and consolidation behavior of slurry-deposited, desiccated tailings and compacted filtered tailings. In general, the evaluation supports the hypothesis that desiccation yields a higher peak undrained shear strength relative to compacted filtered tailings when considering the same initial conditions. The increase in undrained strength was attributed to stiffening of the tailings fabric.

The main practical implications of this study are (i) the justification of thin-lift deposition and desiccation as an alternative to compacted filtered tailings, and (ii) the understanding of consolidation behavior difference due to fabric in TSF operations. The target applications for desiccated tailings in TSF operation and long-term management depend on the shear strength behavior and relevant parameters need to be defined for stability analyses. The results on desiccated tailings obtained from this study can be used for the evaluation of operational costs of a TSF to efficiently use climate to aid in tailings dewatering, strength gain, and ideally a method to increase TSF stability via increased strength and reduced liquefaction potential.

The other practical implication is while no specimen preparation method can fully replicate the intact fabric of tailings in a TSF, the described laboratory testing procedure can be utilized to represent slurry, thickened, or paste tailings deposition followed by desiccation to create laboratory test specimens that can be used to better understand the behavior of tailings in arid environments. Additional testing is needed to (i) evaluate how the critical state line of desiccated tailings varies relative to compacted filtered tailings and (ii) optimize the lift thickness during deposition to promote the maximum amount of desiccation.

Table 4.1. Summary of consolidated undrained triaxial tests conducted on desiccated and filtered tailings.

Test	Target σ'_c [kPa]	Actual σ'_c [kPa]	Failure Criteria	$\varepsilon_{a,f}$	$\Delta\sigma_f$ [kPa]	σ'_{3f} [kPa]	σ'_{1f} [kPa]	$u_{e,f}$ [kPa]	p'_f [kPa]	q_f [kPa]	q/P'	e_i	e_f	φ'_s (deg)	S_u [kPa]	S_u/σ'_c
PT-1	50	50	Peak $U_{e,f}$	4%	36.7	18.3	55.0	31.4	36.7	18.3	0.50	1.12	0.81	30.0	18.3	0.37
			Peak $\Delta\sigma_f$	24%	49.6	24.1	73.6	25.1	48.9	24.8	0.51			30.5	24.8	0.50
			ε_a=25%	25%	48.2	24.2	72.4	25.1	48.3	24.1	0.50			30.0	24.1	0.49
FT-1	50	41	Peak $U_{e,f}$	8%	31.5	15.6	47.1	26.0	31.3	15.8	0.50	1.08	0.80	30.2	15.8	0.38
			Peak $\Delta\sigma_f$	19%	36.3	17.4	53.7	24.2	35.5	18.1	0.51			30.7	18.1	0.44
			ε_a=25%	25%	34.4	17.9	52.3	23.9	35.1	17.2	0.49			29.3	17.2	0.41
PT-2	100	101	Peak $U_{e,f}$	5%	71.8	35.0	106.8	66.2	70.9	35.9	0.51	1.16	0.75	30.4	35.9	0.35
			Peak $\Delta\sigma_f$	23%	98.1	43.9	142.0	56.7	93.0	49.0	0.53			31.8	49.0	0.48
			ε_a=25%	25%	97.7	44.3	142.0	56.5	93.2	48.8	0.52			31.6	48.8	0.48
FT-2	100	77	Peak $U_{e,f}$	8%	59.3	26.9	86.2	48.6	56.6	29.7	0.52	1.10	0.74	31.6	29.7	0.39
			Peak $\Delta\sigma_f$	19%	66.4	29.9	96.3	45.1	63.1	33.2	0.53			31.8	33.2	0.43
			ε_a=25%	25%	64.0	31.1	95.1	43.7	63.1	32.0	0.51			30.5	32.0	0.42
PT-3	50	59	Peak $U_{e,f}$	4%	52.3	29.1	81.5	30.2	55.3	26.2	0.47	1.08	0.77	28.2	26.2	0.44
			Peak $\Delta\sigma_f$	20%	65.3	33.6	98.8	25.7	66.2	32.6	0.49			29.5	32.6	0.55
			ε_a=25%	25%	61.1	33.8	94.9	25.4	64.3	30.5	0.47			28.3	30.5	0.52
FT-3	50	54	Peak $U_{e,f}$	5%	45.5	20.3	65.8	34.3	43.1	22.8	0.53	0.96	0.76	31.9	22.8	0.42
			Peak $\Delta\sigma_f$	17%	51.6	22.4	74.0	31.7	48.2	25.8	0.53			32.3	25.8	0.48
			ε_a=25%	25%	48.8	23.5	72.3	31.0	47.9	24.4	0.51			30.6	24.4	0.45
PT-4	100	111	Peak $U_{e,f}$	4%	80.3	44.3	124.6	67.3	84.4	40.1	0.48	1.01	0.78	28.4	40.1	0.36
			Peak $\Delta\sigma_f$	18%	100.3	51.4	151.7	59.8	101.5	50.1	0.49			29.6	50.1	0.45
			ε_a=25%	25%	97.4	52.6	150.0	58.6	101.3	48.7	0.48			28.7	48.7	0.44
FT-4	100	101	Peak $U_{e,f}$	9%	57.5	27.8	85.4	73.3	56.6	28.8	0.51	1.04	0.76	30.6	28.8	0.28
			Peak $\Delta\sigma_f$	20%	64.6	31.3	95.9	70.1	63.6	32.3	0.51			30.5	32.3	0.32
			ε_a=25%	25%	63.2	32.1	95.4	69.1	63.7	31.6	0.50			29.7	31.6	0.31

Notes: σ_c' = effective confining stress; $\varepsilon_{a,f}$ = axial strain at failure; $\Delta\sigma_f$ = deviator stress at failure; σ'_{3f} = minor effective principle stress at failure; σ'_{1f} = major effective principle stress at failure; $u_{e,f}$ = excess pore pressure at failure; p'_f = effective stress at failure; q = mean shear stress at failure; e_i = initial void ratio; e_f = final void ratio after consolidation and shearing; ϕ'_s = secant friction angle; S_u = undrained shear strength; S_u/σ_c' = undrained shear strength ratio

Table 4.1. Summary of consolidated undrained triaxial tests conducted on desiccated and filtered tailings (continued).

Test	Target σ'_c [kPa]	Actual σ'_c [kPa]	Failure Criteria	$\varepsilon_{a,f}$	$\Delta\sigma_f$ [kPa]	σ'_{3f} [kPa]	σ'_{1f} [kPa]	$u_{e,f}$ [kPa]	p'_f [kPa]	q_f [kPa]	q/P'	e_i	e_f	φ'_s (deg)	S_u [kPa]	S_u/σ'_c
PT-5	50	58	Peak $U_{e,f}$	3%	62.2	38.6	100.8	18.9	69.7	31.1	0.45	0.85	0.79	26.5	31.1	0.53
			Peak $\Delta\sigma_f$	17%	81.6	43.0	124.6	14.3	83.8	40.8	0.49			29.1	40.8	0.70
			ε_a=25%	25%	77.7	44.0	121.7	12.9	82.9	38.8	0.47			27.9	38.8	0.67
FT-5	50	48	Peak $U_{e,f}$	4%	34.2	23.9	58.1	24.8	41.0	17.1	0.42	0.87	0.78	24.7	17.1	0.35
			Peak $\Delta\sigma_f$	20%	41.9	26.5	68.3	21.9	47.4	20.9	0.44			26.2	20.9	0.43
			ε_a=25%	25%	40.9	27.0	67.9	21.3	47.4	20.4	0.43			25.5	20.4	0.42
PT-6	100	113	Peak $U_{e,f}$	5%	93.5	48.6	142.0	64.2	95.3	46.7	0.49	0.84	0.76	29.4	46.7	0.41
			Peak $\Delta\sigma_f$	15%	113.2	53.8	166.9	58.1	110.4	56.6	0.51			30.9	56.6	0.50
			ε_a=25%	25%	110.6	56.5	167.0	50.9	111.8	55.3	0.49			29.6	55.3	0.49
FT-6	100	76	Peak $U_{e,f}$	8%	53.3	38.0	91.3	38.2	64.6	26.6	0.41	0.88	0.76	24.3	26.6	0.35
			Peak $\Delta\sigma_f$	22%	60.2	41.5	101.7	34.4	71.6	30.1	0.42			24.9	30.1	0.40
			ε_a=25%	25%	58.9	41.7	100.6	34.0	71.2	29.5	0.41			24.5	29.5	0.39
PT-7	50	59	Peak $U_{e,f}$	2%	61.3	37.2	98.4	22.2	67.8	30.6	0.45	0.84	0.76	26.9	30.6	0.52
			Peak $\Delta\sigma_f$	16%	88.2	44.8	133.1	14.3	89.0	44.1	0.50			29.7	44.1	0.74
			ε_a=25%	25%	85.8	46.4	132.2	12.6	89.3	42.9	0.48			28.7	42.9	0.72
FT-7	50	59	Peak $U_{e,f}$	9%	40.3	25.1	65.4	34.2	45.3	20.1	0.45	0.90	0.78	26.4	20.1	0.34
			Peak $\Delta\sigma_f$	18%	43.3	26.1	69.4	33.2	47.7	21.7	0.45			27.0	21.7	0.37
			ε_a=25%	25%	41.6	26.8	68.5	32.3	47.7	20.8	0.44			25.9	20.8	0.35
PT-8	100	106	Peak $U_{e,f}$	6%	85.4	47.2	132.6	58.9	89.9	42.7	0.47	0.85	0.74	28.4	42.7	0.40
			Peak $\Delta\sigma_f$	18%	95.7	51.5	147.2	54.3	99.4	47.9	0.48			28.8	47.9	0.45
			ε_a=25%	25%	92.6	53.7	146.3	52.2	100.0	46.3	0.46			27.6	46.3	0.44
FT-8	100	78	Peak $U_{e,f}$	3%	53.2	33.5	86.7	43.8	60.1	26.6	0.44	0.86	0.74	26.3	26.6	0.34
			Peak $\Delta\sigma_f$	18%	67.2	37.1	104.3	39.9	70.7	33.6	0.47			28.3	33.6	0.43
			ε_a=25%	25%	63.9	38.3	102.1	38.5	70.2	31.9	0.45			27.1	31.9	0.41

Notes: σ_c' = effective confining stress; $\varepsilon_{a,f}$ = axial strain at failure; $\Delta\sigma_f$ = deviator stress at failure; σ'_{3f} = minor effective principle stress at failure; σ'_{1f} = major effective principle stress at failure; $u_{e,f}$ = excess pore pressure at failure; p'_f = effective stress at failure; q = mean shear stress at failure; e_i = initial void ratio; e_f = final void ratio after consolidation and shearing; ϕ'_s = secant friction angle; S_u = undrained shear strength; S_u/σ_c' = undrained shear strength ratio

Table 4.1. Summary of consolidated undrained triaxial tests conducted on desiccated and filtered tailings (continued).

Test	Target σ'_c [kPa]	Actual σ'_c [kPa]	Failure Criteria	$\varepsilon_{a,f}$	$\Delta\sigma_f$ [kPa]	σ'_{3f} [kPa]	σ'_{1f} [kPa]	$u_{e,f}$ [kPa]	p'_f [kPa]	q_f [kPa]	q/P'	e_i	e_f	φ'_s (deg)	S_u [kPa]	S_u/σ'_c
PT-9	50	59	Peak $U_{e,f}$	2%	53.9	34.6	88.6	24.5	61.6	27.0	0.44	0.83	0.78	26.0	27.0	0.46
			Peak $\Delta\sigma_f$	16%	79.1	40.8	119.9	18.3	80.3	39.5	0.49			29.5	39.5	0.67
			ε_a=25%	25%	74.7	42.4	117.1	16.7	79.8	37.4	0.47			27.9	37.4	0.63
FT-9	50	59	Peak $U_{e,f}$	8%	40.3	27.3	67.6	31.3	47.4	20.1	0.42	0.89	0.79	25.1	20.1	0.34
			Peak $\Delta\sigma_f$	18%	44.9	28.5	73.4	30.4	50.9	22.5	0.44			26.2	22.5	0.38
			ε_a=25%	25%	44.1	29.1	73.2	29.6	51.1	22.0	0.43			25.5	22.0	0.38
PT-10	100	107	Peak $U_{e,f}$	6%	96.5	50.3	146.7	38.4	98.5	48.2	0.49	0.80	0.75	29.3	48.2	0.45
			Peak $\Delta\sigma_f$	18%	106.4	55.2	161.7	33.0	108.5	53.2	0.49			29.4	53.2	0.50
			ε_a=25%	25%	102.6	56.2	158.8	32.0	107.5	51.3	0.48			28.5	51.3	0.48
FT-10	100	106	Peak $U_{e,f}$	8%	66.1	39.4	105.5	66.1	72.5	33.1	0.46	0.88	0.73	27.1	33.1	0.31
			Peak $\Delta\sigma_f$	18%	71.8	41.6	113.4	63.6	77.5	35.9	0.46			27.6	35.9	0.34
			ε_a=25%	25%	69.5	43.0	112.5	62.0	77.8	34.7	0.45			26.5	34.7	0.33

Notes: σ_c' = effective confining stress; $\varepsilon_{a,f}$ = axial strain at failure; $\Delta\sigma_f$ = deviator stress at failure; σ'_{3f} = minor effective principle stress at failure; σ'_{1f} = major effective principle stress at failure; $u_{e,f}$ = excess pore pressure at failure; p'_f = effective stress at failure; q = mean shear stress at failure; e_i = initial void ratio; e_f = final void ratio after consolidation and shearing; ϕ'_s = secant friction angle; S_u = undrained shear strength; S_u/σ_c' = undrained shear strength ratio

Table 4.2. Summary of consolidation tests conducted on desiccated and filtered tailings. Preconsolidation stress, compression indices, and recompression indices were derived using Casagrande procedures.

Test	Initial Void Ratio, e_i	Final Void Ratio, e_f	Initial Water Content [%]	Final Water Content [%]	Preconsolidation Stress [kPa]	Compression Index, C_c	Recompression Index, C_r
PC-1	1.07	0.67	44%	22%	52	0.225	0.046
PC-2	1.06	0.60	45%	22%	60	0.237	0.056
PC-3	1.06	0.62	33%	22%	52	0.236	0.033
PC-4	0.99	0.64	32%	23%	40	0.240	0.056
PC-5	0.89	0.59	27%	23%	95	0.218	0.042
PC-6	0.90	0.60	27%	23%	150	0.236	0.044
PC-7	0.92	0.59	18%	22%	150	0.210	0.036
PC-8	0.90	0.59	18%	23%	150	0.236	0.065
PC-9	0.79	0.59	10%	22%	200	0.231	0.056
PC-10	0.89	0.58	8%	22%	280	0.259	0.036
FC-1	1.11	0.61	5%	25%	55	0.202	0.014
FC-2	1.19	0.62	5%	22%	25	0.227	0.032
FC-3	1.15	0.62	5%	22%	17	0.195	0.061
FC-4	1.14	0.63	5%	23%	45	0.221	0.065
FC-5	1.07	0.63	5%	21%	47	0.315	0.030
FC-6	0.99	0.62	5%	22%	40	0.213	0.039
FC-7	0.85	0.60	5%	22%	95	0.206	0.030
FC-8	0.84	0.63	5%	21%	90	0.189	0.032
FC-9	0.85	0.60	5%	21%	125	0.222	0.041
FC-10	0.96	0.61	5%	21%	55	0.205	0.013

Table 4.3. Initial and final void ratios, initial water content, final dry density, relative compaction, brittleness, and Young's Modulus determined for the consolidated undrained triaxial tests.

Test	Initial Void Ratio, e_i	Initial Water Content [%]	Final Void Ratio, e_f	Final Dry Density [g/cm^3]	Relative Compaction [%]	Brittleness [%]	Young's Modulus, E [kPa]
PT-1	1.12	41.2	0.81	1.30	75.5	2.2%	2736
PT-2	1.16	41.2	0.75	1.28	74.1	0.2%	8357
PT-3	1.08	30.9	0.77	1.33	77.0	5.3%	5357
PT-4	1.01	32.0	0.78	1.37	79.7	2.0%	7583
PT-5	0.85	24.9	0.79	1.49	86.5	3.7%	5724
PT-6	0.84	24.9	0.76	1.50	86.8	1.1%	8116
PT-7	0.84	17.9	0.76	1.50	86.9	1.8%	4320
PT-8	0.85	16.7	0.74	1.49	86.6	2.1%	5311
PT-9	0.83	7.4	0.78	1.51	87.4	4.1%	9340
PT-10	0.80	7.4	0.75	1.53	89.0	2.3%	8210
FT-1	1.08	5.0	0.80	1.33	78.4	3.9%	4019
FT-2	1.10	5.0	0.74	1.31	77.7	2.3%	6870
FT-3	0.96	5.0	0.76	1.41	83.2	3.6%	8915
FT-4	1.04	5.0	0.76	1.35	80.1	1.3%	4887
FT-5	0.87	5.0	0.78	1.48	87.4	1.8%	3355
FT-6	0.88	5.0	0.76	1.47	86.8	1.8%	6699
FT-7	0.90	5.0	0.78	1.45	85.9	3.0%	6517
FT-8	0.86	5.0	0.74	1.48	87.7	3.7%	7651
FT-9	0.89	5.0	0.79	1.46	86.5	1.4%	6147
FT-10	0.88	5.0	0.73	1.47	87.0	2.3%	7237

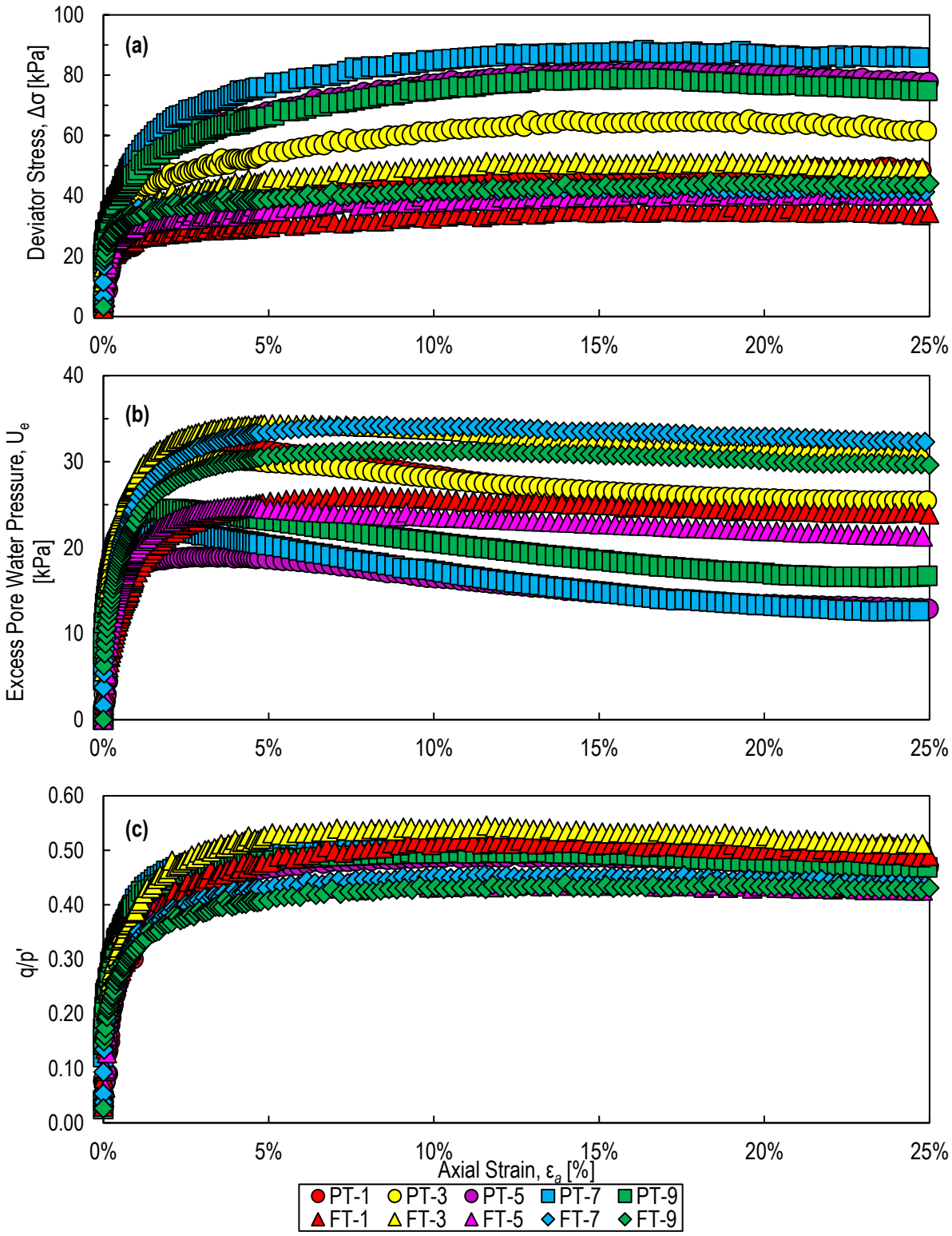

Fig. 4.1. Relationships of (a) deviator stress, (b) excess pore water pressure, (c) and q/p' ratio versus axial strain for consolidated undrained triaxial compression tests on filtered tailings and desiccated tailings prepared to a target confining stress (σ'_c) of 50 kPa.

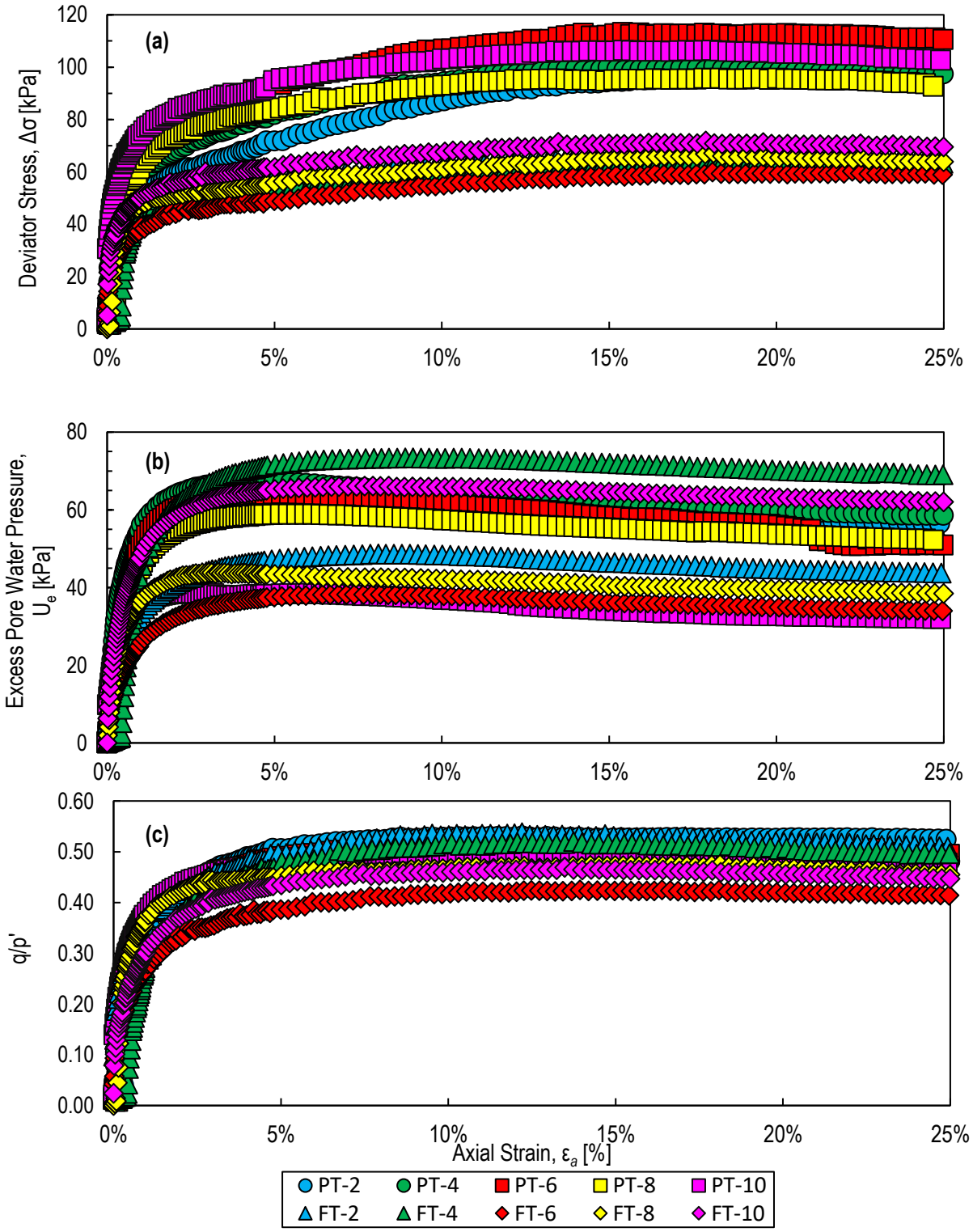

Fig. 4.2. Relationships of (a) deviator stress, (b) excess pore water pressure, (c) and q/p' ratio versus axial strain for consolidated undrained triaxial compression tests on filtered tailings and desiccated tailings prepared to a target confining stress (σ'_c) of 100 kPa.

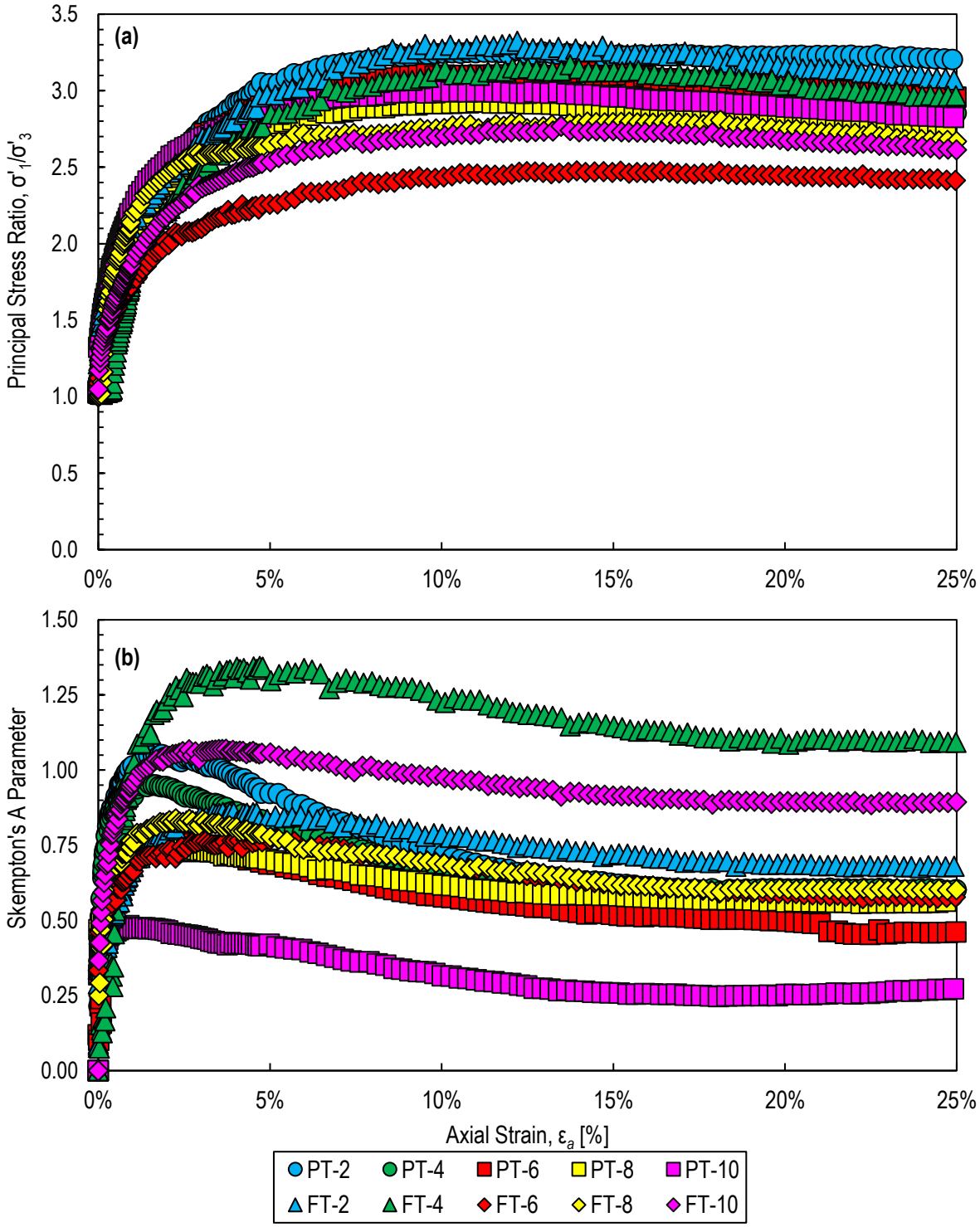

Fig. 4.3. Relationships of (a) principal stress ratio and (b) Skempton's A Parameter versus axial strain for consolidated undrained triaxial compression tests on filtered tailings and desiccated thickened tailings prepared to a target confining stress (σ'_c) of 50 kPa.

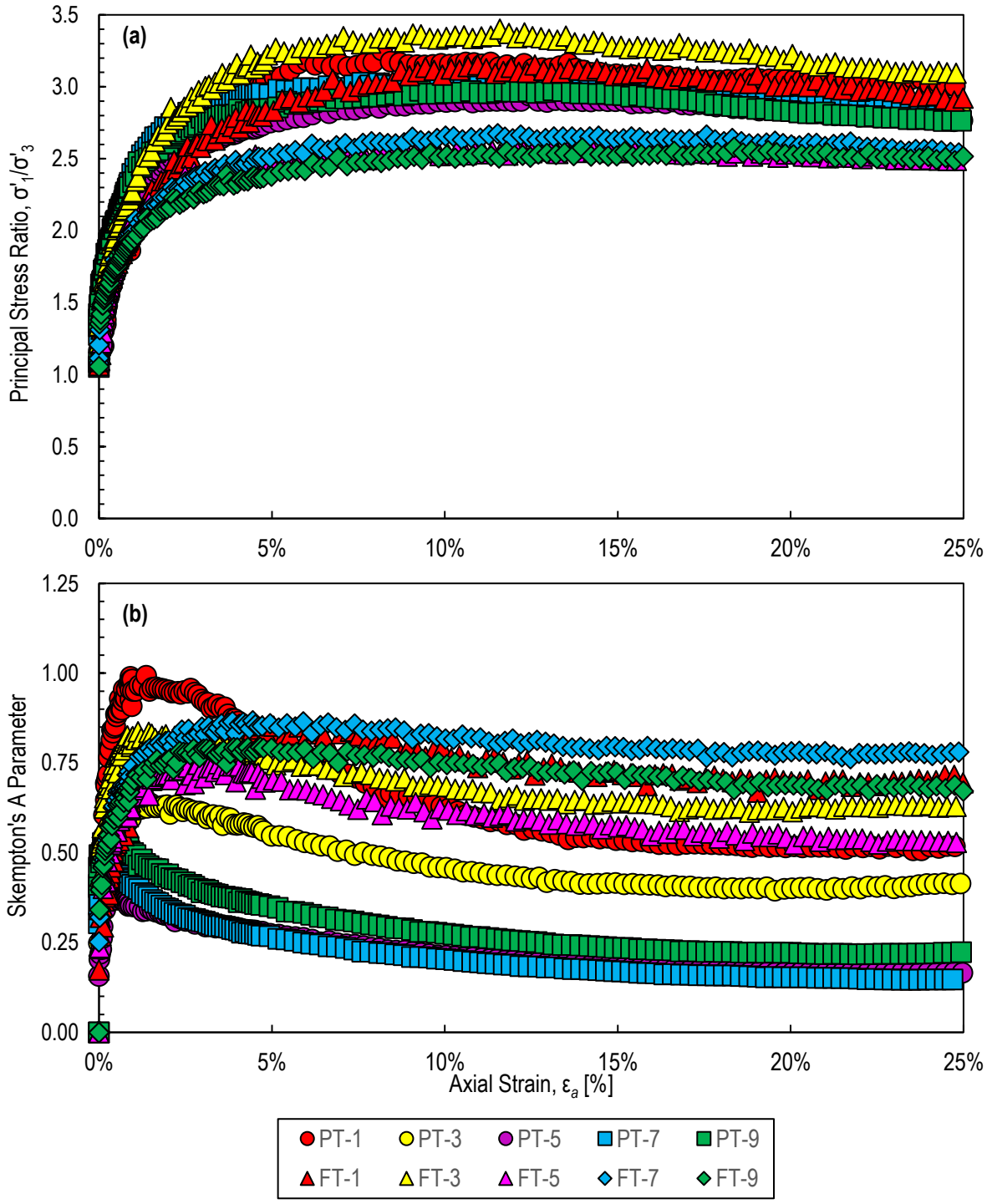

Fig. 4.4. Relationships of (a) principal stress ratio and (b) Skempton's A Parameter versus axial strain for consolidated undrained triaxial compression tests on filtered tailings and desiccated thickened tailings prepared to a target confining stress (σ'_c) of 100 kPa.

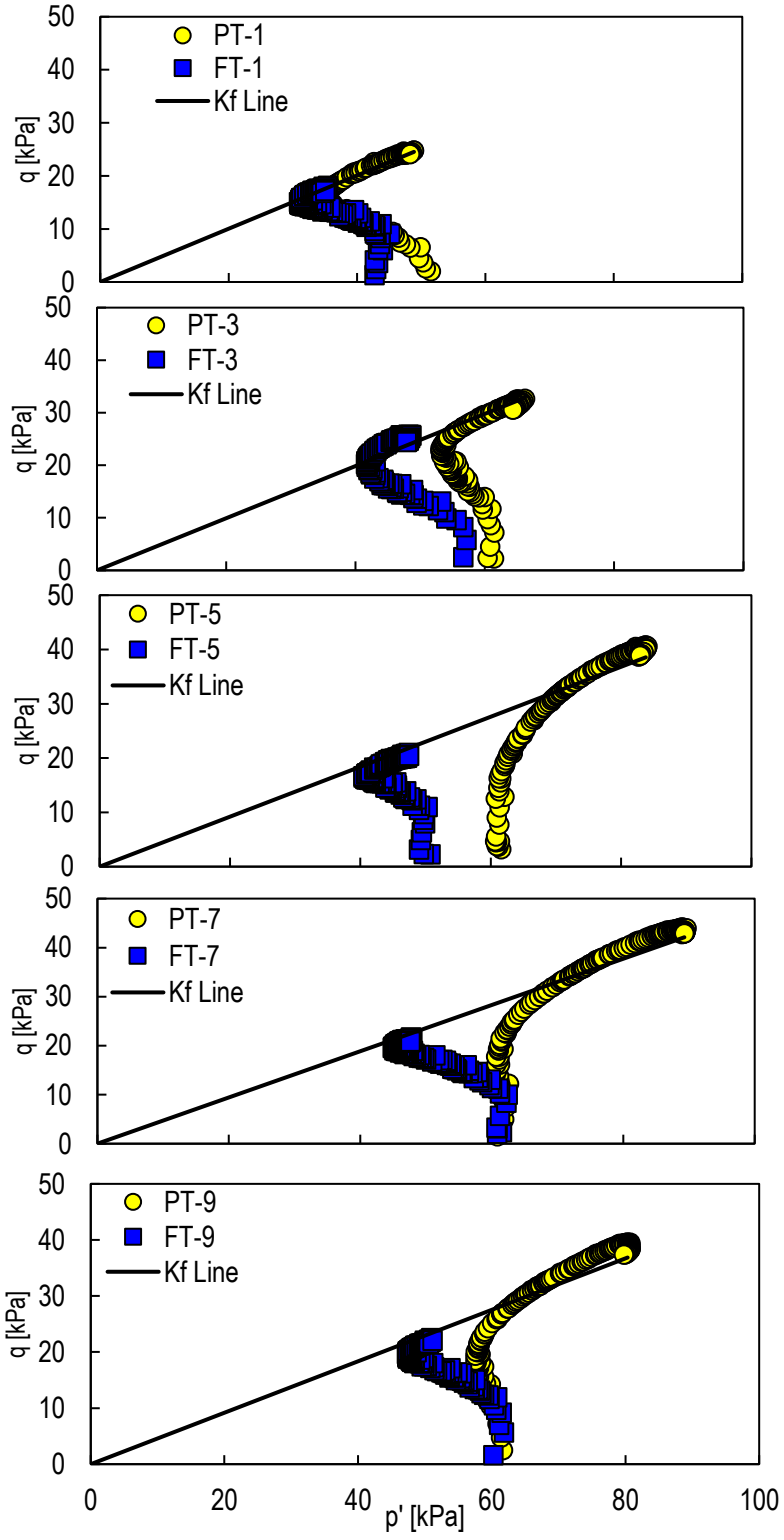

Fig. 4.5. Effective stress paths in q versus p' space for consolidated undrained triaxial compression tests on filtered tailings and desiccated tailings at target confining stress (σ'_c) of 50 kPa.

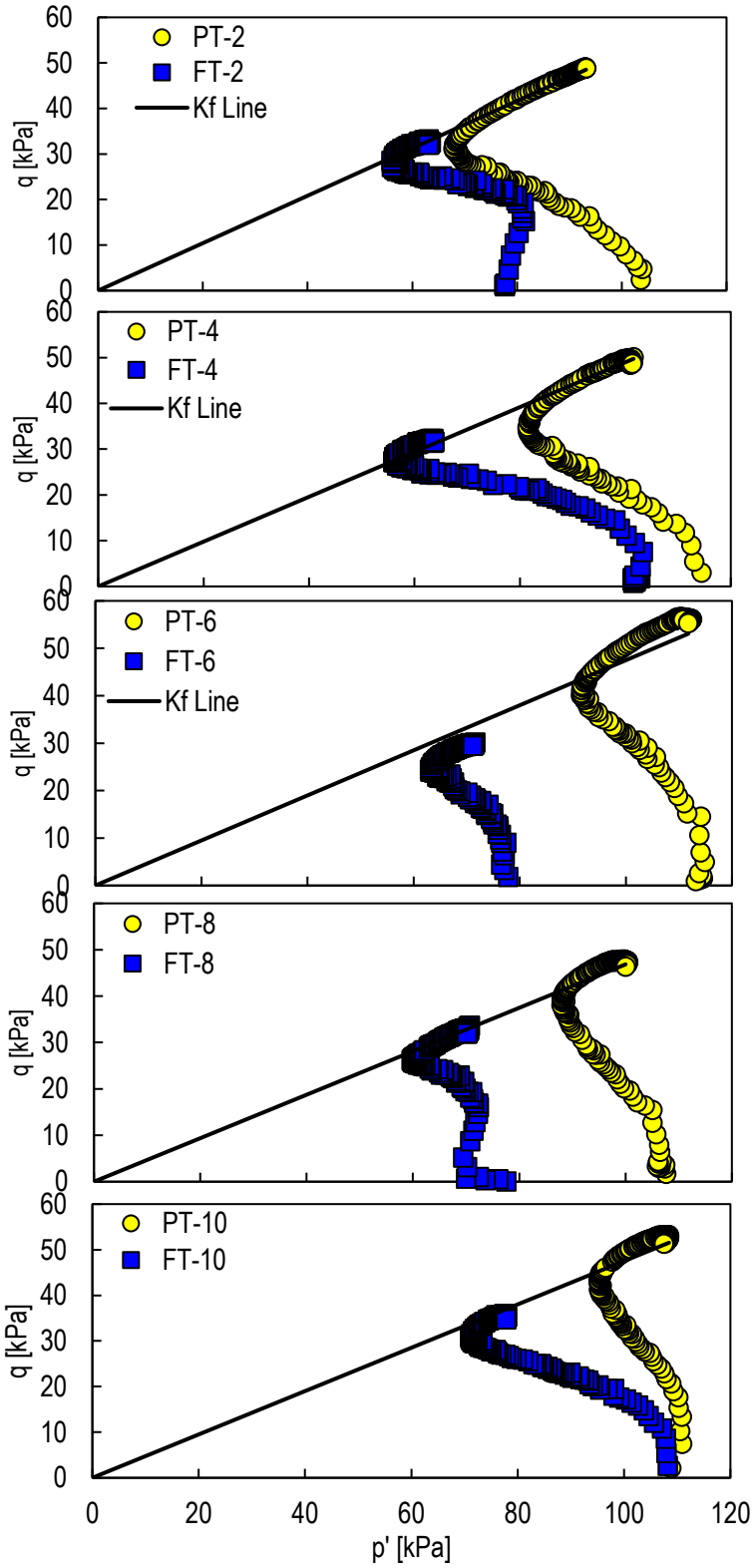

Fig. 4.6. Effective stress paths in q versus p' space for consolidated undrained triaxial compression tests on filtered tailings and desiccated tailings at target confining stress (σ'_c) of 100 kPa.

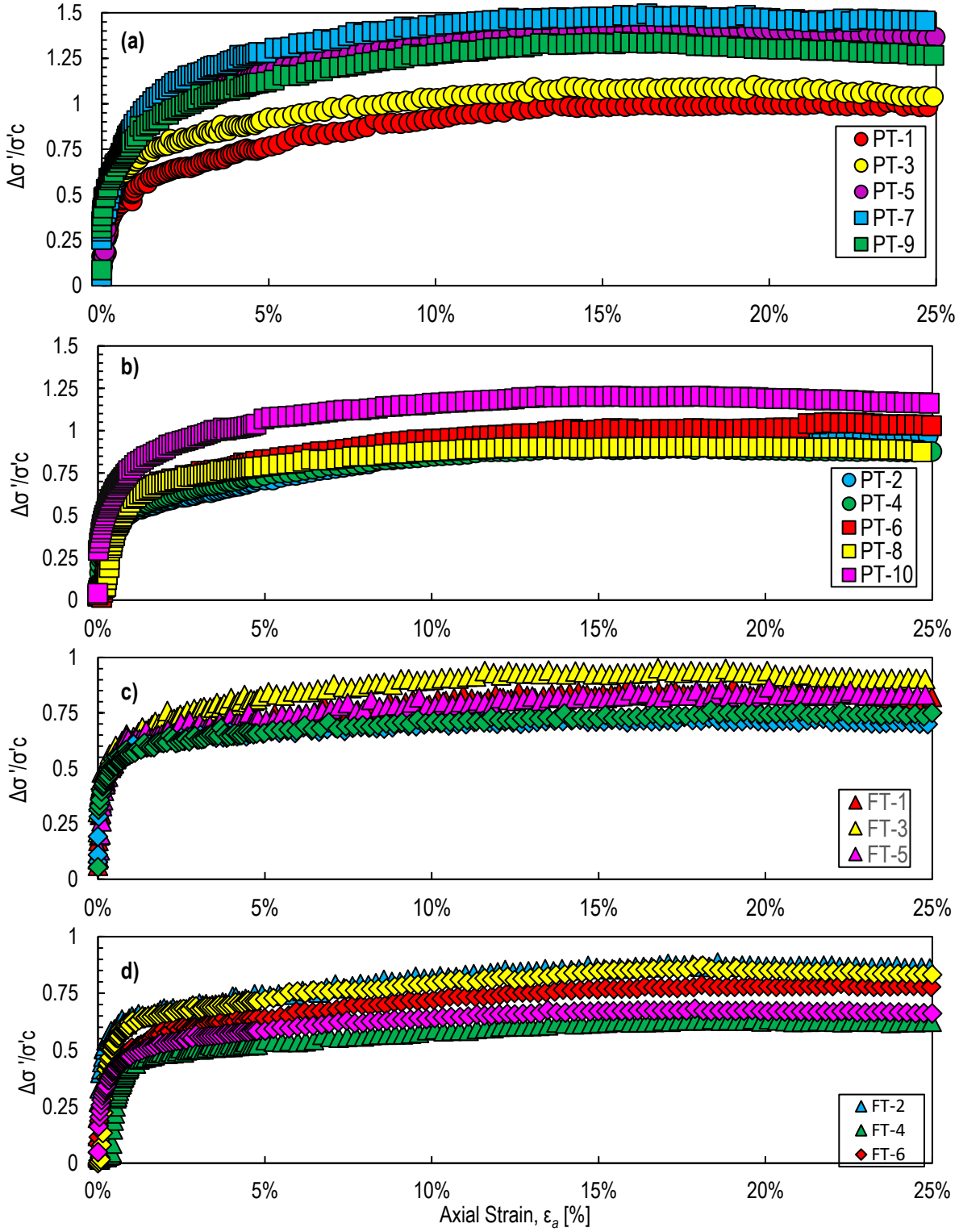

Fig. 4.7. Deviatoric stress normalized by the effective confining stress ($\Delta\sigma_d/\sigma'_c$) vs. axial strain for desiccated tailings at target stress (σ'_c) of (a) 50 kPa and (b) 100 kPa and compacted filtered tailings (c) 50 kPa and (d) 100 kPa tested in consolidated undrained triaxial compression tests.

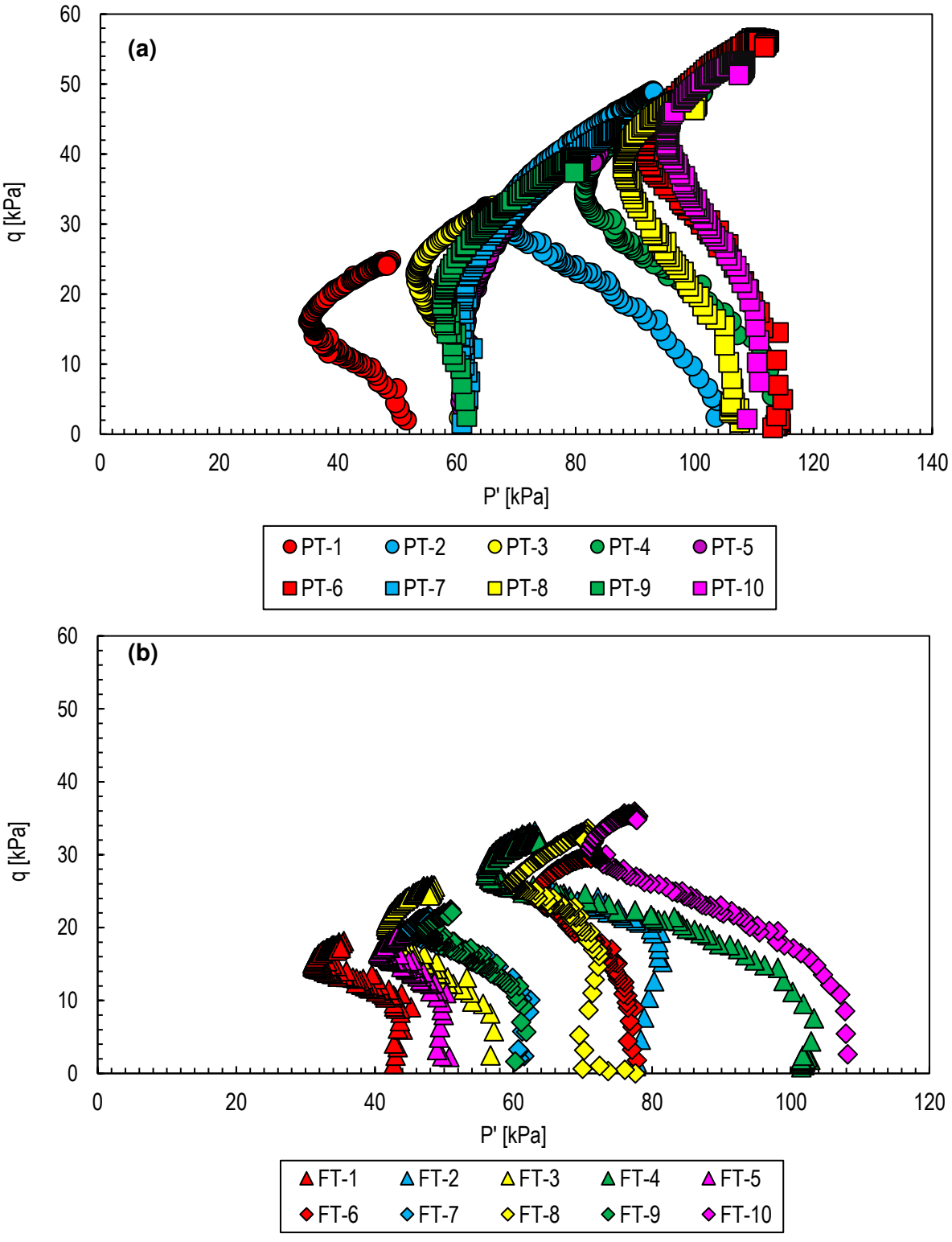

Fig. 4.8. Effective stress paths in q versus p' space for (a) desiccated tailings and (b) compacted filtered tailings prepared to a target confining stresses (σ'_c) of 50 kPa and 100 kPa tested in consolidated undrained triaxial compression tests.

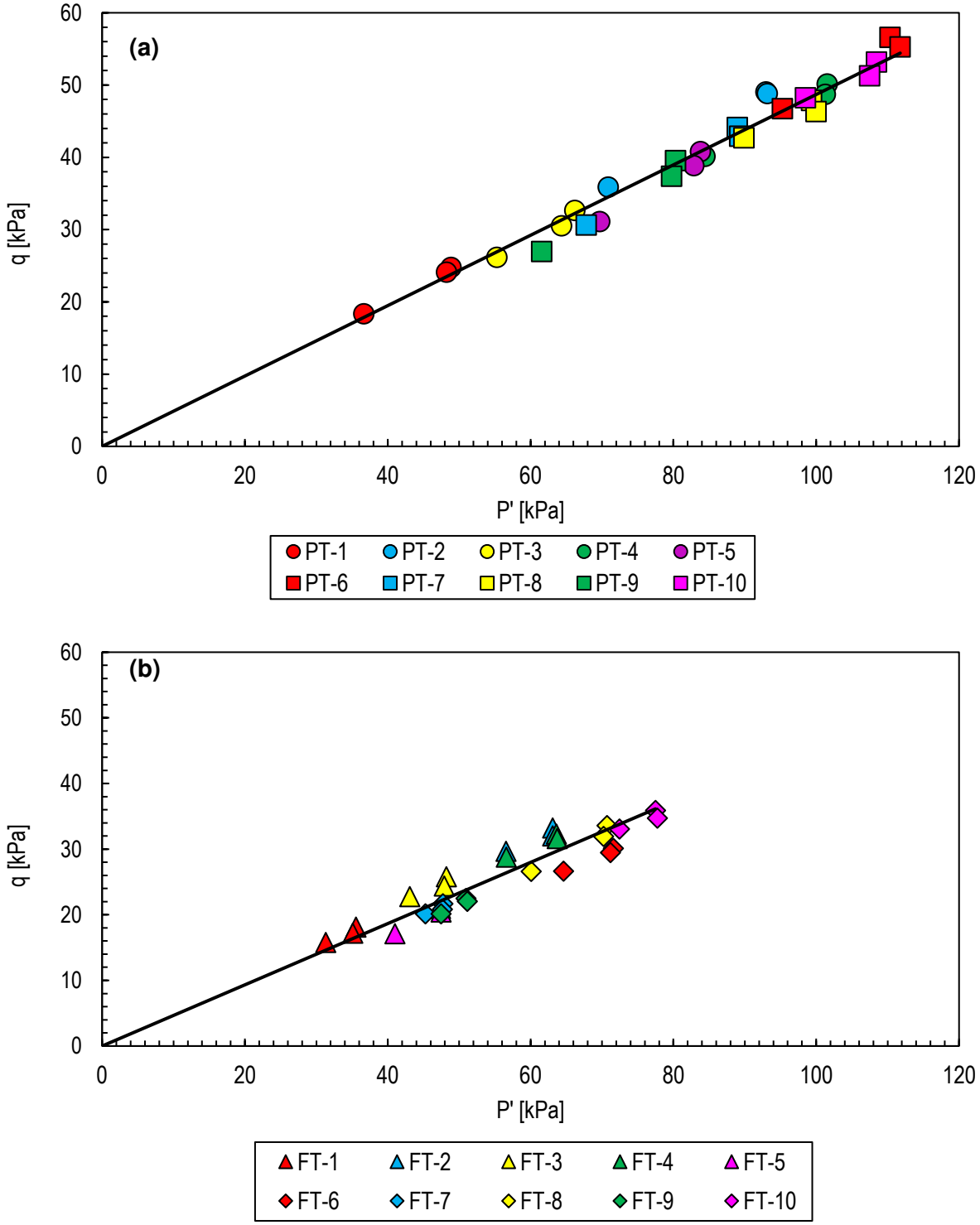

Fig. 4.9. Stress states at failure for (a) desiccated tailings and (b) compacted filtered tailings prepared to a target confining stresses (σ'_c) of 50 kPa and 100 kPa tested in consolidated undrained triaxial compression tests. The K_f Line was regressed through all failure points and the origin.

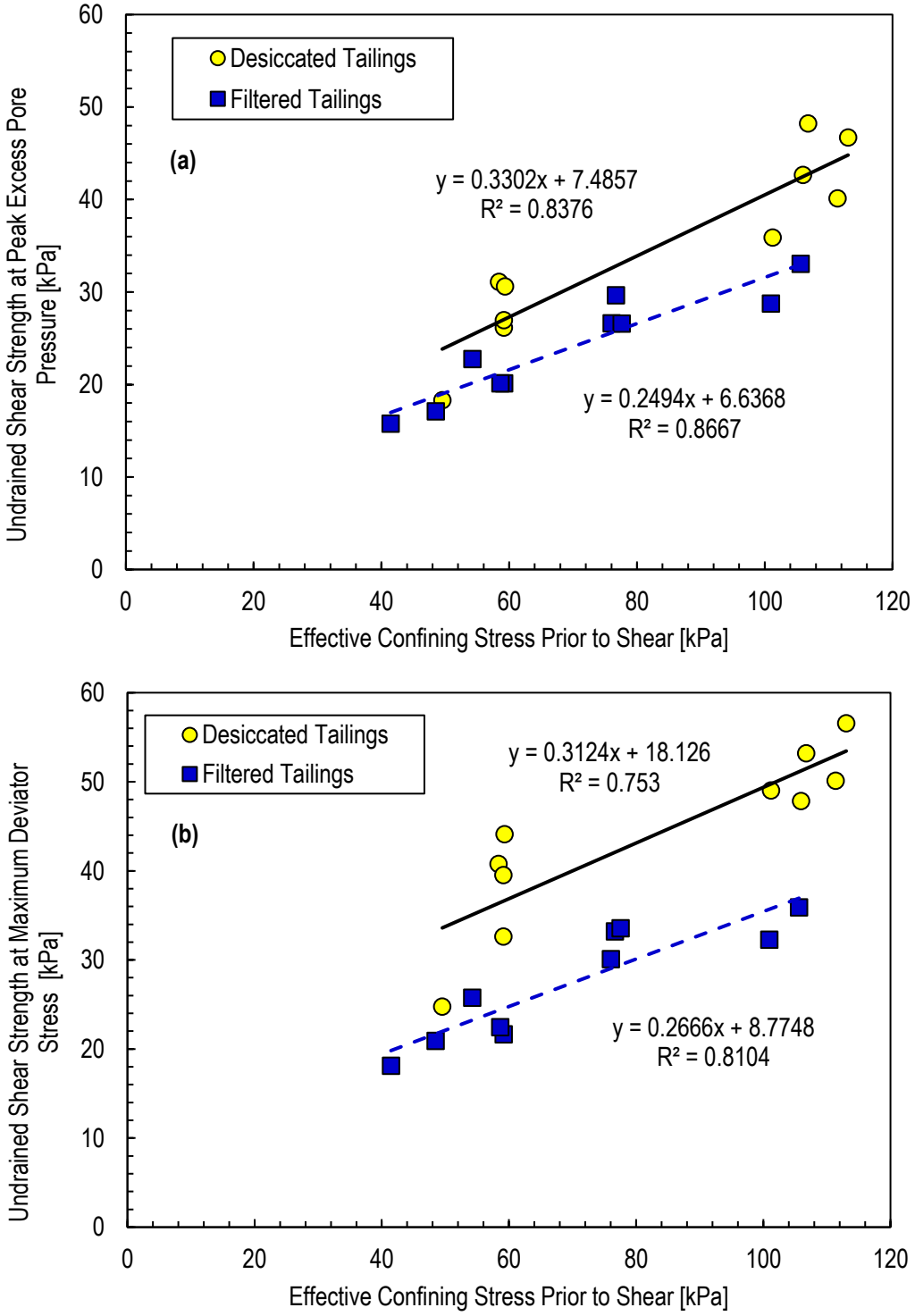

Fig. 4.10. Relationships of undrained shear strength (S_u) defined at (a) peak excess pore pressure and (b) maximum deviator stress versus effective confining stresses for filtered tailings and desiccated thickened tailings tested in consolidated undrained triaxial compression.

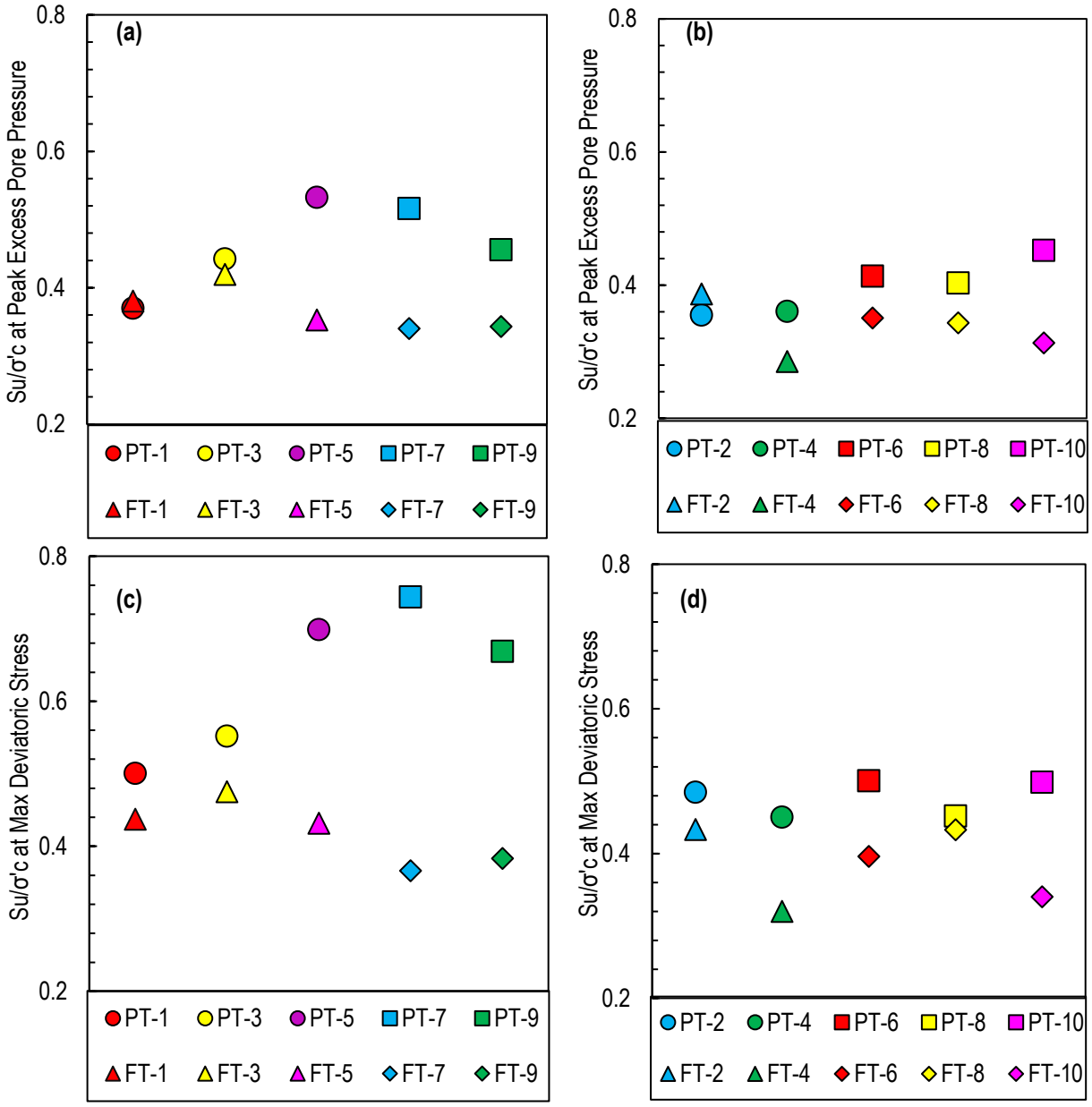

Fig. 4.11. Undrained shear strength ratio (S_u/σ'_c) with S_u defined at peak excess pore pressure for target confining stress (σ'_c) of (a) 50 kPa and (b) 100 kPa and maximum deviator stress for target confining stress (σ'_c) of (c) 50 kPa and (d) 100 kPa for all desiccated tailings and compacted filtered tailings. Note that the legend at the bottom of the figures aligns vertically with the data points plotted.

(a)

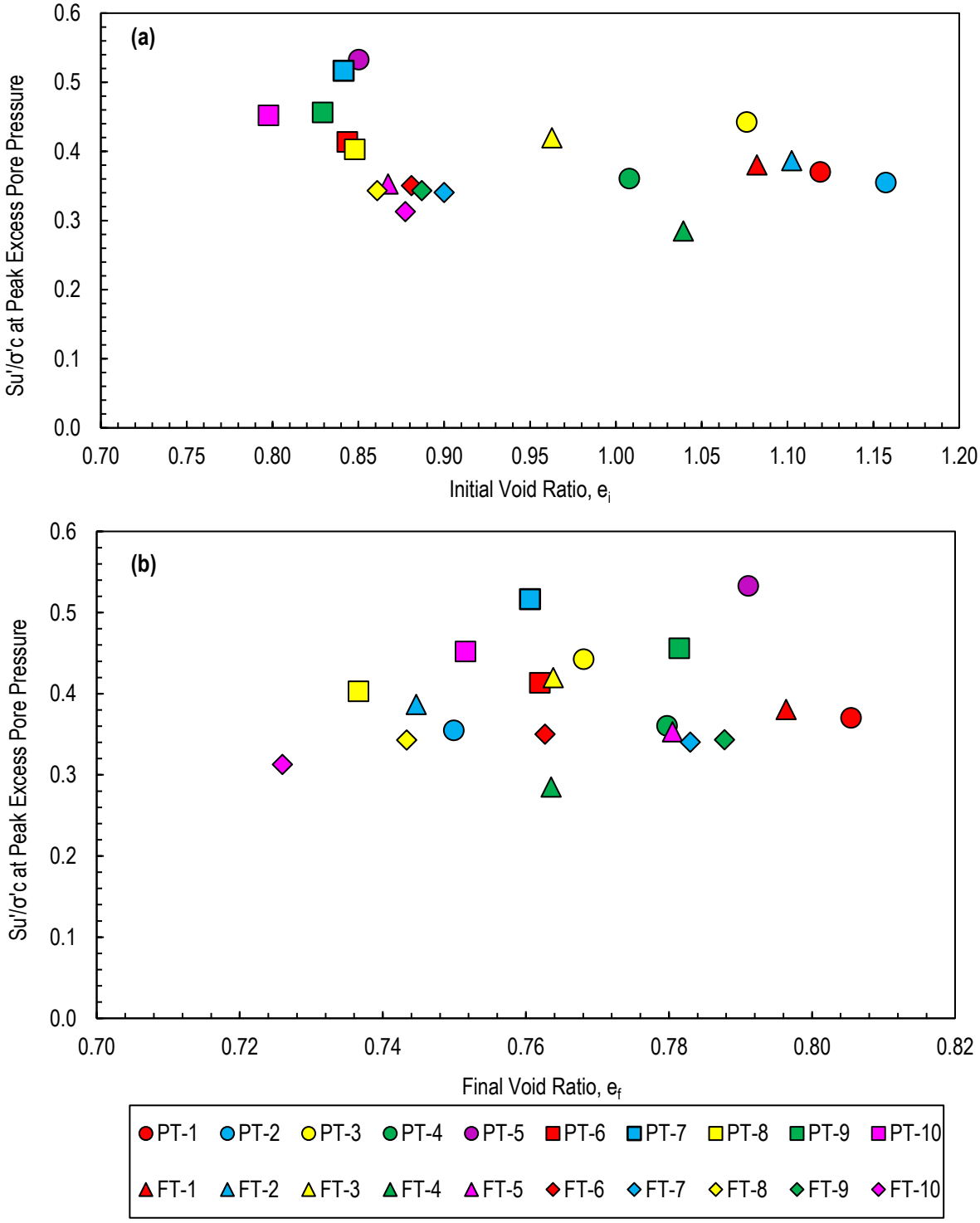

Fig. 4.12. Ratio of effective undrained shear strength over effective confining stresses versus the initial pre-consolidation void ratio (a) and final void ratio (a) at peak excess pore pressure conditions comparing compacted filtered tailings and desiccated thickened tailings prepared to similar initial void ratios and tested in consolidated undrained triaxial compression.

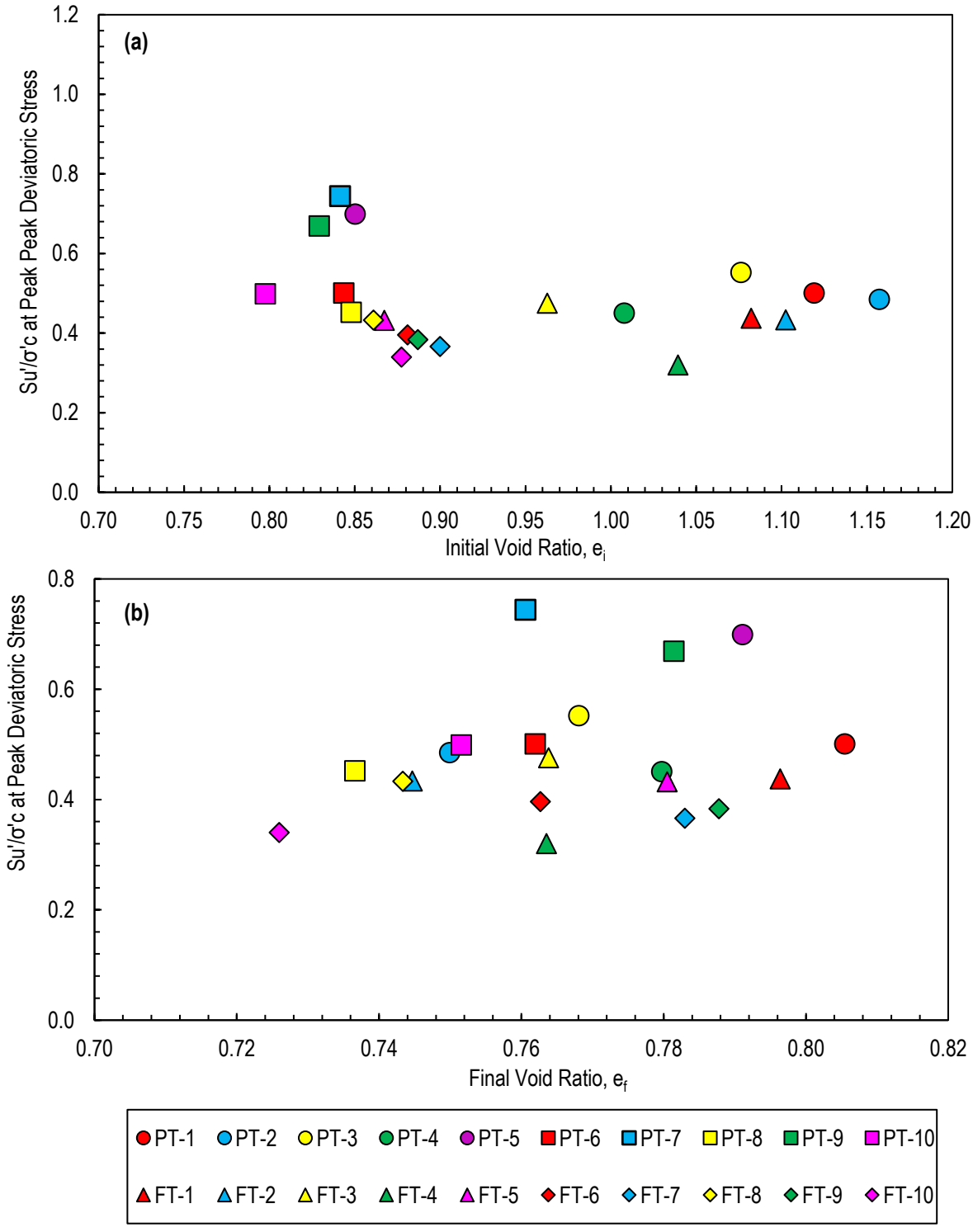

Fig. 4.13. Ratio of effective undrained shear strength over effective confining stresses versus the initial pre-consolidation void ratio (a) and final void ratio (a) at peak deviatoric stress conditions comparing compacted filtered tailings and desiccated thickened tailings prepared to similar initial void ratios and tested in consolidated undrained triaxial compression.

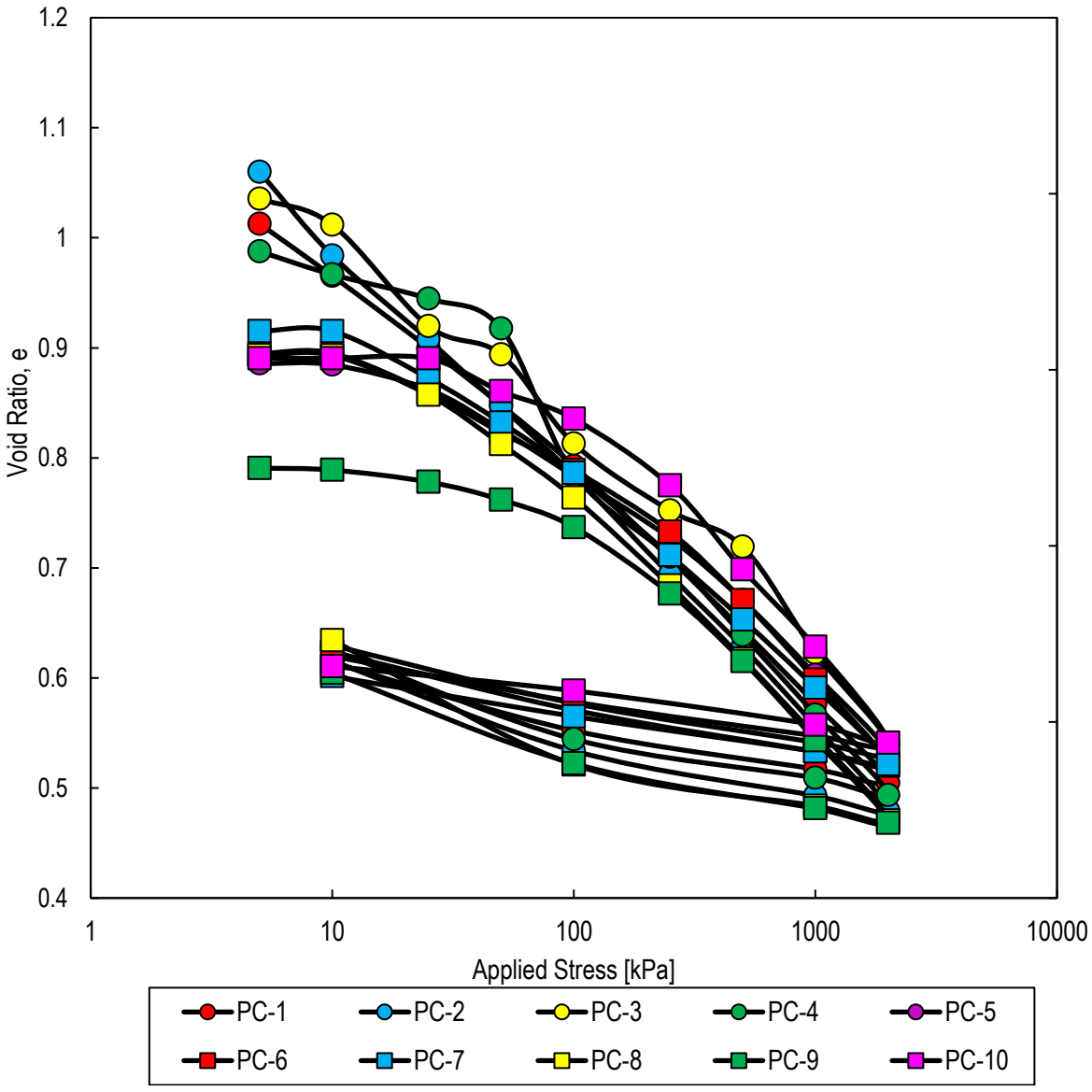

Fig. 4.14. Consolidation data for desiccated tailings tested in one-dimensional consolidation prepared at different initial void ratios and loading with the same loading schedule.

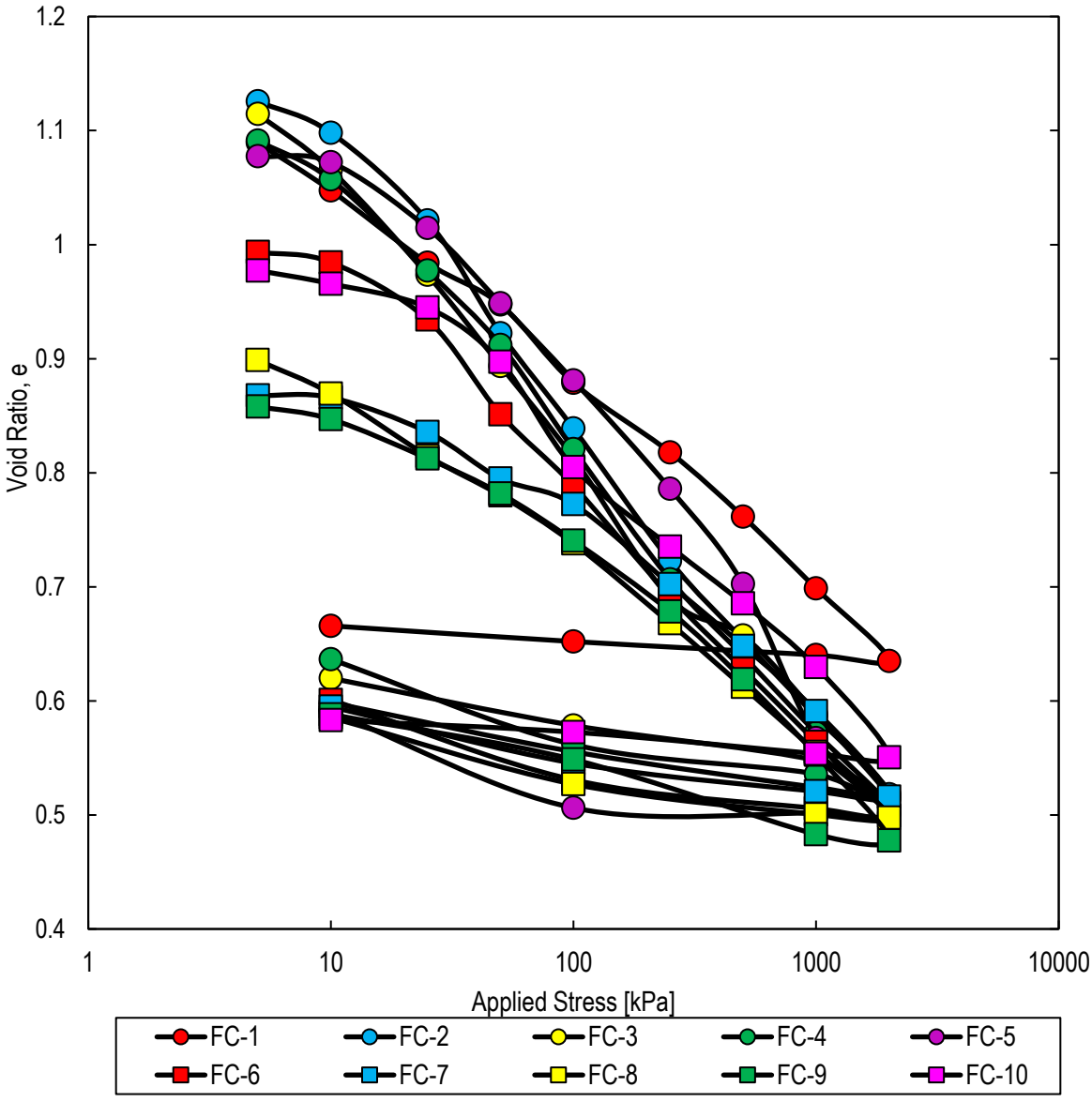

Fig. 4.15. Consolidation data for filtered tailings tested in one-dimensional consolidation prepared at different initial void ratios and loading with the same loading schedule.

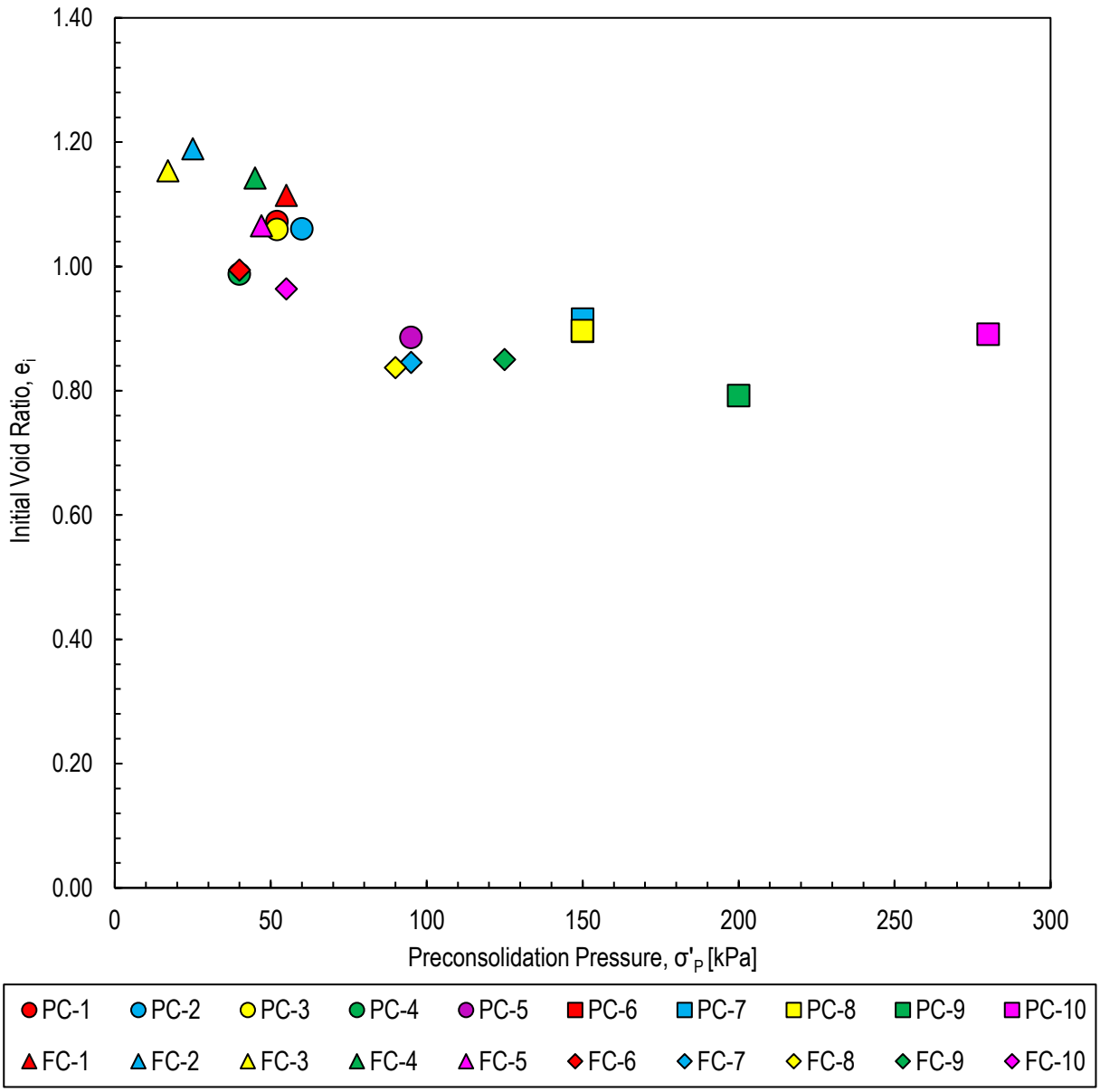

Fig. 4.16. Estimated preconsolidation pressure (σ'_P) [kPa] vs initial void ratio data for both desiccated and filtered tailings tested in one-dimensional consolidation prepared at different initial void ratios and loading with the same loading schedule. Preconsolidation pressure was estimated graphically using Casagrande procedures.

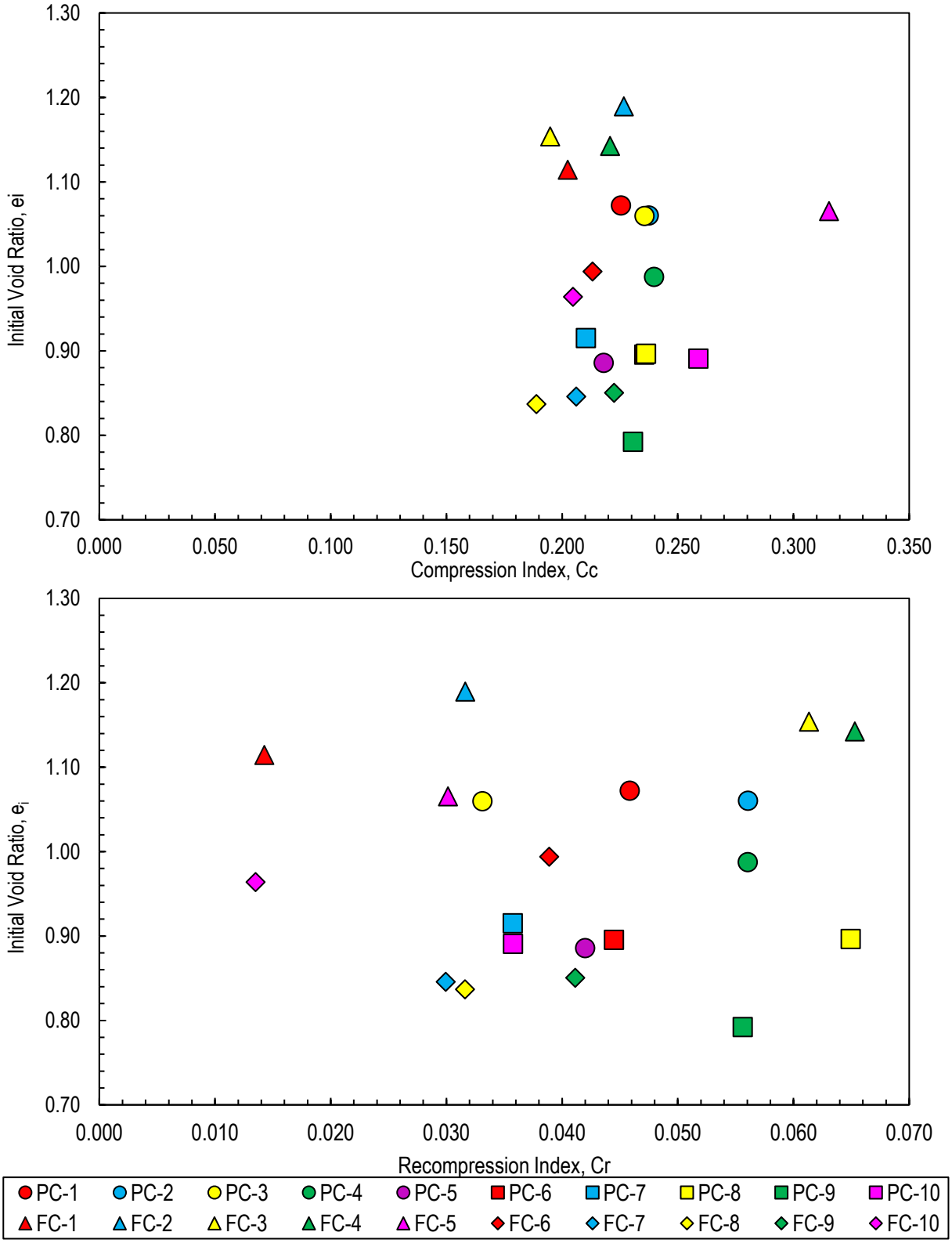

Fig. 4.17. Relationships of initial void ratio versus (a) compression Index (Cc) and (b) recompression Index (Cr) for both desiccated and filtered tailings tested in one-dimensional consolidation prepared at different initial void ratios.

CHAPTER 5: SUMMARY, CONCLUSIONS, AND FUTURE WORK

5.1 Summary and Conclusions

The effect desiccation in thickened tailing that undergo resaturation was evaluated to analyze the strength and consolidation behavior compared to filtered tailings. Consolidated undrained (CU) triaxial compression and one-dimensional consolidation tests were performed on thickened and filtered tailings prepared to represent field conditions. The undrained shear and consolidation behavior of each depositional method of tailings was evaluated to establish a baseline for comparison. The following conclusions were drawn from this study:

- The evaporative drying method in buckets yields a continuum of water contents and void ratios unless equilibrium is reached.
- There is an observable change in the shear behavior and shear strength of slurry deposited tailings with higher amounts of desiccation.
- The effective stress paths, coupled with the trends of Skempton's A parameter suggest the desiccated fabric is uniquely different from the fabric created via compacting filtered tailings. Desiccation creates a stiffer and more dilative fabric relative to compacting filtered tailings prepared at similar initial void ratios.
- Desiccation produces overconsolidated fabrics that exhibit smaller a more pronounced phase transition from contractive to dilative behavior than mechanically compacted, filtered prepared at similar initial void ratios.
- Desiccated tailings yielded an effective stress friction angle of 29.1°. Filtered tailings yielded an effective stress friction angle of 27.7°.
- There is observable increase in the effects of stress-history due to desiccation at lower stresses indicated by a higher $\Delta\sigma_d/\sigma'_c$ ratio for increased levels of desiccation.
- Desiccated tailings samples showed a stiffer initial peak $\Delta\sigma$ than filtered samples and continued to exhibit slower decreasing rate of change than the filtered tailings. The

desiccated fabric produced stiffer response compared to compacted, filtered tailings prepared at the similar initial void ratios.

- The effective stress paths in *q-p'* space for the filtered tailings all show similar nonlinear behavior that is representative of a soft, contractive material. The effective stress paths for *q-p'* space for the desiccated tailings show transitional behavior that is more prominent with increased desiccation.
- The undrained shear strength for a given effective confining stress is larger for desiccated tailings relative to filtered tailings.
- In general, the undrained strength ratios for the desiccated tailings (0.37 to 0.53 for peak excess pore pressure and 0.45 to 0.74 for maximum deviator stress) were consistently greater than the filtered tailings (0.29 to 0.39 for peak excess pore pressure and 0.32 to 0.48 maximum deviator stress).
- In general, there is an increase in Su/σ'_C for desiccated tailings that experience higher amounts of desiccation, and also that were tested at lower effective confining stress. These trends suggest that increasing desiccation led to higher undrained strength under a given level of effective stress. Increasing effective confining stress reduces the undrained strength ratio for a given level of desiccation, verifying desiccated fabrics exhibit stress-history imparted from desiccation-induced overconsolidation.
- The comparison of undrained shear behavior between the slight transitional behavior of desiccated tailings compared and overall contractive behavior of filtered tailings yields the conclusion that the increased shear resistance is attributed to the previously desiccated fabric and differences in soil structure.
- While shear resistance varied, there was not an indication of a significant difference in the effective principal stress ratio (σ'_1/σ'_3) between tailings preparation methods.

- Desiccated tailings samples showed a stiffer initial peak deviatoric stress and slower decreasing rate of change in stress relative to the filtered tailings.
- There was no indication of a difference in stiffness or brittleness between tailings preparation methods. The higher shear strength of the desiccated tailings was attributed to more pronounced inter-particle reinforcing effects and densification from stress-history of desiccation.
- Desiccated, resaturated tailings yield a higher peak undrained shear strength relative to compacted filtered tailings prepared to the same void ratio when consolidated under the same effective stress.
- Increased desiccation yielded more curvature in the consolidation curves at low stress as a result of desiccation-induced overconsolidation. The overconsolidation is more prominent in desiccated tailings than filtered tailing, which produced less prominent modest overconsolidation from mechanical compaction.
- Preconsolidation stress generally increased with decreasing initial void ratio for both the desiccated and filtered tailings. For both methods, a decrease in initial void ratio corresponded to an increase in preconsolidation stress. A higher preconsolidation stress was observed for the desiccated tailings relative to the filtered tailings at lower ranges of the initial void ratios, coinciding with the most desiccated tailings specimens.
- Although data provides scatter, there is a slight linear trend of increased compression indexes with higher initial void ratios. Desiccated tailings tend to exhibit a steeper response in compression indexes with each increase in initial void ratio than filtered tailings.
- The data for recompression index also exhibits a large amount of scatter; however, there is a slight increasing linear trend for the filtered tailings and decreasing linear trend for the

desiccated tailings. Overall, the compression and recompression indices found in the desiccated tailings were slightly higher, on average, relative to the filtered tailings.

5.2 Future Work

This study was conducted to evaluate the effects desiccation in thickened tailing to analyze the strength and consolidation behavior compared to filtered tailings. Additional data is necessary to study the effects of fabric in desiccated, resaturated thickened tailings when compared to filtered tailings at different void ratios. Further testing should be done to evaluate how different initial solids contents prior to desiccation can affect the undrained shear and consolidation behavior compared to filtered tailings. Additionally, an analysis of soil fabric using an electron scanning microscope to assess fabric conditions both prior to and after undrained shear would add to the understanding of the fabric conditions within the specimen. A larger range of target void ratios should be assessed for the effects desiccation, with a focus on thin-lift deposition and long-term evaporative drying. Lastly, a critical state assessment should be done at varying consolidation stresses to assess whether the critical state line of the material shifts due to the effects of desiccation and whether there is a diminishing value in the level of desiccation that is allowed to occur within a tailings facility.

REFERENCES

Al-Tarhouni, M., Simms, P., & Sivathayalan, S. (2011). Cyclic behaviour of reconstituted and

desiccated–rewet thickened gold tailings in simple shear. Canadian Geotechnical Journal, 48(7), 1044–1060. https://doi.org/10.1139/t11-022

Alarcon, A., Leonards, G., Chameau, J.L. (1988). Undrained monotonic and cyclic strength of sands. *Journal of Geotechnical Engineering*, 114(10), 1089–1109.

ASTM D422-63e2 (2007). *Standard Test Method for Particle-Size Analysis of Soils* (Withdrawn 2016), ASTM International, West Conshohocken, PA.

ASTM D854-14 (2014). *Standard Test Methods for Specific Gravity of Soil Solids by Water Pycnometer*, ASTM International, West Conshohocken, PA.

ASTM D2487-17 (2017). *Standard Practice for Classification of Soils for Engineering Purposes*, (Unified Soil Classification System), ASTM International, West Conshohocken, PA.

ASTM D4648-16 (2016). Standard Test Methods for Laboratory Miniature Vane Shear Test for

Saturated Fine-Grained Clayey Soil, ASTM International, West Conshohocken, PA.

ASTM D4767-11 (2011). *Standard Test Method for Consolidated Undrained Triaxial Compression Test for Cohesive Soils*, ASTM International, West Conshohocken, PA.

ASTM D4318-17e1 (2017). *Standard Test Methods for Liquid Limit, Plastic Limit, and Plasticity Index of Soils*, ASTM International, West Conshohocken, PA.

ASTM D7263-21 (2021). *Standard Test Methods for Laboratory Determination of Density and Unit Weight of Soil Specimen*, ASTM International, West Conshohocken, PA.

Barrios, G., Saez, E., & Ledezma, C. (2012). Influence of desiccation cracking on the liquefaction Potential of Thickened Tailing Deposits. *Proceeds 15 WCEE 2012*.

Bedin, J., Schnaid, F., Da Fonseca, A. V., &; Costa Filho, L. D. E. M. (2012). Gold tailings liquefaction under Critical State Soil Mechanics. Géotechnique, 62(3), 263–267. https://doi.org/10.1680/geot.10.p.037

Been, K., Jefferies, M.G. (1985). A state parameter for sands, *Géotechnique*, 35(2), 99-112.

Been, K., Jefferies, M.G., Hachey, J. (1991). The critical state of sands. *Geotechnique* 41(3), 365-381.

Been, K., & Li, A. (2009). Soil liquefaction and paste tailings. *Proceedings of the Twelfth International Seminar on Paste and Thickened Tailings*. https://doi.org/10.36487/acg_repo/963_32

Belem, T., & Benzaazoua, M. (2008). Design and application of underground mine paste backfill technology. *Geotechnical and Geological Engineering*, *26*, 147-174.

Blight, G. (2010). *Geotechnical Engineering for Mine Waste Storage Facilities*, CRC Press, Taylor & Francis Group, London, UK.

Bligth G.E. & Fourie A.B. (2005) Catastrophe revisited – disastrous flow failures of mine and municipal solid waste. *Geotechnical and Geological Engineering* 23(3): 219-248.

Bowker L.N. & Chambers D.M. (2015). The risk, public liability, and economics of tailing storage facility failures. *Earthwork Act* 1-56.

Bobei, D.C., Lo, S.R., Wanatowski, D., Gnanendran, C.T., Rahman, M.M. (2009). Modified state parameter for characterizing static liquefaction of sand with fines. *Canadian Geotechnical Journal*, 46(3), 281-295.

Boger, D.V. (2009), Rheology and the resource industries. *Chemical Engineering Science*, 64 (09) 4525-4536.

Borja, R.N., Bareither, C.A. (2020). Shear Behavior of Waste Rock and Filtered Tailings. Geo-Congress, GSP, 1339-1354.

Boulanger, R.W. (2003). Relating Ka to Relative State parameter index. *Journal of Geotechnical and Geoenvironmental Engineering,* 129(8): 770-773.

Brandon, T.L., Rose, A.T., Duncan, J.M. (2006). Drained and undrained strength interpretation for low-plasticity silts. *Journal of Geotechnical and Geoenvironmental Engineering*, 132(2), 250-257.

Bray, J.D., Sancio, R.B. (2006). Assessment of the liquefaction susceptibility of fine-grained soils. *Journal of Geotechnical and Geoenvironmental Engineering*, 132 (9): 1165-1177.

Bray J.D. & Frost J.D. (2010). *Geo-Engineering Reconnaissance of the 2010 Maule, Chile Earthquake, A Report of the SNF-Sponsored GEER Association Team.*

Bishop, A.W. (1967). Progressive failure – with special reference to the mechanism causing it., Proc. Geotech. Conf., Oslo, 2:142-150.

Bishop, A.W. (1973). The stability of tips and soil heaps. Quart. J. Eng. Geol., 6:335-376.

Bussière, B. (2007). Colloquium 2004: Hydrogeotechnical properties of hard rock tailings from metal mines and emerging geoenvironmental disposal approaches. *Canadian Geotechnical* Journal, 44(9), 1019-1052.

Casagrande, A. (1936). Characteristics of cohesionless soils affecting the stability or earth fills. *Journal of Boston Society of Civil Engineers*, 23, 257-276.

Casagrande, A. (1975) Liquefaction and Cyclic Deformation of Sands, a Critical Review.

Proceedings of 5th Pan American Conference Soil Mechanic, Foundation Engineering, Buenos Aires, 80-133.

Chang, N., Heymann, G., & Clayton, C. (2011). The effect of fabric on the behaviour of gold tailings. *Géotechnique*, *61*(3), 187–197. https://doi.org/10.1680/geot.9.p.066

Davies, M.P. (2002). Tailings impoundment failures: are geotechnical engineers listening? *Geotechnical News* 20(3): 31-36.he

Daliri, F. (2013). *The influence of desiccation and stress history on monotonic and cyclic shear response of thickened gold tailings* (dissertation). Carleton University, Ottawa.

Daliri, F., Kim, H., Simms, P., & Sivathayalan, S. (2012). Contribution of desiccation to monotonic and cyclic strength of thickened gold tailings – not the same as over-consolidation. *Proceedings of the 15th International Seminar on Paste and Thickened Tailings*. https://doi.org/10.36487/acg_rep/1263_07_daliri

Daliri, F., Kim, H., Simms, P., Sivathayalan, S. (2014). Impact of desiccation on monotonic and cyclic shear strength of thickened gold tailings. *Journal of Geotechnical and Geoenvironmental Engineering*, 140(9), 1-13.

Damian, D., Jorge Cardenas, Soto, C., & Rivas, L. (2022). Tailings critical state curve estimation using standard instrumented triaxial equipment. *Proceedings Tailings and Mine Waste 2022*.

Fall, M., Benzaazoua, M., & Ouellet, S. (2005). Experimental characterization of the influence of tailings fineness and density on the quality of cemented paste backfill. *Minerals engineering*, *18*(1), 41-44.

Fisseha, B., Bryan, R., & Simms, P. (2010). Evaporation, unsaturated flow, and salt accumulation in multilayer deposition of paste gold tailings. *Journal of Geotechnical and Geoenvironmental Engineering.* 136(12): 1703-1712.

Fitton, TG & Roshdieh, A 2013, 'Filtered tailings versus thickened slurry: four case studies', in R

Jewell, AB Fourie, J Caldwell & J Pimenta (eds), Paste 2013: Proceedings of the 16th International Seminar on Paste and Thickened Tailings, Australian Centre for Geomechanics, Perth, pp. 275-288, https://doi.org/10.36487/ACG_rep/1363_21_Fitton

Garino Libardi L.M., Oldecop L.A., Romero Morales E.E., Rodriguez Pacheco R.L. (2022).

Tailings desiccation process studied in environmental chamber experiment. *Proceedings of the Institution of Civil Engineers – Geotechnical Engineering* 172(2): 261-271, https://doi.org/10.1680/jgeen.21.00109

Global Industry Standard on Tailings Management – Global Tailings Review. (2020). . International Council on Mining and Metals, United Nations Environment Programme and the Principles for Responsible Investment.

Hale C.R. (2022). Critical state analysis of gold mine tailings via isotropically consolidated undrained compression. Colorado State University.

Høeg, K., Dyvik, R., & Sandbækken, G. (2000). Strength of undisturbed versus reconstituted silt and silty sand specimens. Journal of geotechnical and geoenvironmental engineering, 126(7), 606-617.

ICOLD (International Commission on Large Dams) (2001). *Tailing Dams Risk of Dangerous*

Occurrences, Lessons Learnt from Practical Experiences, Bulletin 121. United Nations Environmental Programme (UNEP) Division of Technology, Industry and Economics (DTIE) and International Commission on Large Dams (ICOLD), Paris, France.

Jefferies, M. Been, K. (2006). *Soil Liquefaction, A Critical State Approach*. Taylor and Francis.

Jefferies, M., & Been, K. (2019). *Soil liquefaction: A critical state approach*. CRC Press.

Jehring, M.M., Bareither, C.A. (2016). Tailings composition effects on shear strength behavior of co-mixed mine waste rock and tailings. *Acta Geotechnica*, 1-20.

Khalili, A., Wijewickreme, D., Wilson, G.W. (2005). Some observations on the mechanical response of mixtures of mine waste and tailings. Proc. 58th Canadian Geotechnical Conference.

Konrad, J.-M., & Ayad, R. (1997). A idealized framework for the analysis of cohesive soils undergoing desiccation. *Canadian Geotechnical Journal*, *34*(4), 477–488. https://doi.org/10.1139/t97-015

Ladd, R.S. (1993). Area Correction in Triaxial Testing. Geotechnical Testing Journal, GTODJ, Vol. 1, No. 1, March 1978, 16-23.

Lambe, T.W. and Whitman, R.V. (1969). Soil Mechanics. John Wiley & Sons, Inc. New York.

Macedo, J., & Vergaray, L. (2022). Properties of mine tailings for static liquefaction assessment. Canadian Geotechnical Journal, 59(5), 667–687. https://doi.org/10.1139/cgj-2020-0600

Morgenstern, N.R., Vick, S.G., Viotti, C.B., Watts, B.D. (2016). Fundão Tailings Dam Review Panel – Report on the Immediate Causes of the Failure of the Fundão Dam, Copyright – *Cleary Gottlieb Steen & Hamilton LLP, Vale S.A., BHP Billiton Brasil Ltda. and Samarco Mineração S.A*,

Morrison, K. F. (2022). Tailings management handbook: A life-cycle approach. Society for Mining, Metallurgy & Exploration.

Plewes, H.D., Davies, M.P., Jefferies, M.G. (1992). CPT based screening procedure for evaluating liquefaction susceptibility. 45th Canadian Geotechnical Conference, Proc., Toronto, Ont. 26-28.

Poulos, J. (1981). The steady state of deformation. Journal of Geotechnical Engineering Division, ASCE, 107(GT5), 553- 562.

Qiu, Y., Sego, D.C. (2001). Lab properties of mine tailings, *Canadian Geotechnical Journal*, 38(1), 183-190.

Rassam, D. W., & Williams, D. J. (1999). Bearing capacity of desiccated tailings. *Journal of Geotechnical and Geoenvironmental Engineering*, *125*(7), 600–609. https://doi.org/10.1061/(asce)1090-0241(1999)125:7(600)

Reid, D., Fanni, R., & Fourie, A. (2022a). Effect of tamping conditions on the shear strength of tailings. *International Journal of Geomechanics*, *22*(3). https://doi.org/10.1061/(asce)gm.1943-5622.0002247

Reid, D., Fanni, R., & Fourie, A. (2022b). Slurry deposition preparation method for tailings characterisation – history, debates, techniques and benefits. *Proceeds Tailings 2022 - Online Conference*.

Reid, D., Fanni, R., & Fourie, A. B. (2021a). Some considerations when preparing thickened tailings for shear strength testing in the laboratory from a slurry. In *Paste 2021: 24th International Conference on Paste, Thickened and Filtered Tailings* (pp. 203-216). Australian Centre for Geomechanics.

Reid, D., Fourie, A., Castro, J., & Lupo, J. (2018). Undrained shear strength evolution with loading on an undisturbed block sample of desiccated gold tailings. *Proceedings Tailings and Mine Waste 2018*.

Reid, D., Fourie, A., Ayala, J.L., Dickinson, S., Ochoa-Cornejo, F., Fanni, R., Garfias, J., Viana Da Fonseca, A., Ghafghazi, M., Ovalle, C., Reimer, M., Rismanchian, A., Olivera, R., Suazo, G. (2020). Results of a Critical State Line Testing Round Robin Programme. Geotechnique, July 2020 , 1-15.

Reid, D., Fourie, A., & Russell, A. (2022c). Effects of desiccation on shear strength of tailings - comparison clayey and sandy tailings. *Proceedings Tailings and Mine Waste 2022*.

Reid, D., Simms, P., Sivathayalan, S., Fanni, R., & Fourie, A. (2022d). The "air dried" specimen reconstitution technique - review, refinements, and applications. *Proceedings Tailings and Mine Waste 2022*.

Rico M., Benito G., Salgueiro A.R., Diez-Herrero A., & Pereira H.G. (2008). Reported tailings dam failures – a review of the European incidents in the worldwide context. *Joural of Hazardous Materials* 152(2): 846-852.

Robertson P.K., de Melo L., Williams D.J., and Ward Wilson G. (2019). *Report on the Expert Panel on the Technical Causes of Failure of Feijao Dam I,* 12 December, 2019.

Robertson, P. K. (2017). Evaluation of flow liquefaction: influence of high stresses. In *Proceedings of the 3rd international conference on performance based design (PBD-III)*.

Roche C., Thygesen K., & Baker E. (2017). *Mine Tailings Storage: Safety Is No Accident. A UNEP Rapid Response Assessment.* United Nations Environmental Programme and GRID-Arendal, Nairobi, Kenya and Arendal, Norway.

Roscoe, K. Shofield, A.S., Wroth, C.P. (1958). On the yielding of soils. Geotechnique, 8(1), 22-53.

Saleh-Mbemba, F., Aubertin, M., & Mbonimpa, M. (2010a). Desiccation and shrinkage of low plasticity tailings: testing and preliminary modeling. In *Proceedings of the 63rd Canadian*

Geotechnical Conference and 6th Canadian Permafrost Conference Geo2010, Calgary, Alta.

Saleh-Mbemba, F., Aubertin, M., Mbonimpa, M., & Li, L. (2010b). A new testing procedure to assess shrinkage of paste tailings. In *Proc. of the 13th International Seminar on Paste and Thickened Tailings* (pp. 495-504).

Schofield, A., Wroth, C.P (1968). *Critical State Soil Mechanics*. London, McGrawHill.

Sheshpari, M. (2015). A review of underground mine backfilling methods with emphasis on cemented paste backfill. *Electronic Journal of Geotechnical Engineering*, *20*(13), 5183-5208.

Simms, P. (2021). The role of unsaturated soil mechanics in unconventional tailings deposition. *Soils and Rocks*: *An International Journal of Geotechnical and Geoenvironmental Engineering.* 44(3).

Simms, P., Grabinsky, M., & Zhan, G. (2006). Evaporation from Surface Deposited Thickened Gold Tailings. In *Paste 2006: Proceedings of the Ninth International Seminar on Paste and Thickened Tailings* (pp. 267-274). Australian Centre for Geomechanics.

Simms, P., Sivathayalan, S., & Daliri, F. (2013). Desiccation in dewatering and strength development of high-density hard rock tailings. *Proceedings of the 16th International Seminar on Paste and Thickened Tailings*. https://doi.org/10.36487/acg_rep/1363_06_simms

Simms, P., Soleimani, S., Mizani, S., Daliri, F., Dunmola, A., Rozina, E., & Innocent-Bernard, T. (2017). Cracking, salinity and evaporation in mesoscale experiments on three types of tailings. *Environmental Geotechnics*, *6*(1), 3-17.

Skempton, A. W. (1952). The pore-pressure coefficients A and B. *Geotechnique, 4*(4), 143-147.

Sonntag, C., Freistadt, K., & Haug, M. (2022). Impact of solids content on sub-aerially deposited potash fine tailings. *Proceedings Tailings and Mine Waste 2022*.

Tian, Z., Bareither, C.A., and Scalia, J. (2020). Development and assessment of a seepage-induced consolidation test apparatus, Geotechnical Testing Journal, 43(4), 894-917. DOI: 10.1520/GTJ20180375.

Verdugo R., Sitar N., Frost J.D. (2012) Seismic performance of earth structures during the

February 2010 Maule, Chile, earthquake: dams, levees, tailings dams, and retaining walls.

Earthquake Spectra 28(1): 75-96.

Vick, S. G. (1990). Nature and Production of Tailings. In *Planning, design, and analysis of tailings dams* (pp. 1–40). essay, BiTech.

Wang, S., Luna, R. (2012). Monotonic behavior of Mississippi River Valley silt in triaxial compression. *Journal of Geotechnical and Geoenvironmental Engineering*, 138(4), 516-525.

Williams, D. J., Paterson, S., Yau, R., & Goddard, D. (2015). Selection of shear strength profile for desiccated tailings to support an upstream raise. *Proceedings Tailings and Mine Waste 2015*.

APPENDIX A: Results from Consolidated Undrained Triaxial Compression Tests

Tests PT-1 and FT-1 Comparison

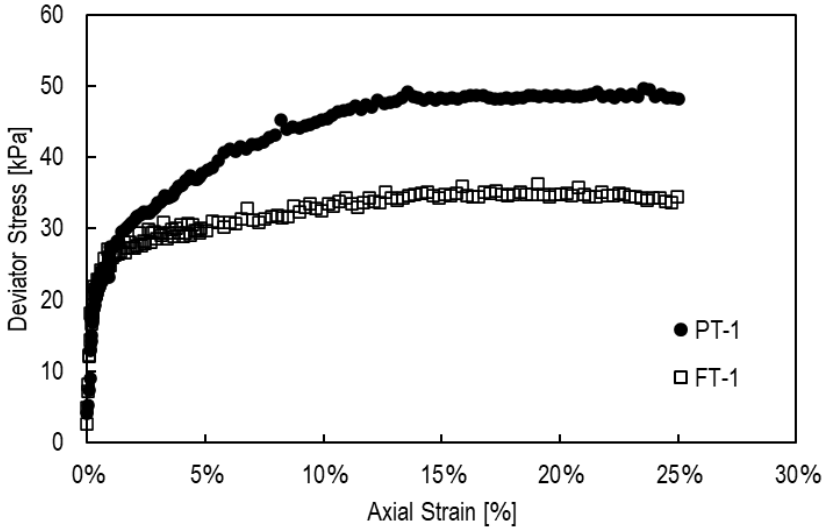

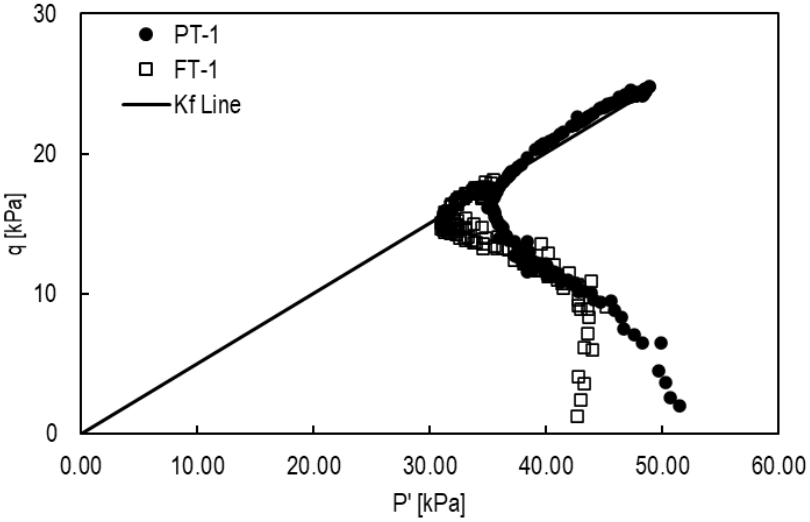

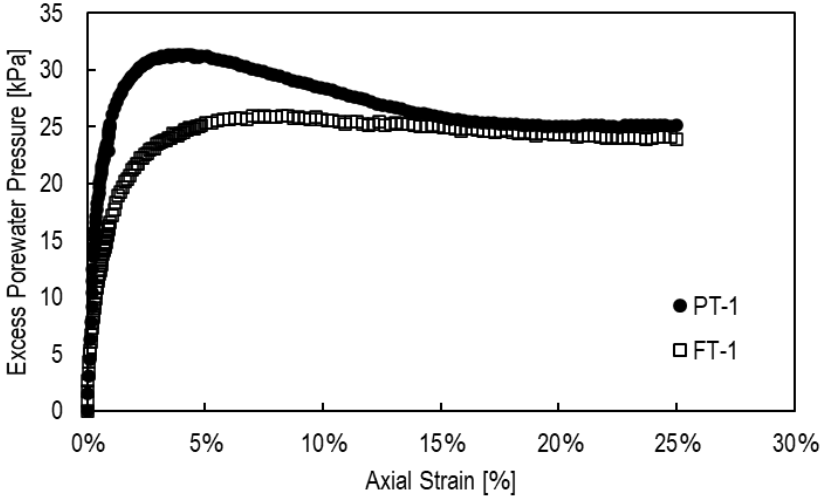

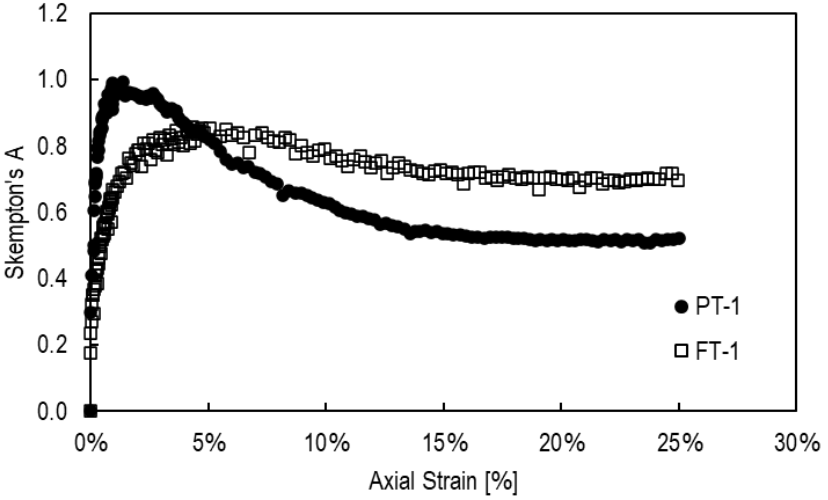

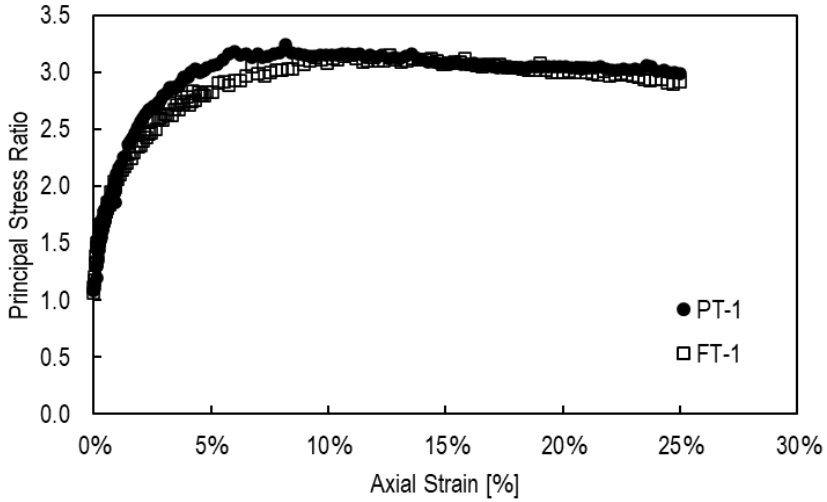

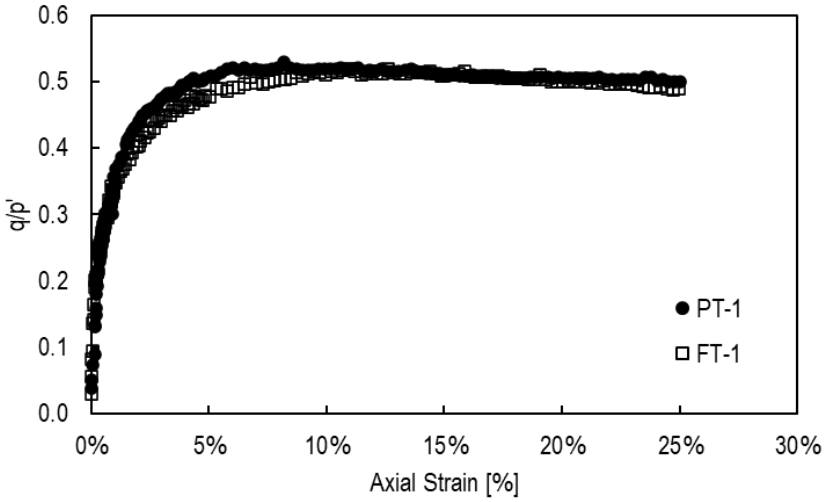

Test	Target σ'_c [kPa]	Actual σ'_c [kPa]	Failure Criteria	$\varepsilon_{a,f}$	$\Delta\sigma_d$ [kPa]	σ'_{3f} [kPa]	σ'_{1f} [kPa]	$u_{e,f}$ [kPa]	p'_f [kpa]	q_f [kPa]	q/P'	Initial Void Ratio, e_i	Consolidated Void Ratio, e_C	Final Void Ratio, e_f	φ'_s (°)	φ'_f (°)	S_u' [kPa]
PT-1	50	50	Peak $U_{e,f}$	4%	36.7	18.3	55.0	31.4	36.7	18.3	0.50	1.12	0.81	0.81	30.0	30.5	15.9
			Peak $\Delta\sigma f$	24%	49.6	24.1	73.6	25.1	48.9	24.8	0.51				30.5		21.4
			ε_a=25%	25%	48.2	24.2	72.4	25.1	48.3	24.1	0.50				30.0		20.9
FT-1	50	41	Peak $U_{e,f}$	8%	31.5	15.6	47.1	26.0	31.3	15.8	0.50	1.08	0.80	0.80	30.2	30.7	13.6
			Peak $\Delta\sigma f$	19%	36.3	17.4	53.7	24.2	35.5	18.1	0.51				30.7		15.6
			ε_a=25%	25%	34.4	17.9	52.3	23.9	35.1	17.2	0.49				29.3		15.0

Tests PT-2 and FT-2 Comparison

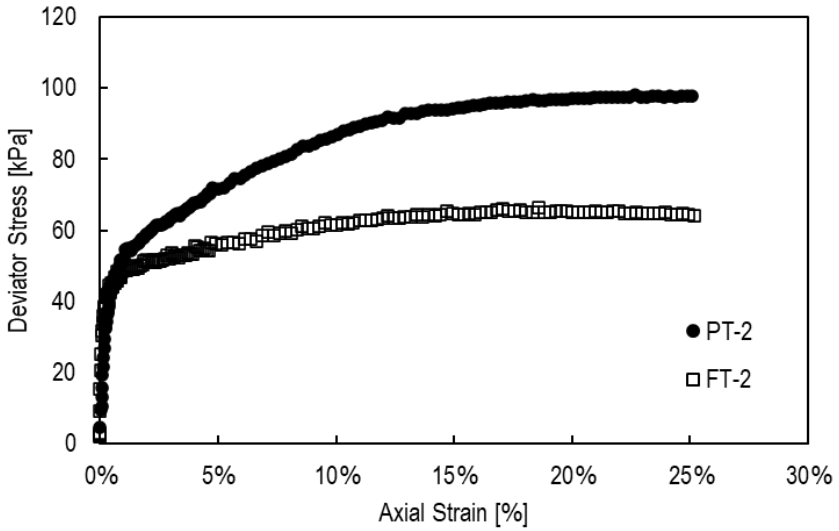

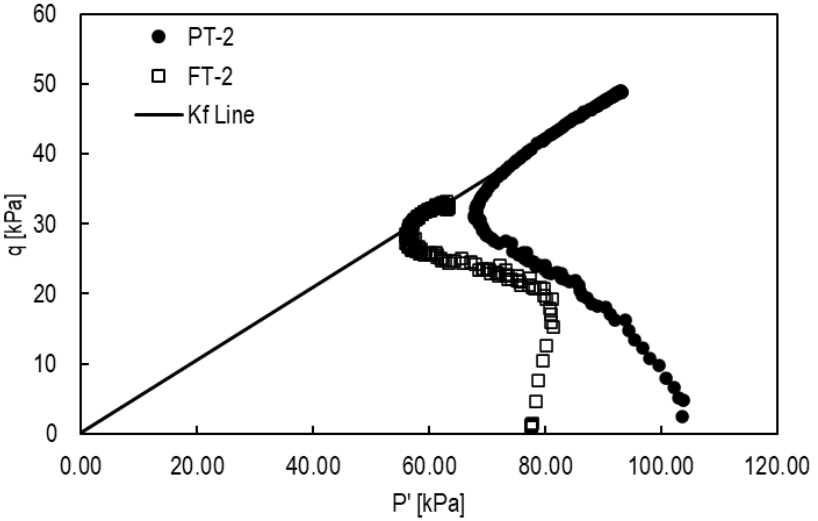

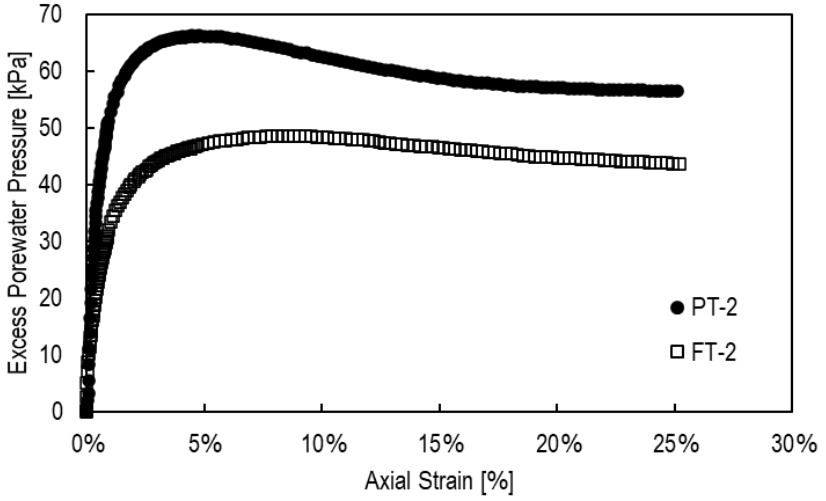

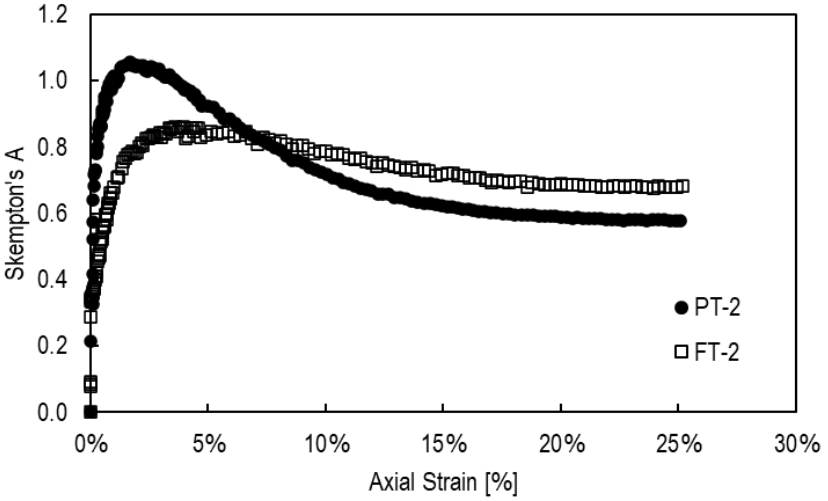

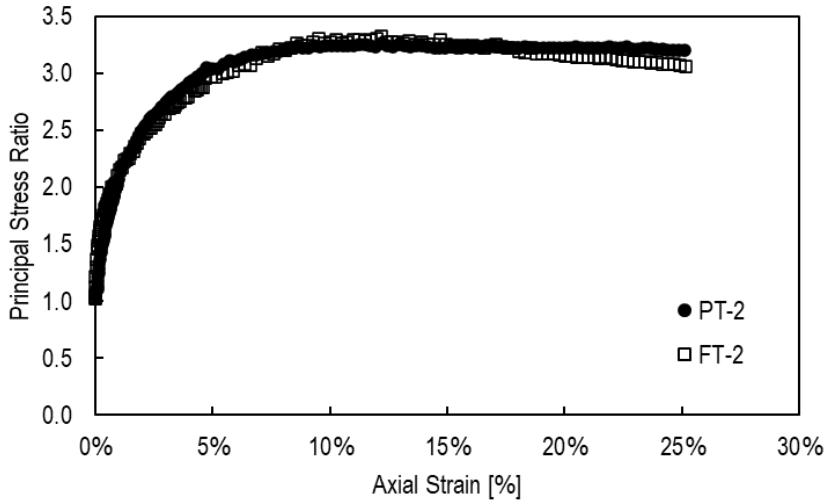

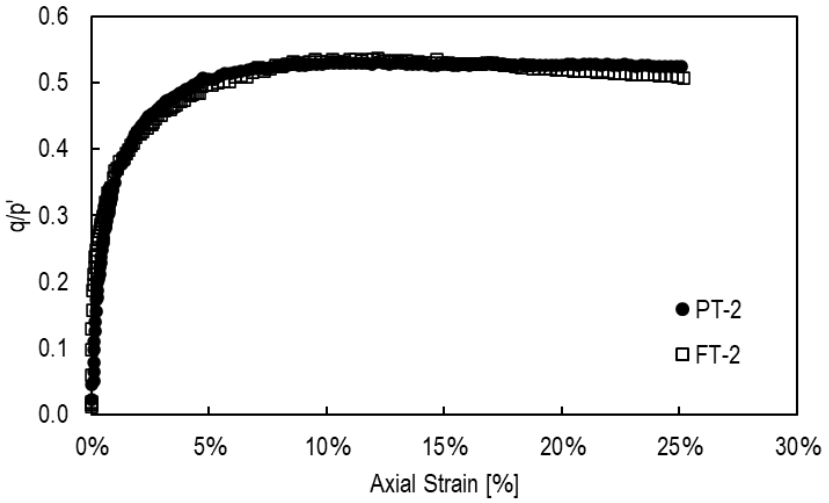

Test	Target σ'_c [kPa]	Actual σ'_c [kPa]	Failure Criteria	$\varepsilon_{a,f}$	$\Delta\sigma_d$ [kPa]	σ'_{3f} [kPa]	σ'_{1f} [kPa]	$u_{e,f}$ [kPa]	p'_f [kpa]	q_f [kPa]	q/P'	Initial Void Ratio, e_i	Consolidated Void Ratio, e_C	Final Void Ratio, e_f	φ'_s (°)	φ'_f (°)	S_u' [kPa]
PT-2	100	101	Peak $U_{e,f}$	5%	71.8	35.0	106.8	66.2	70.9	35.9	0.51	1.16	0.75	0.75	30.4	31.8	31.0
			Peak $\Delta\sigma f$	23%	98.1	43.9	142.0	56.7	93.0	49.0	0.53				31.8		41.7
			ε_a=25%	25%	97.7	44.3	142.0	56.5	93.2	48.8	0.52				31.6		41.6
FT-2	100	77	Peak $U_{e,f}$	8%	59.3	26.9	86.2	48.6	56.6	29.7	0.52	1.10	0.74	0.74	31.6	31.8	25.3
			Peak $\Delta\sigma f$	19%	66.4	29.9	96.3	45.1	63.1	33.2	0.53				31.8		28.2
			ε_a=25%	25%	64.0	31.1	95.1	43.7	63.1	32.0	0.51				30.5		27.6

Tests PT-3 and FT-3 Comparison

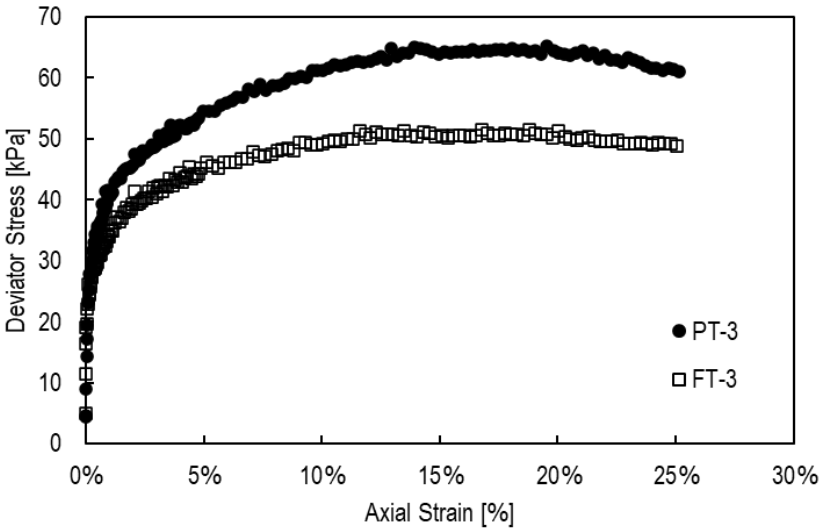

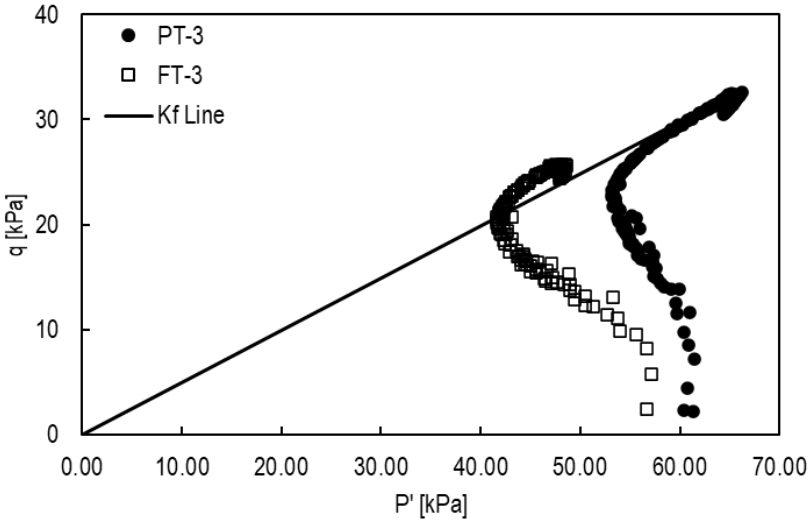

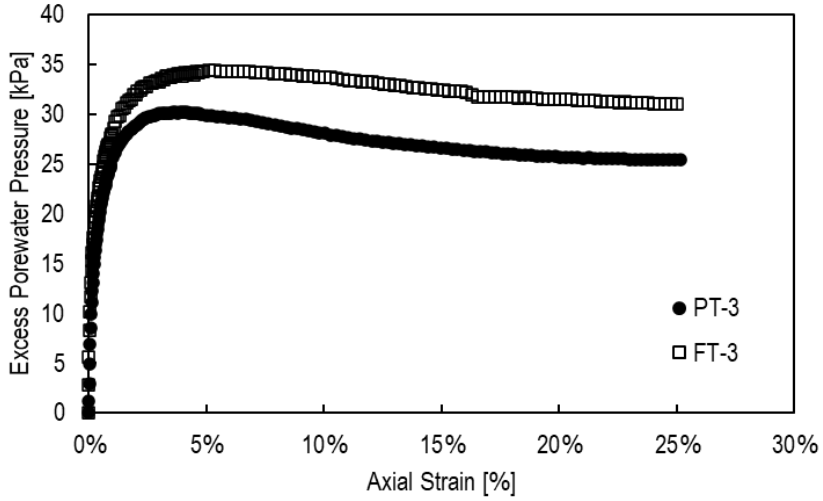

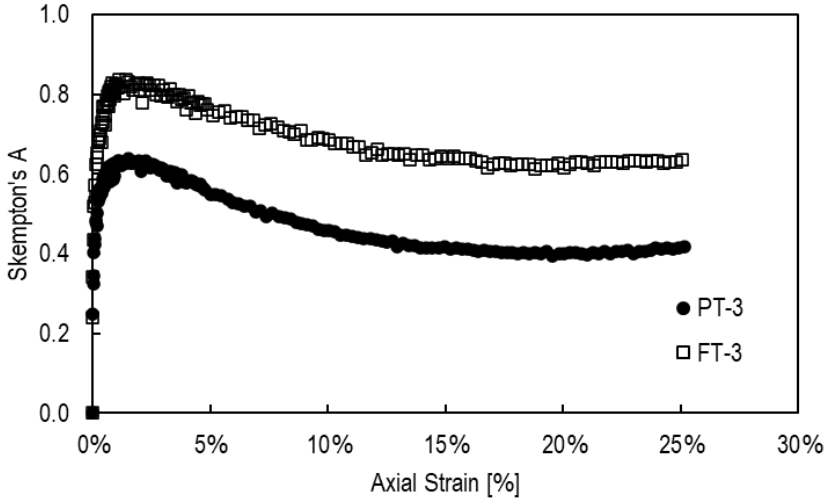

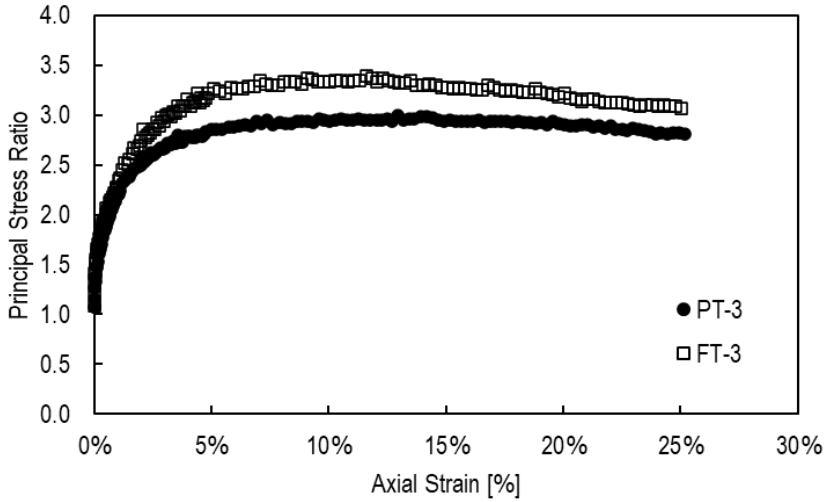

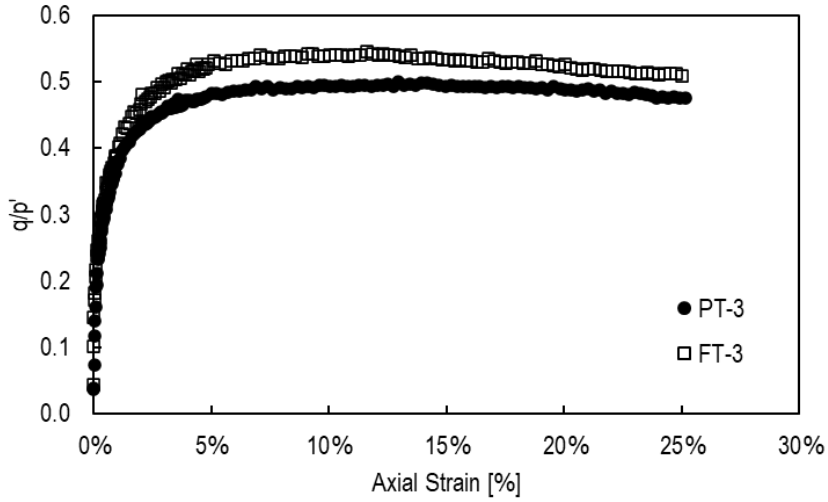

Test	Target σ'_c [kPa]	Actual σ'_c [kPa]	Failure Criteria	$\varepsilon_{a,f}$	$\Delta\sigma_d$ [kPa]	σ'_{3f} [kPa]	σ'_{1f} [kPa]	$u_{e,f}$ [kPa]	p'_f [kpa]	q_f [kPa]	q/P'	Initial Void Ratio, e_i	Consolidated Void Ratio, e_C	Final Void Ratio, e_f	φ'_s (°)	φ'_f (°)	S_u' [kPa]
PT-3	50	59	Peak $U_{e,f}$	4%	52.3	29.1	81.5	30.2	55.3	26.2	0.47	1.08	0.77	0.77	28.2	29.5	23.0
			Peak $\Delta\sigma f$	20%	65.3	33.6	98.8	25.7	66.2	32.6	0.49				29.5		28.4
			ε_a=25%	25%	61.1	33.8	94.9	25.4	64.3	30.5	0.47				28.3		26.9
FT-3	50	54	Peak $U_{e,f}$	5%	45.5	20.3	65.8	34.3	43.1	22.8	0.53	0.96	0.76	0.76	31.9	32.3	19.3
			Peak $\Delta\sigma f$	17%	51.6	22.4	74.0	31.7	48.2	25.8	0.53				32.3		21.8
			ε_a=25%	25%	48.8	23.5	72.3	31.0	47.9	24.4	0.51				30.6		21.0

Tests PT-4 and FT-4 Comparison

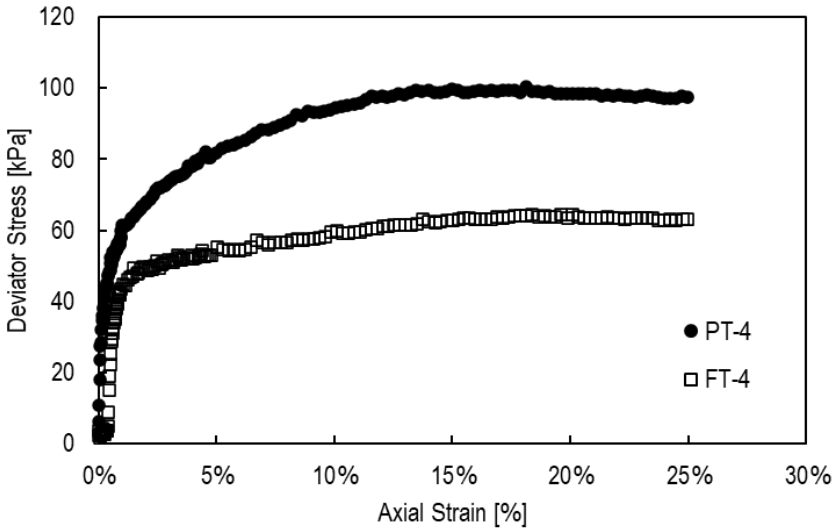

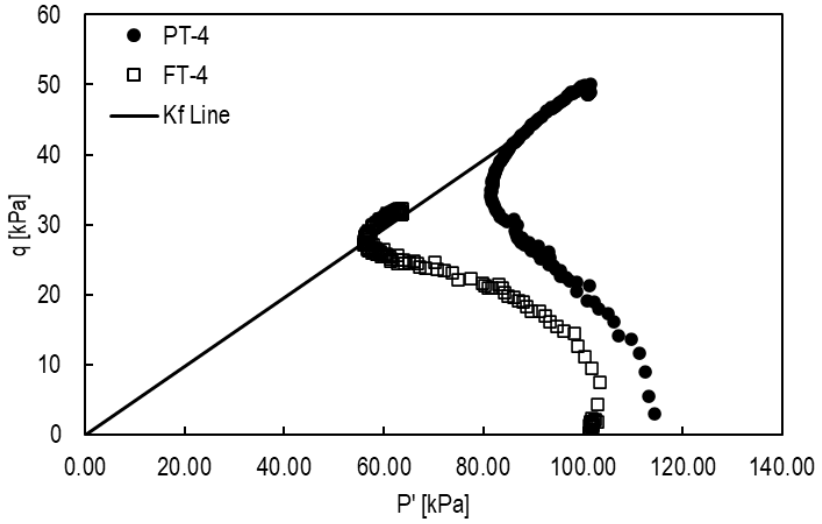

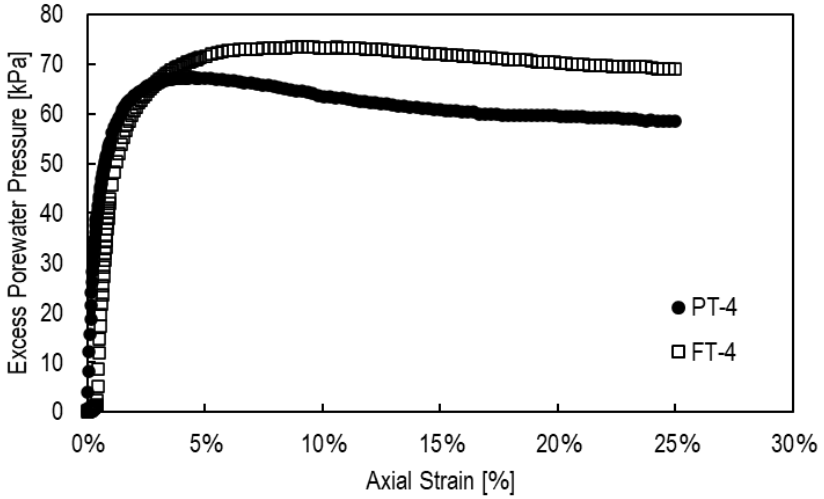

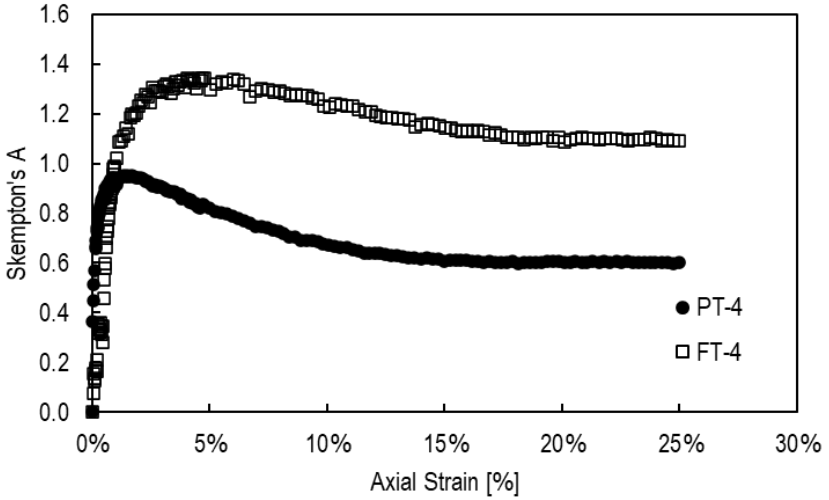

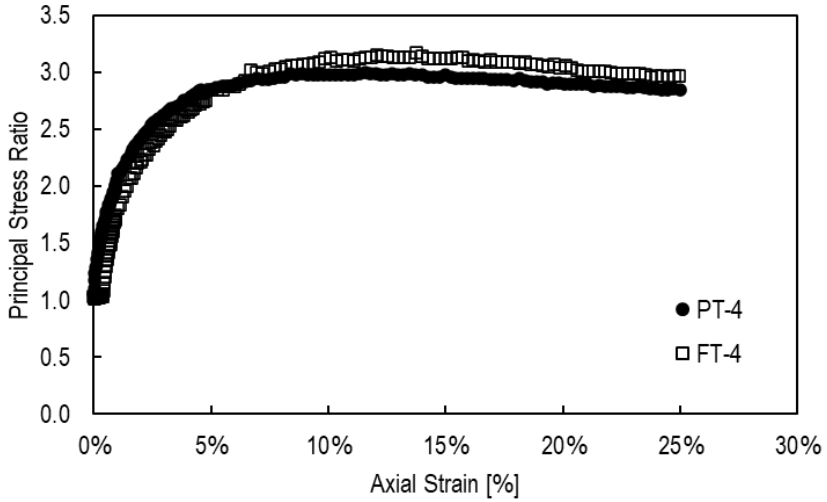

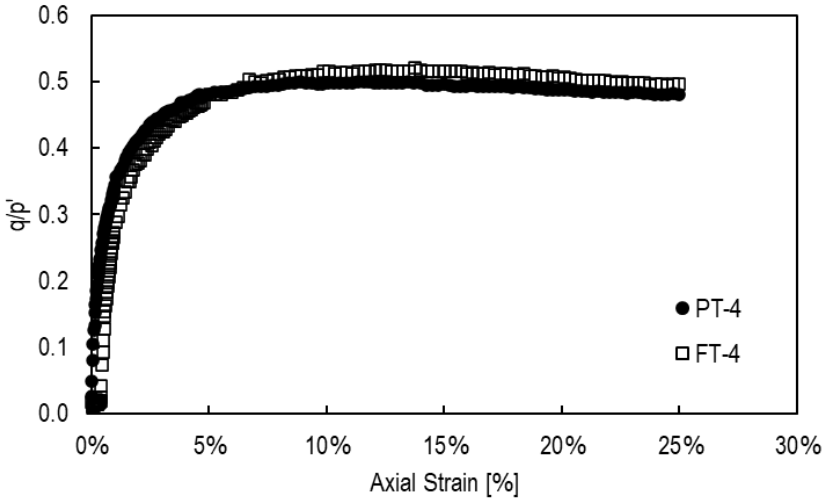

Test	Target σ'_c [kPa]	Actual σ'_c [kPa]	Failure Criteria	$\varepsilon_{a,f}$	$\Delta\sigma_d$ [kPa]	σ'_{3f} [kPa]	σ'_{1f} [kPa]	$u_{e,f}$ [kPa]	p'_f [kpa]	q_f [kPa]	q/P'	Initial Void Ratio, e_i	Consolidated Void Ratio, e_C	Final Void Ratio, e_f	φ'_s (°)	φ'_f (°)	S_u' [kPa]
PT-4	100	111	Peak $U_{e,f}$	4%	80.3	44.3	124.6	67.3	84.4	40.1	0.48	1.01	0.78	0.78	28.4	29.6	35.3
			Peak $\Delta\sigma f$	18%	100.3	51.4	151.7	59.8	101.5	50.1	0.49				29.6		43.6
			ε_a=25%	25%	97.4	52.6	150.0	58.6	101.3	48.7	0.48				28.7		42.7
FT-4	100	101	Peak $U_{e,f}$	9%	57.5	27.8	85.4	73.3	56.6	28.8	0.51	1.04	0.76	0.76	30.6	30.6	24.8
			Peak $\Delta\sigma f$	20%	64.6	31.3	95.9	70.1	63.6	32.3	0.51				30.5		27.8
			ε_a=25%	25%	63.2	32.1	95.4	69.1	63.7	31.6	0.50				29.7		27.5

Tests PT-5 and FT-5 Comparison

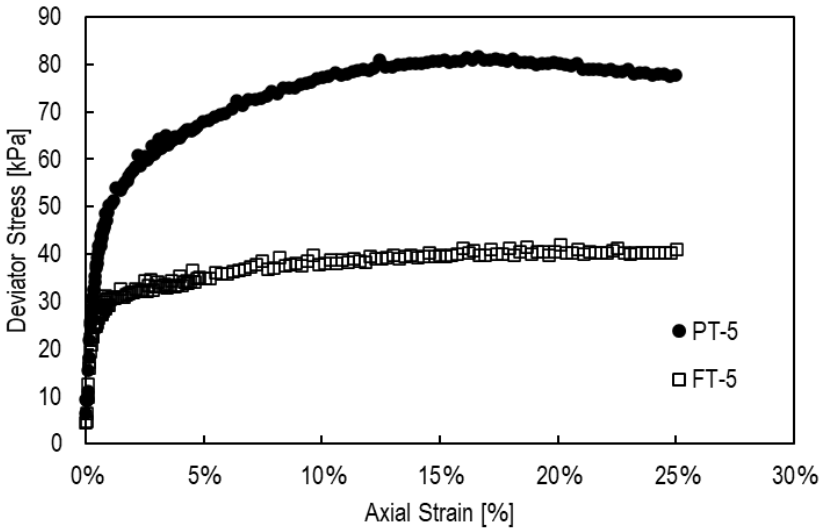

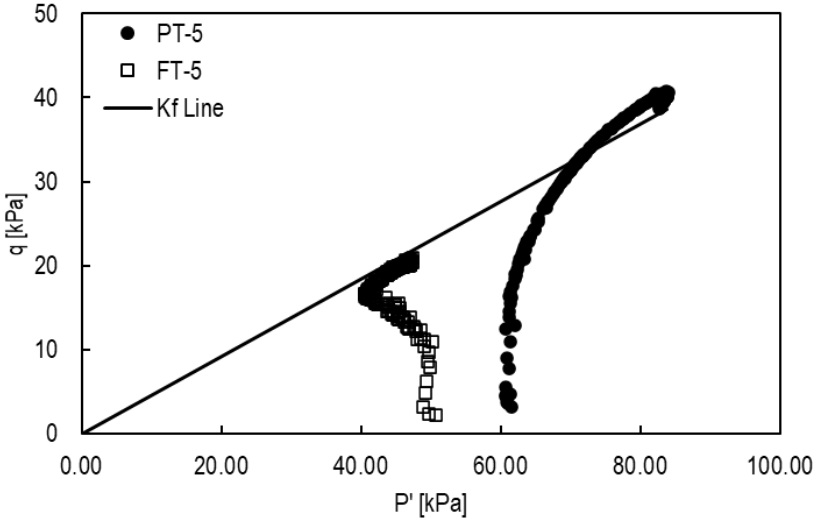

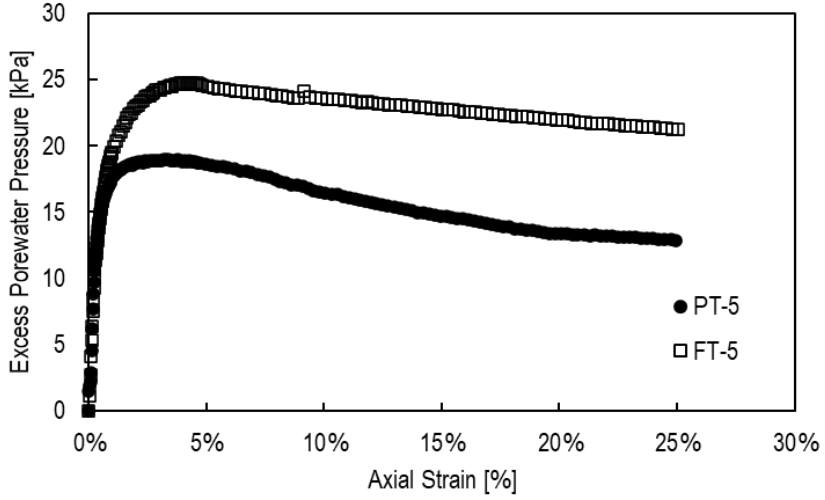

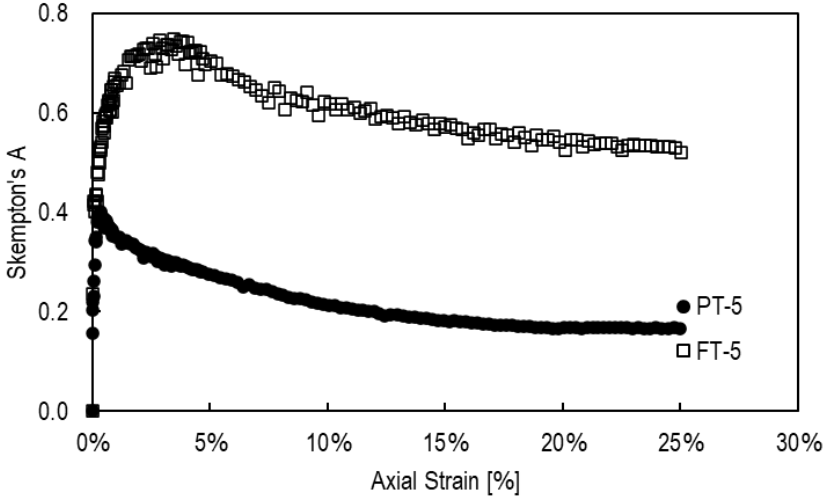

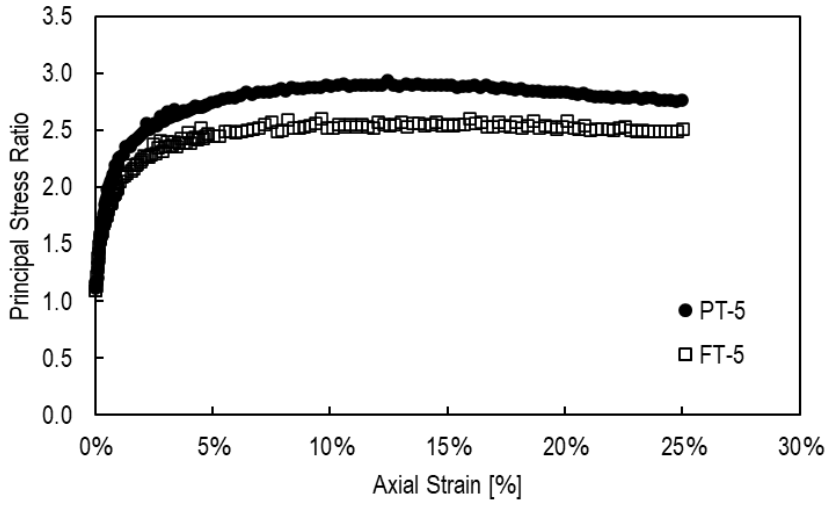

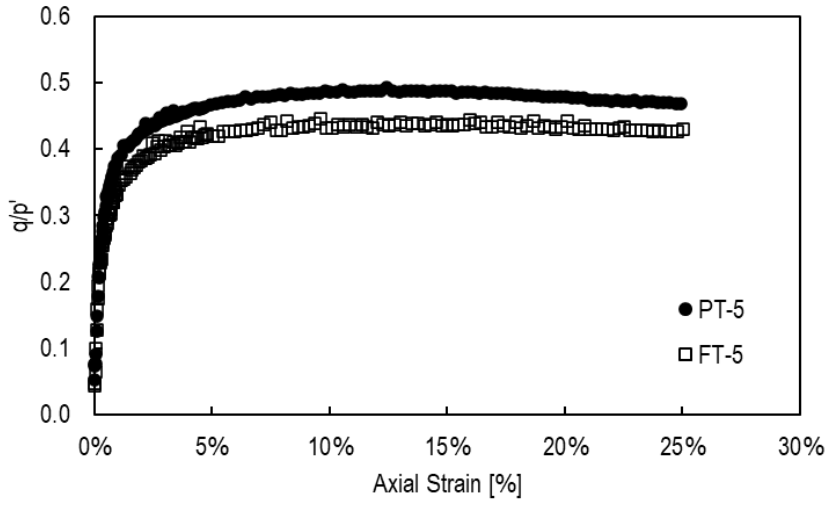

Test	Target σ'_c [kPa]	Actual σ'_c [kPa]	Failure Criteria	$\varepsilon_{a,f}$	$\Delta\sigma_d$ [kPa]	σ'_{3f} [kPa]	σ'_{1f} [kPa]	$u_{e,f}$ [kPa]	p'_f [kpa]	q_f [kPa]	q/P'	Initial Void Ratio, e_i	Consolidated Void Ratio, e_C	Final Void Ratio, e_f	φ'_s (°)	φ'_t (°)	S_u' [kPa]
PT-5	50	58	Peak $U_{e,f}$	3%	62.2	38.6	100.8	18.9	69.7	31.1	0.45	0.85	0.79	0.79	26.5	29.1	27.8
			Peak $\Delta\sigma f$	17%	81.6	43.0	124.6	14.3	83.8	40.8	0.49				29.1		35.6
			ε_a=25%	25%	77.7	44.0	121.7	12.9	82.9	38.8	0.47				27.9		34.3
FT-5	50	48	Peak $U_{e,f}$	4%	34.2	23.9	58.1	24.8	41.0	17.1	0.42	0.87	0.78	0.78	24.7	26.2	15.6
			Peak $\Delta\sigma f$	20%	41.9	26.5	68.3	21.9	47.4	20.9	0.44				26.2		18.8
			ε_a=25%	25%	40.9	27.0	67.9	21.3	47.4	20.4	0.43				25.5		18.4

Tests PT-6 and FT-6 Comparison

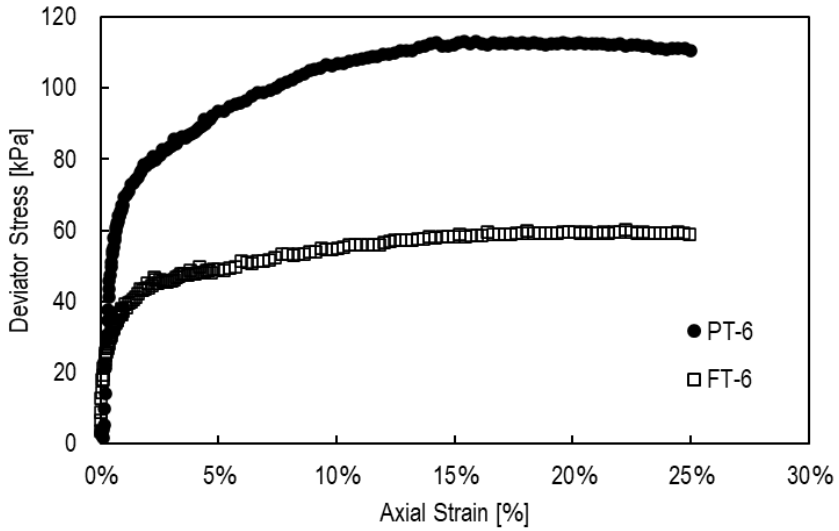

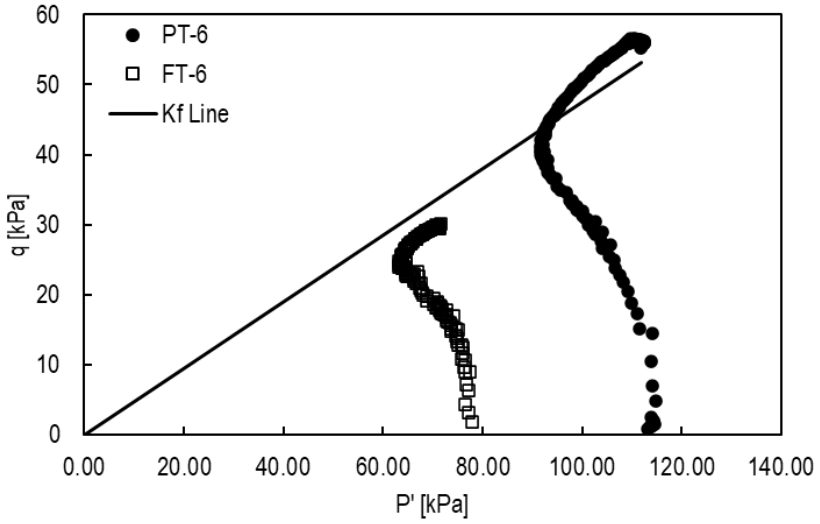

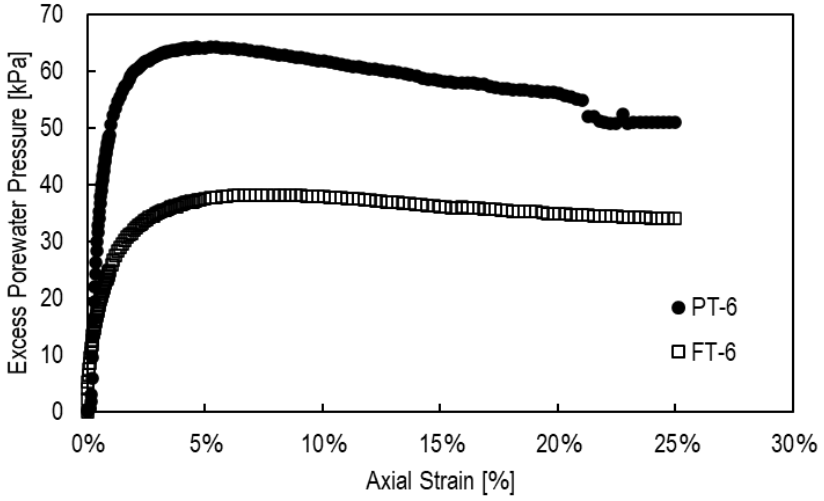

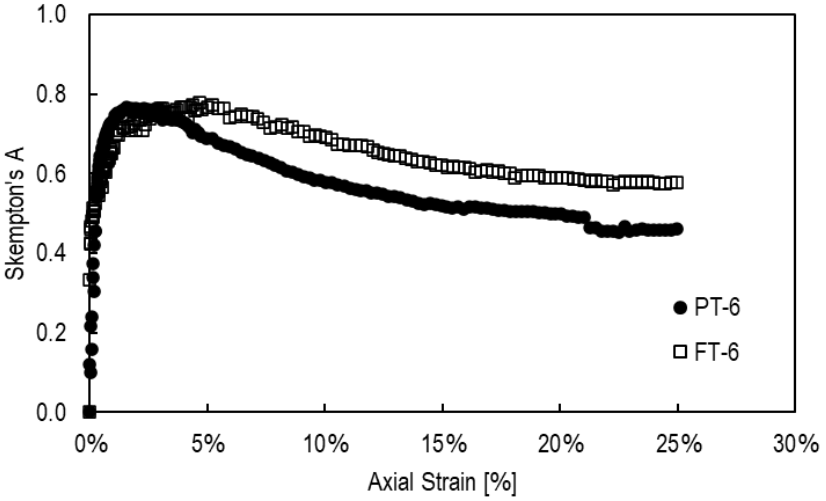

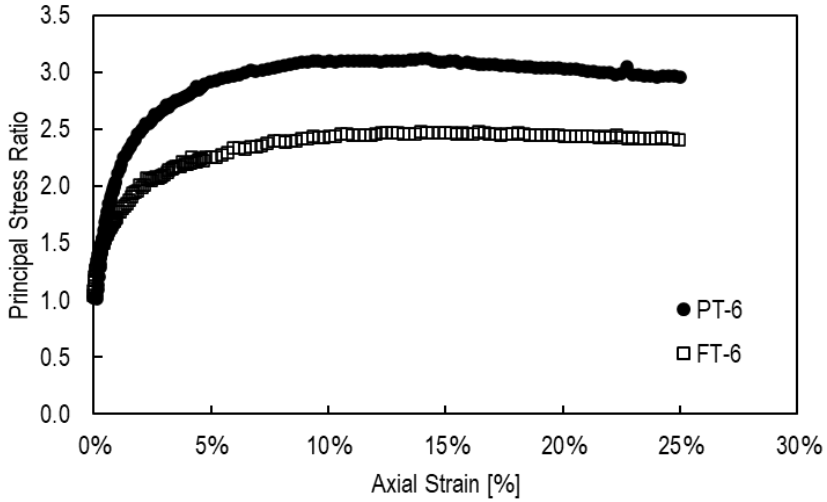

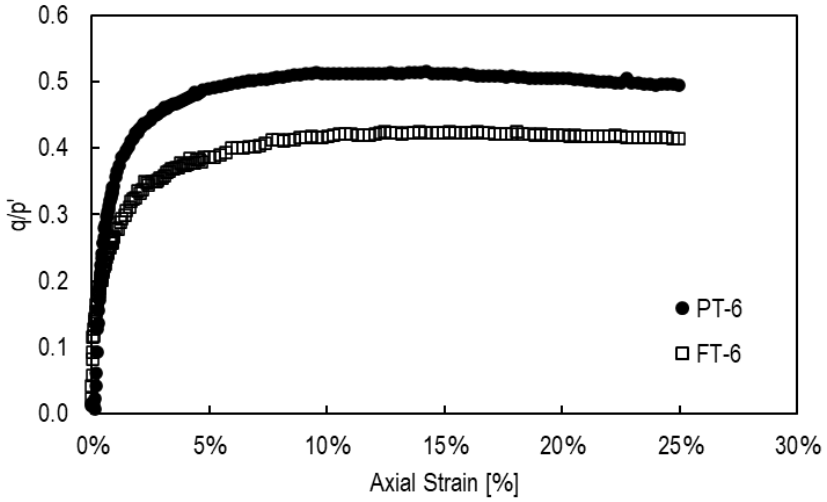

Test	Target σ'_c [kPa]	Actual σ'_c [kPa]	Failure Criteria	$\varepsilon_{a,f}$	$\Delta\sigma_d$ [kPa]	σ'_{3f} [kPa]	σ'_{1f} [kPa]	$u_{e,f}$ [kPa]	p'_f [kpa]	q_f [kPa]	q/P'	Initial Void Ratio, e_i	Consolidated Void Ratio, e_C	Final Void Ratio, e_f	φ'_s (°)	φ'_f (°)	S_u' [kPa]
PT-6	100	113	Peak $U_{e,f}$	5%	93.5	48.6	142.0	64.2	95.3	46.7	0.49	0.84	0.76	0.76	29.4	30.9	40.7
			Peak $\Delta\sigma f$	15%	113.2	53.8	166.9	58.1	110.4	56.6	0.51				30.9		48.6
			ε_a=25%	25%	110.6	56.5	167.0	50.9	111.8	55.3	0.49				29.6		48.0
FT-6	100	76	Peak $U_{e,f}$	8%	53.3	38.0	91.3	38.2	64.6	26.6	0.41	0.88	0.76	0.76	24.3	24.9	24.3
			Peak $\Delta\sigma f$	22%	60.2	41.5	101.7	34.4	71.6	30.1	0.42				24.9		27.3
			ε_a=25%	25%	58.9	41.7	100.6	34.0	71.2	29.5	0.41				24.5		26.8

Tests PT-7 and FT-7 Comparison

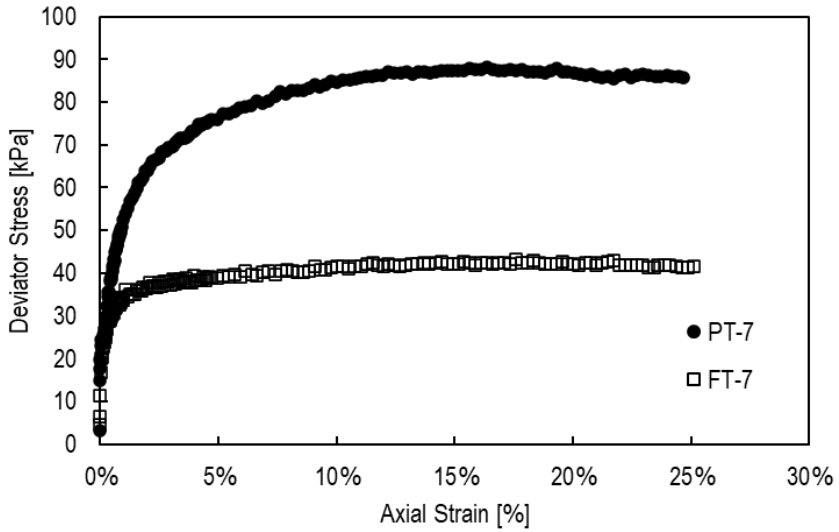

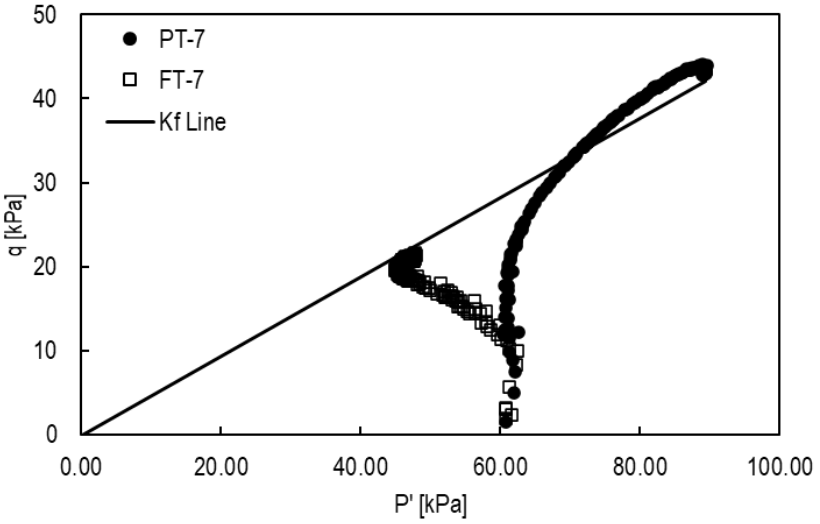

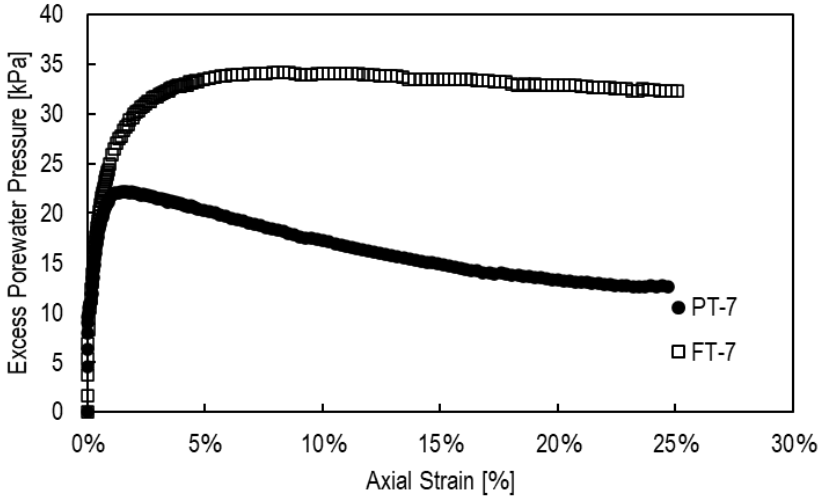

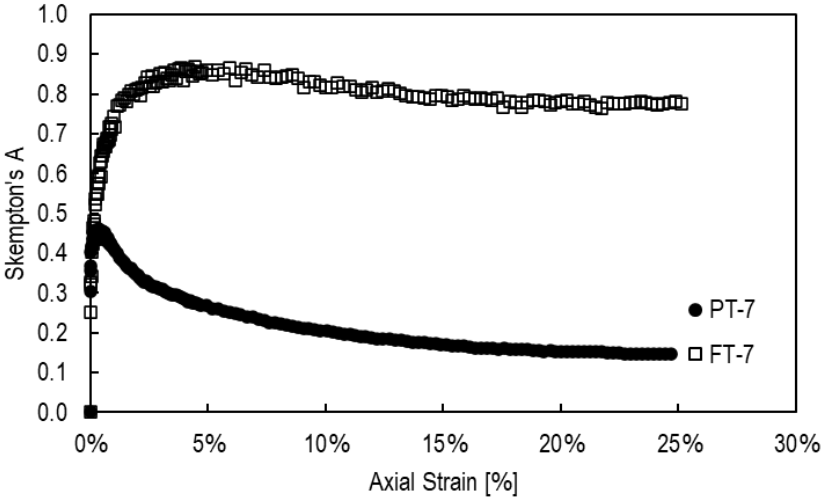

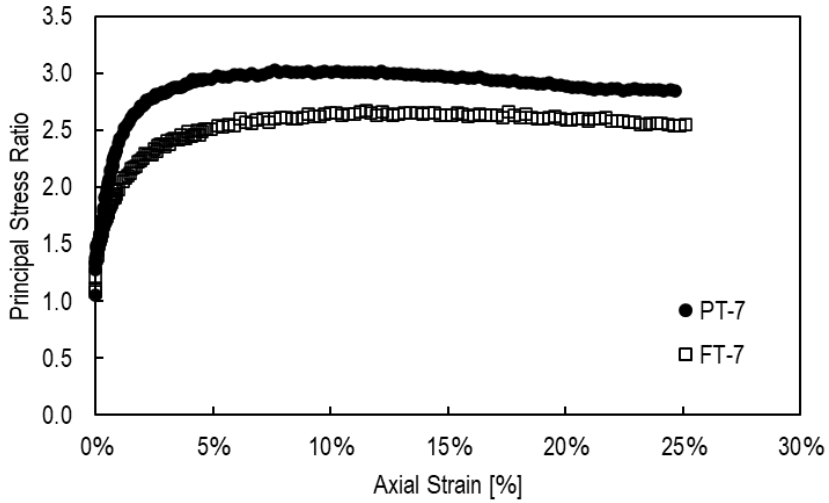

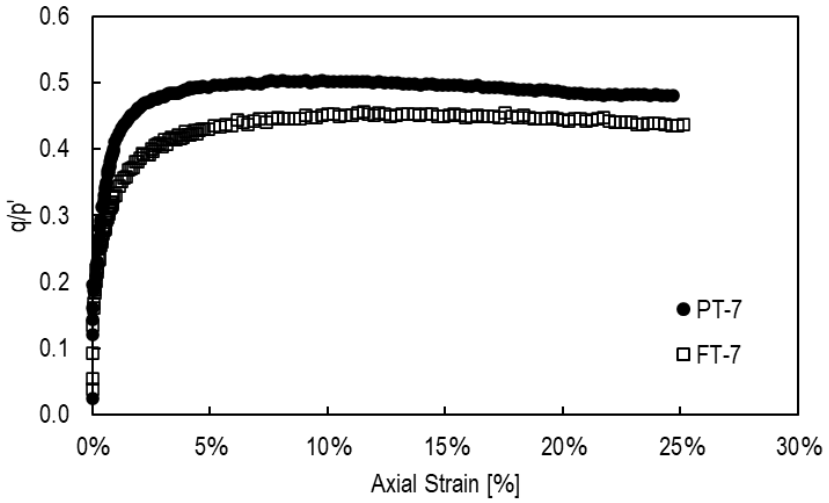

Test	Target σ'_c [kPa]	Actual σ'_c [kPa]	Failure Criteria	$\varepsilon_{a,f}$	$\Delta\sigma_d$ [kPa]	σ'_{3f} [kPa]	σ'_{1f} [kPa]	$u_{e,f}$ [kPa]	p'_f [kpa]	q_f [kPa]	q/P'	Initial Void Ratio, e_i	Consolidated Void Ratio, e_C	Final Void Ratio, e_f	φ'_s (°)	φ'_f (°)	S_u' [kPa]
PT-7	50	59	Peak $U_{e,f}$	2%	61.3	37.2	98.4	22.2	67.8	30.6	0.45	0.84	0.76	0.76	26.9	29.7	27.3
			Peak $\Delta\sigma f$	16%	88.2	44.8	133.1	14.3	89.0	44.1	0.50				29.7		38.3
			ε_a=25%	25%	85.8	46.4	132.2	12.6	89.3	42.9	0.48				28.7		37.6
FT-7	50	59	Peak $U_{e,f}$	9%	40.3	25.1	65.4	34.2	45.3	20.1	0.45	0.90	0.78	0.78	26.4	27.0	18.0
			Peak $\Delta\sigma f$	18%	43.3	26.1	69.4	33.2	47.7	21.7	0.45				27.0		19.3
			ε_a=25%	25%	41.6	26.8	68.5	32.3	47.7	20.8	0.44				25.9		18.7

Tests PT-8 and FT-8 Comparison

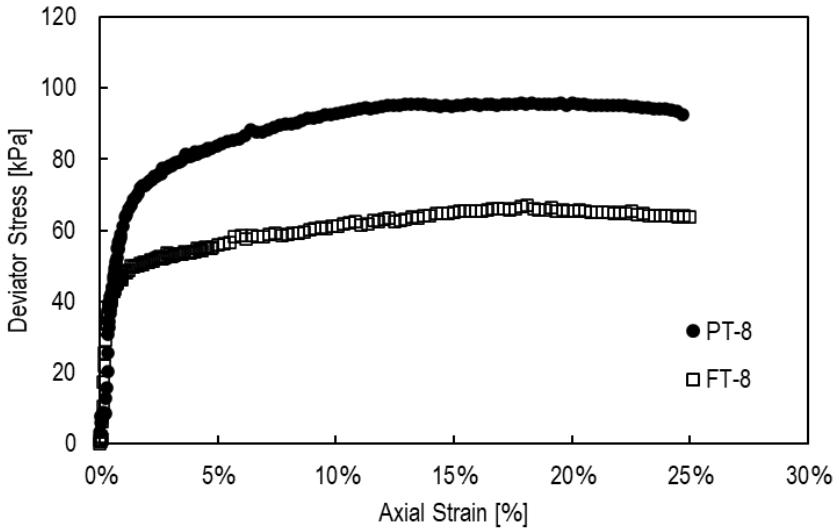

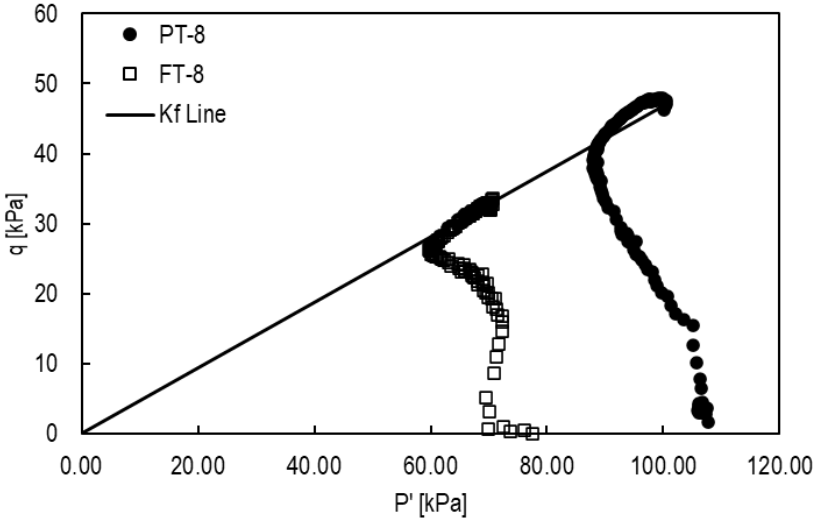

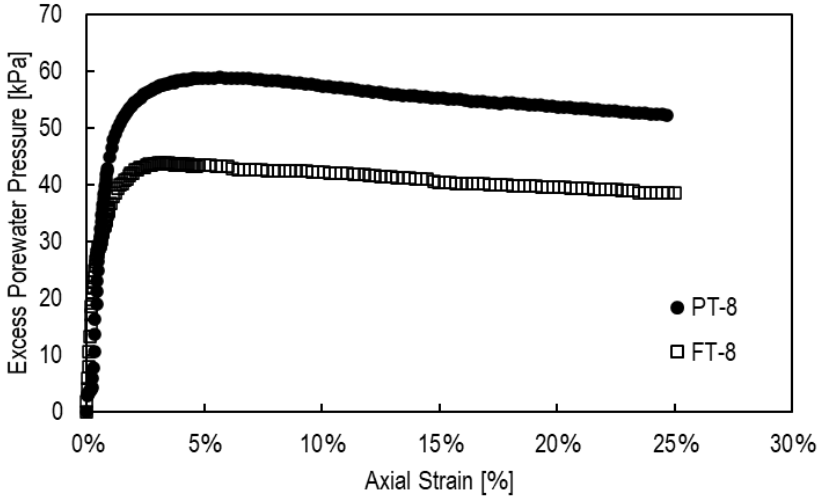

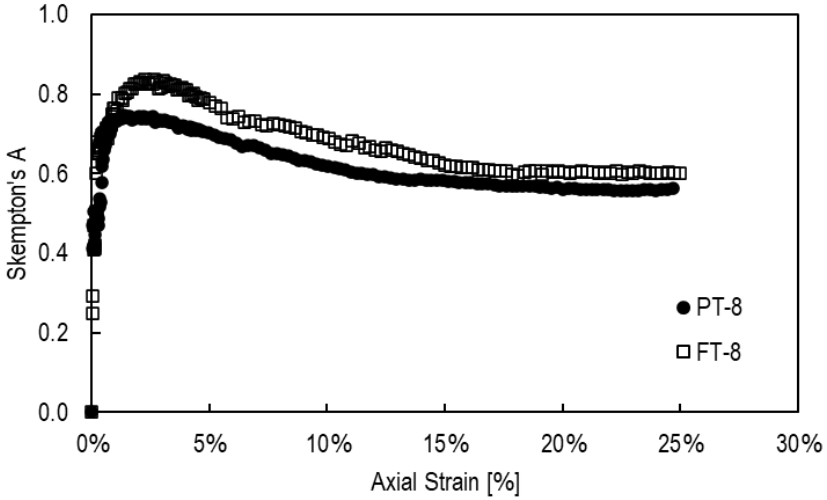

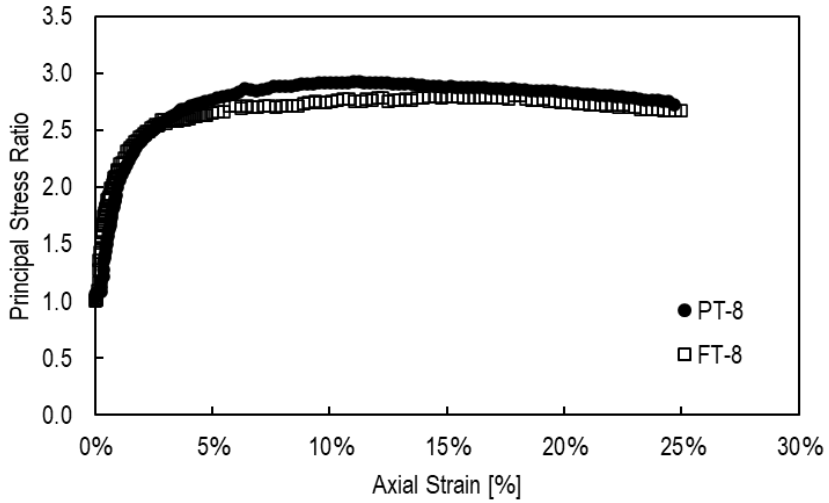

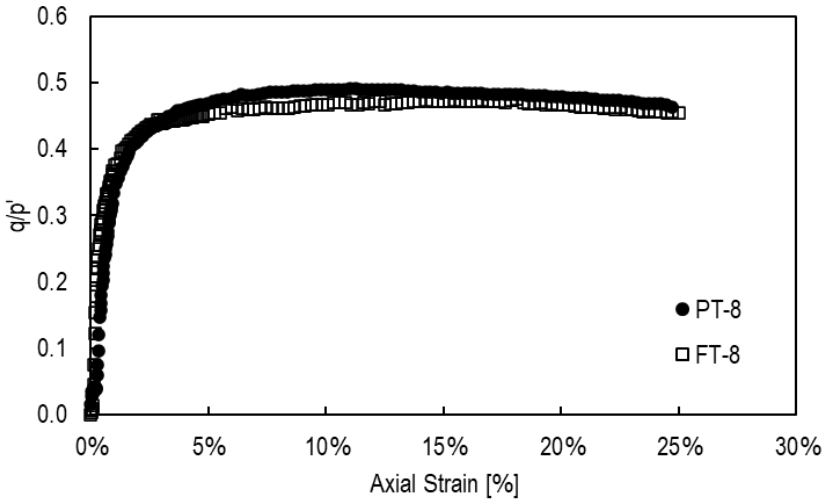

Test	Target σ'_c [kPa]	Actual σ'_c [kPa]	Failure Criteria	$\varepsilon_{a,f}$	$\Delta\sigma_d$ [kPa]	σ'_{3f} [kPa]	σ'_{1f} [kPa]	$u_{e,f}$ [kPa]	p'_f [kpa]	q_f [kPa]	q/P'	Initial Void Ratio, e_i	Consolidated Void Ratio, e_C	Final Void Ratio, e_f	φ'_s (°)	φ'_f (°)	S_u' [kPa]
PT-8	100	106	Peak $U_{e,f}$	6%	85.4	47.2	132.6	58.9	89.9	42.7	0.47	0.85	0.74	0.74	28.4	28.8	37.6
			Peak $\Delta\sigma f$	18%	95.7	51.5	147.2	54.3	99.4	47.9	0.48				28.8		41.9
			ε_a=25%	25%	92.6	53.7	146.3	52.2	100.0	46.3	0.46				27.6		41.1
FT-8	100	78	Peak $U_{e,f}$	3%	53.2	33.5	86.7	43.8	60.1	26.6	0.44	0.86	0.74	0.74	26.3	28.3	23.9
			Peak $\Delta\sigma f$	18%	67.2	37.1	104.3	39.9	70.7	33.6	0.47				28.3		29.5
			ε_a=25%	25%	63.9	38.3	102.1	38.5	70.2	31.9	0.45				27.1		28.4

Tests PT-9 and FT-9 Comparison

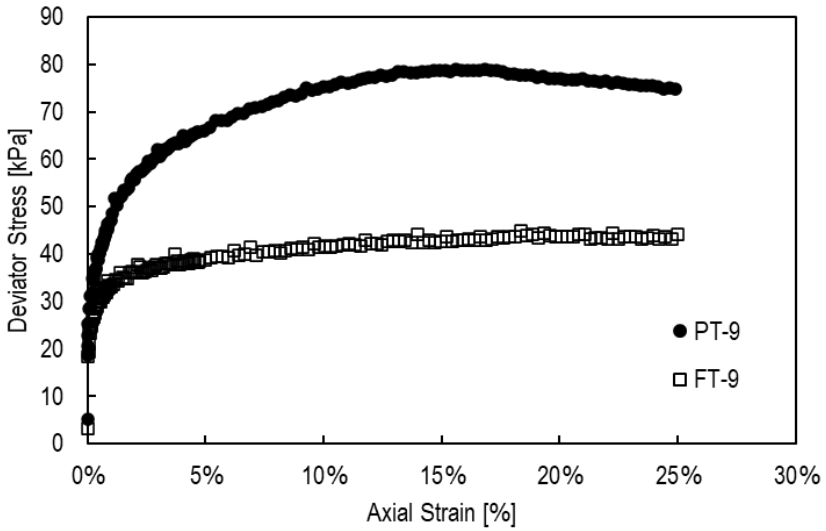

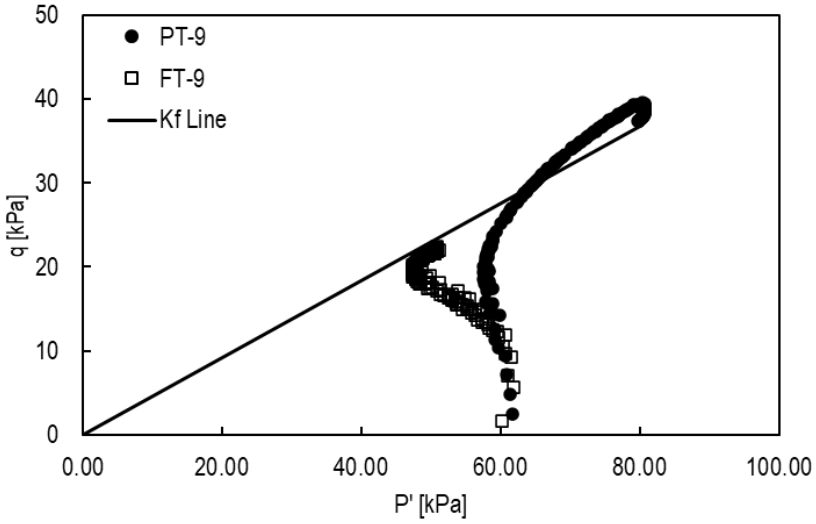

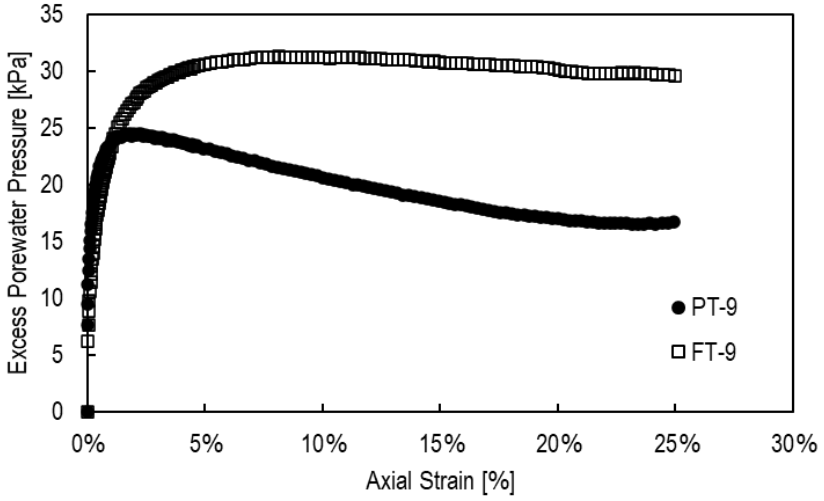

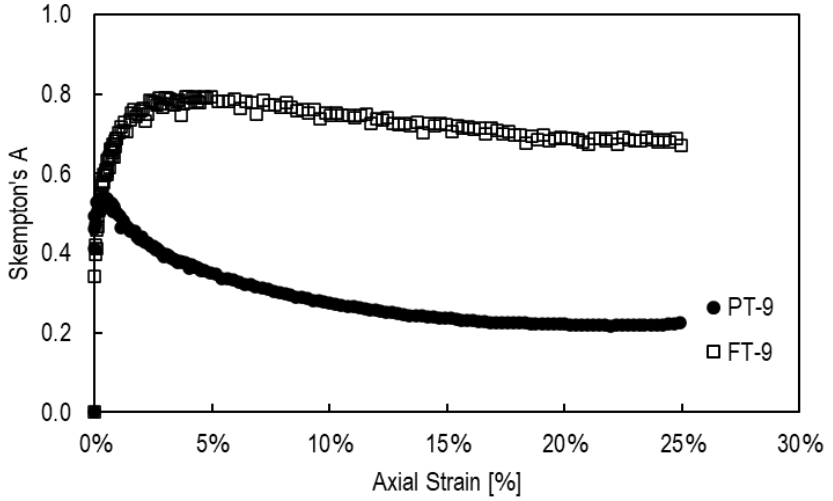

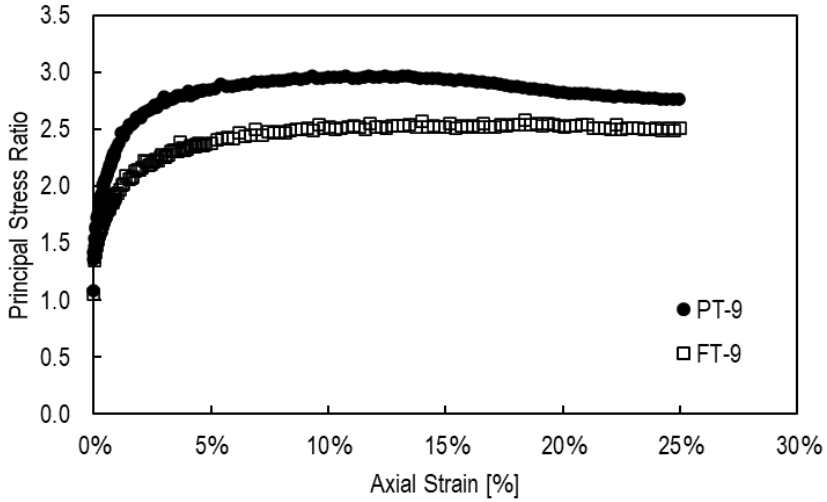

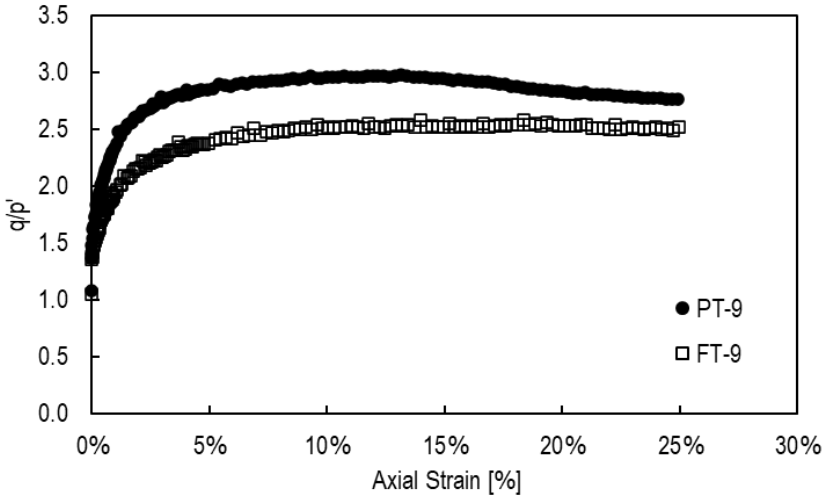

Test	Target σ'_c [kPa]	Actual σ'_c [kPa]	Failure Criteria	$\varepsilon_{a,f}$	$\Delta\sigma_d$ [kPa]	σ'_{3f} [kPa]	σ'_{1f} [kPa]	$u_{e,f}$ [kPa]	p'_f [kpa]	q_f [kPa]	q/P'	Initial Void Ratio, e_i	Consolidated Void Ratio, e_C	Final Void Ratio, e_f	φ'_s (°)	φ'_f (°)	S_u' [kPa]
PT-9	50	59	Peak $U_{e,f}$	2%	53.9	34.6	88.6	24.5	61.6	27.0	0.44	0.83	0.78	0.78	26.0	29.5	24.2
			Peak $\Delta\sigma f$	16%	79.1	40.8	119.9	18.3	80.3	39.5	0.49				29.5		34.4
			ε_a=25%	25%	74.7	42.4	117.1	16.7	79.8	37.4	0.47				27.9		33.0
FT-9	50	59	Peak $U_{e,f}$	8%	40.3	27.3	67.6	31.3	47.4	20.1	0.42	0.89	0.79	0.79	25.1	26.2	18.2
			Peak $\Delta\sigma f$	18%	44.9	28.5	73.4	30.4	50.9	22.5	0.44				26.2		20.2
			ε_a=25%	25%	44.1	29.1	73.2	29.6	51.1	22.0	0.43				25.5		19.9

Tests PT-10 and FT-10 Comparison

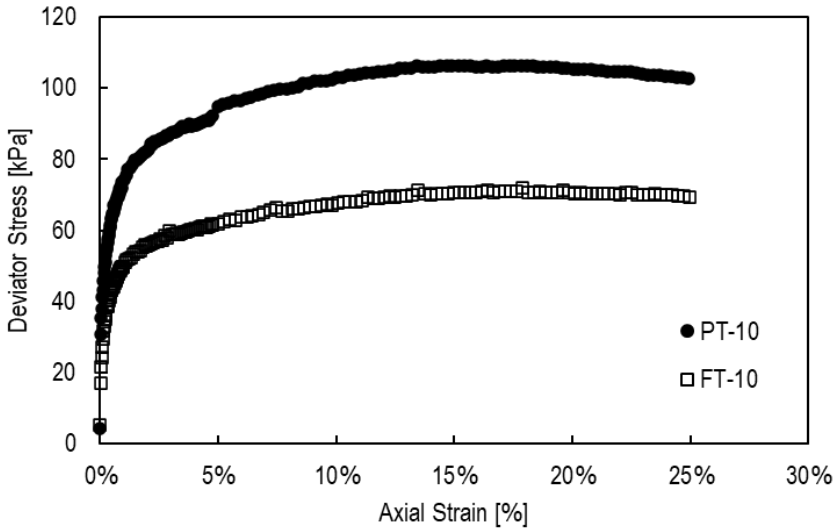

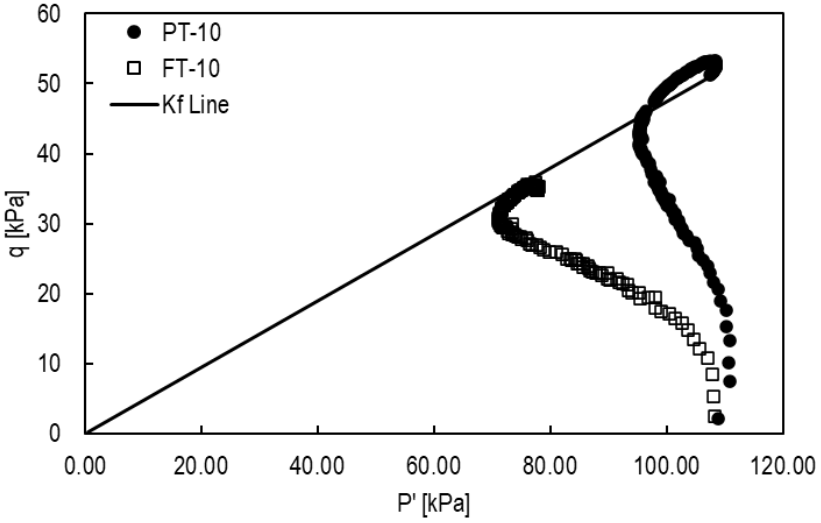

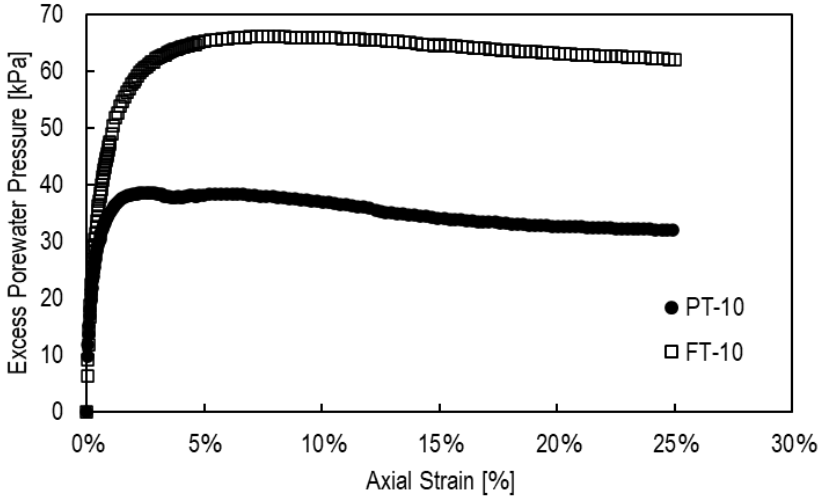

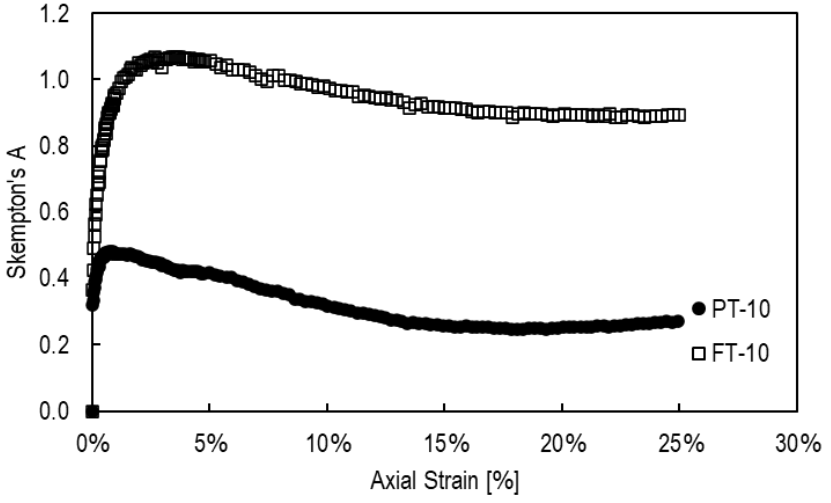

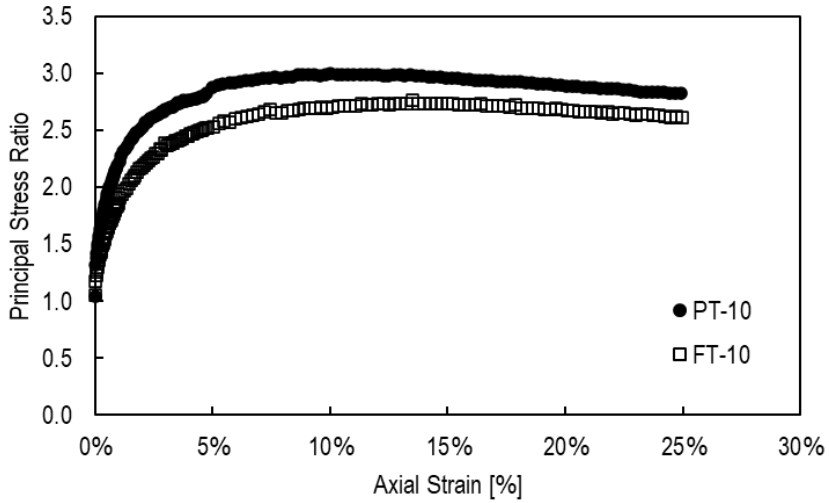

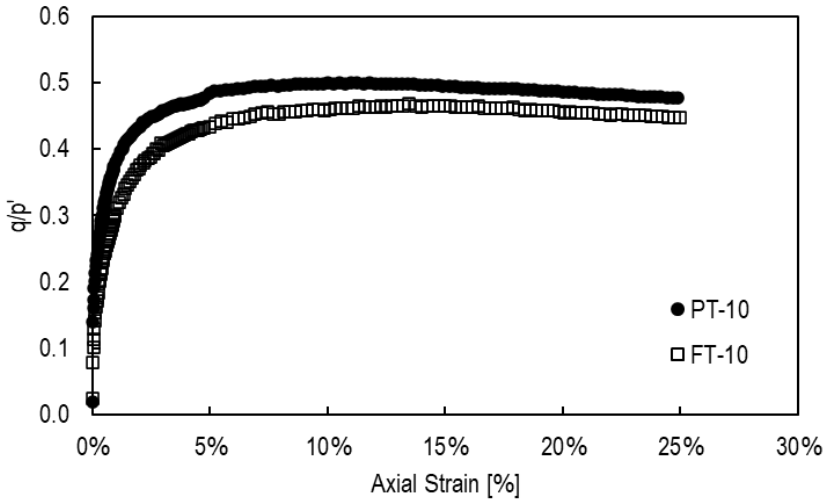

Test	Target σ'_c [kPa]	Actual σ'_c [kPa]	Failure Criteria	$\varepsilon_{a,f}$	$\Delta\sigma_d$ [kPa]	σ'_{3f} [kPa]	σ'_{1f} [kPa]	$u_{e,f}$ [kPa]	p'_f [kpa]	q_f [kPa]	q/P'	Initial Void Ratio, e_i	Consolidated Void Ratio, e_C	Final Void Ratio, e_f	φ'_s (°)	φ'_f (°)	S_u' [kPa]
PT-10	100	107	Peak $U_{e,f}$	6%	96.5	50.3	146.7	38.4	98.5	48.2	0.49	0.80	0.75	0.75	29.3	29.4	42.1
			Peak $\Delta\sigma f$	18%	106.4	55.2	161.7	33.0	108.5	53.2	0.49				29.4		46.4
			ε_a=25%	25%	102.6	56.2	158.8	32.0	107.5	51.3	0.48				28.5		45.1
FT-10	100	106	Peak $U_{e,f}$	8%	66.1	39.4	105.5	66.1	72.5	33.1	0.46	0.88	0.73	0.73	27.1	27.6	29.4
			Peak $\Delta\sigma f$	18%	71.8	41.6	113.4	63.6	77.5	35.9	0.46				27.6		31.8
			ε_a=25%	25%	69.5	43.0	112.5	62.0	77.8	34.7	0.45				26.5		31.1

APPENDIX B: Results from One-Dimensional Consolidation Tests

Desiccated Thickened Tailings One-Dimensional Consolidation Results

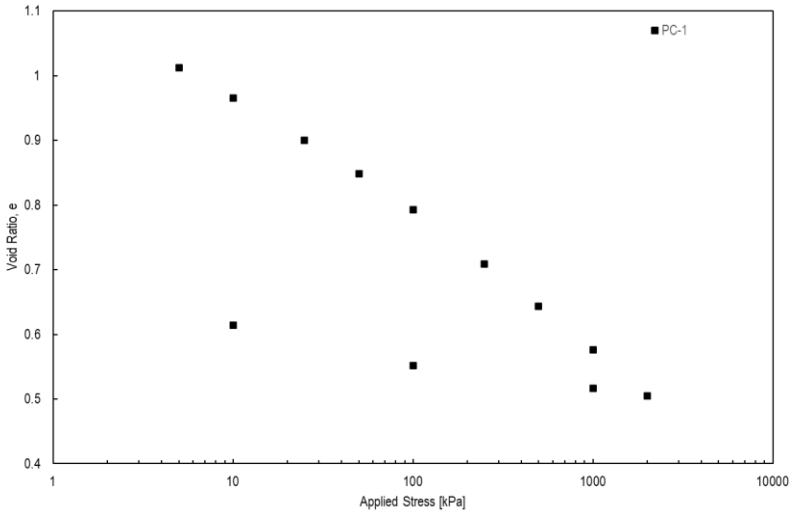

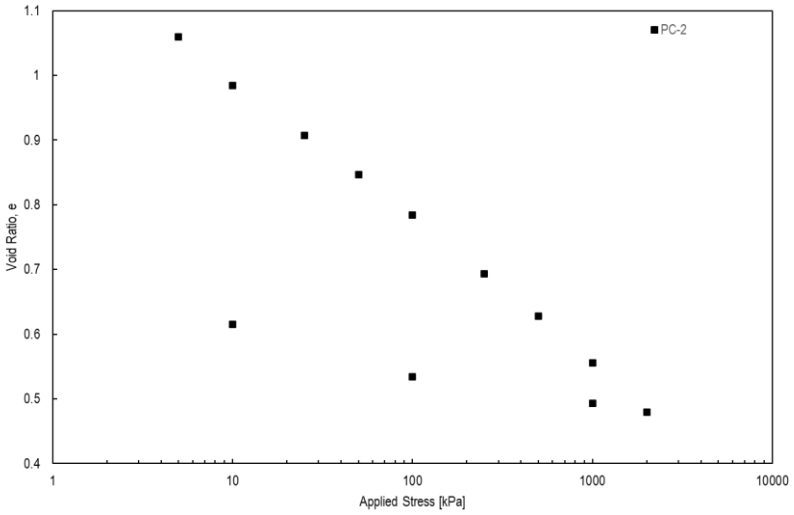

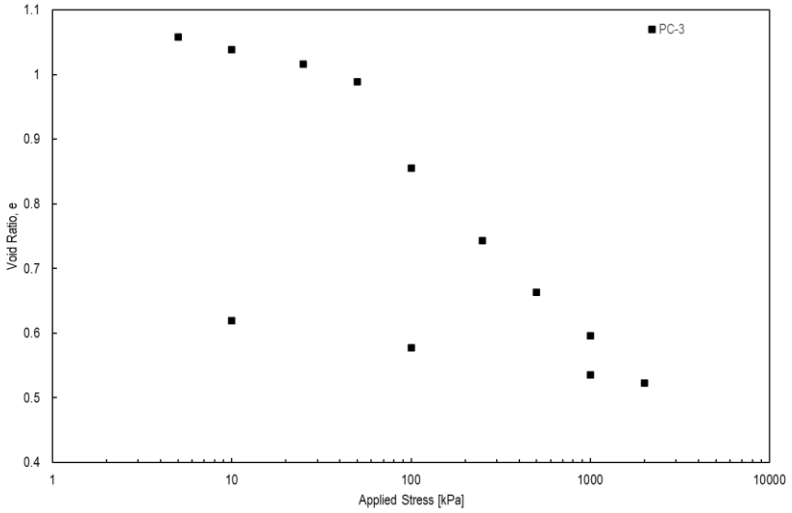

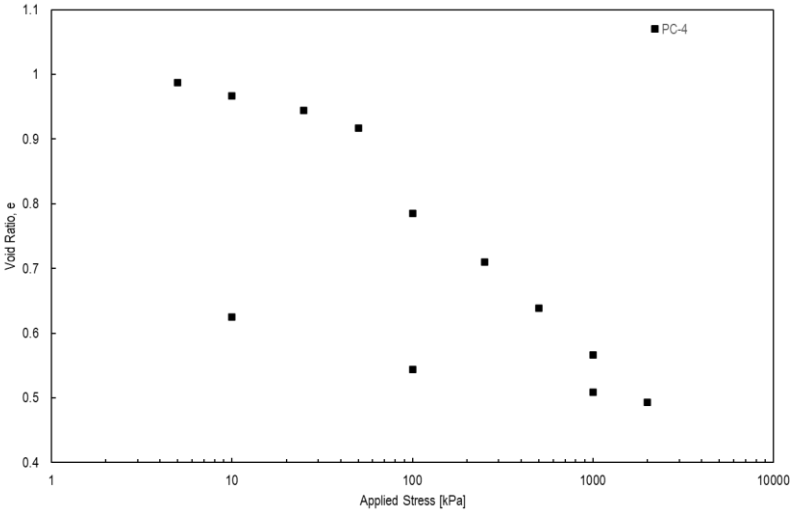

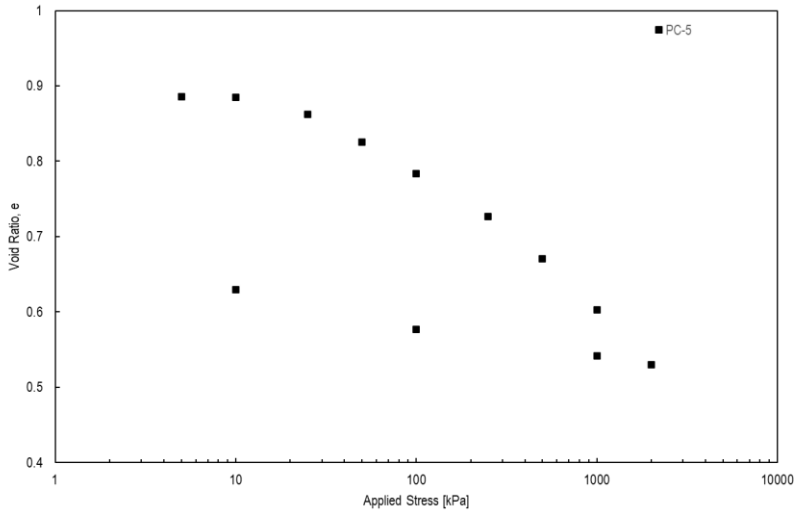
PC-5
Void Ratio, e
Applied Stress [kPa]
1
0.9
0.8
0.7
0.6
0.5
0.4
1
10
100
1000
10000

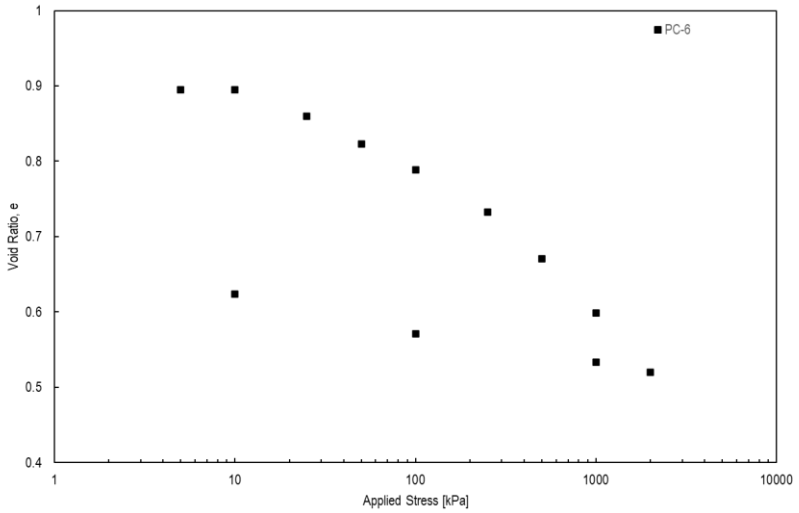
PC-6
Void Ratio, e
Applied Stress [kPa]
1
0.9
0.8
0.7
0.6
0.5
0.4
1
10
100
1000
10000

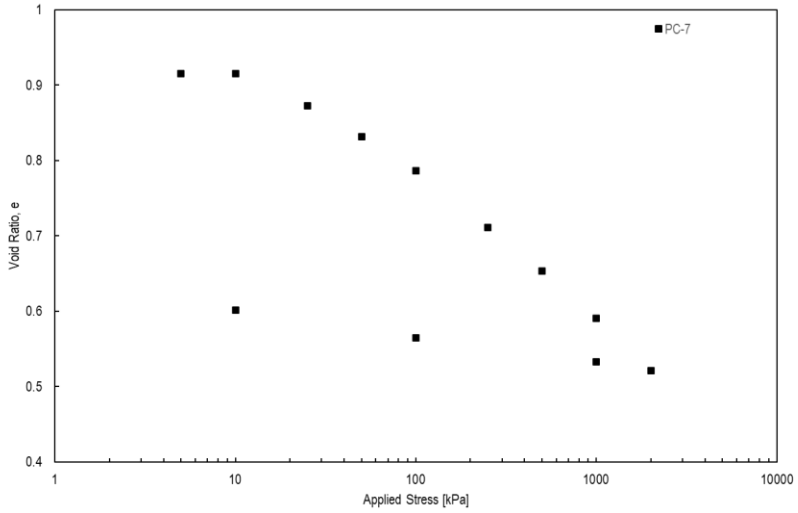
PC-7
Void Ratio, e
Applied Stress [kPa]
1
0.9
0.8
0.7
0.6
0.5
0.4
1
10
100
1000
10000

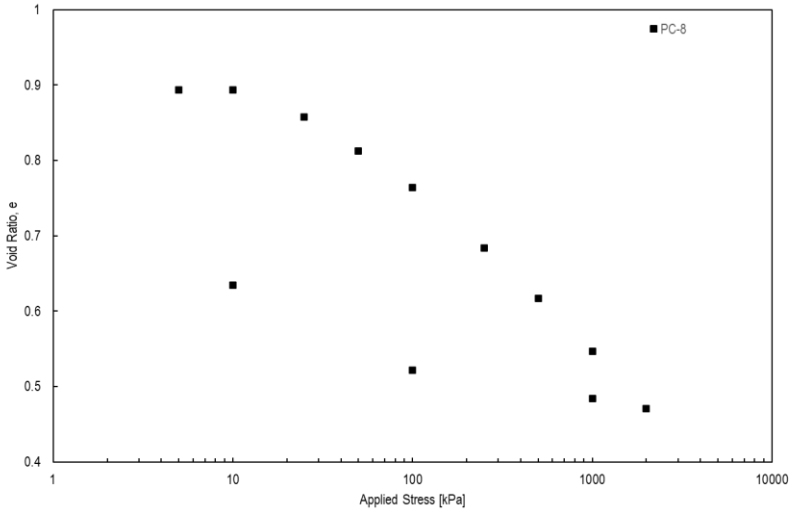
PC-8
Void Ratio, e
Applied Stress [kPa]
1
0.9
0.8
0.7
0.6
0.5
0.4
1
10
100
1000
10000

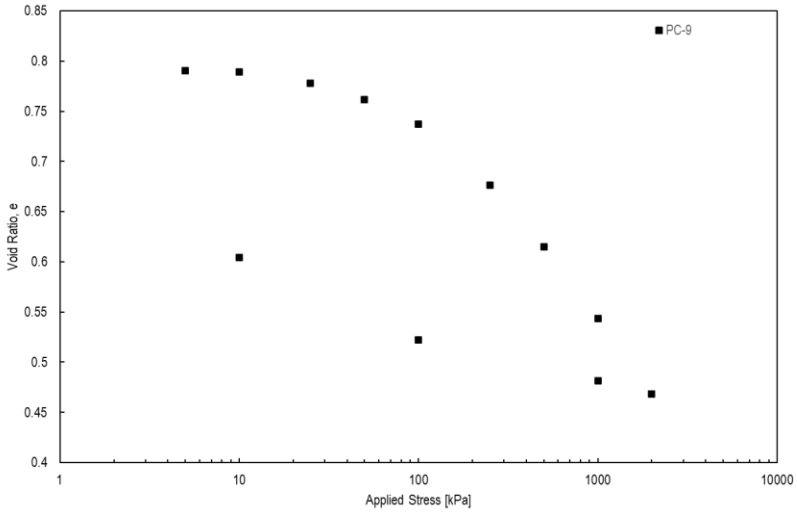
PC-9
Void Ratio, e
Applied Stress [kPa]
0.85
0.8
0.75
0.7
0.65
0.6
0.55
0.5
0.45
0.4
1
10
100
1000
10000

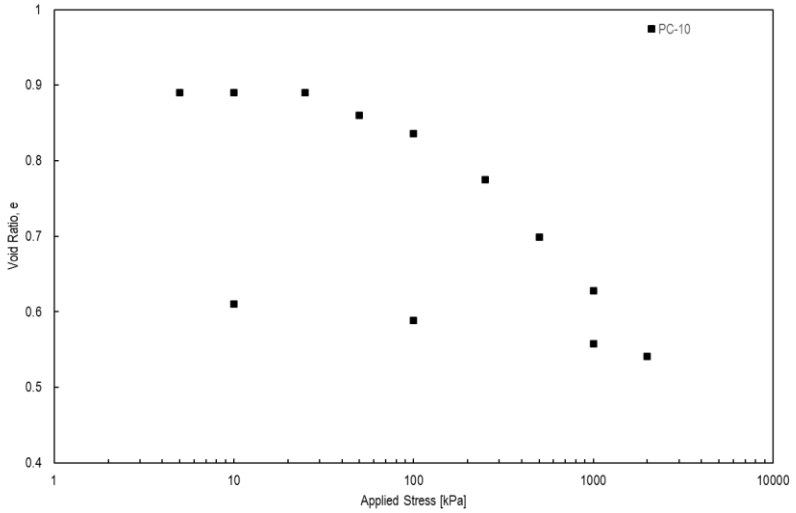
PC-10
Void Ratio, e
Applied Stress [kPa]
1
0.9
0.8
0.7
0.6
0.5
0.4
1
10
100
1000
10000

Compacted Filtered Tailings One-Dimensional Consolidation Results

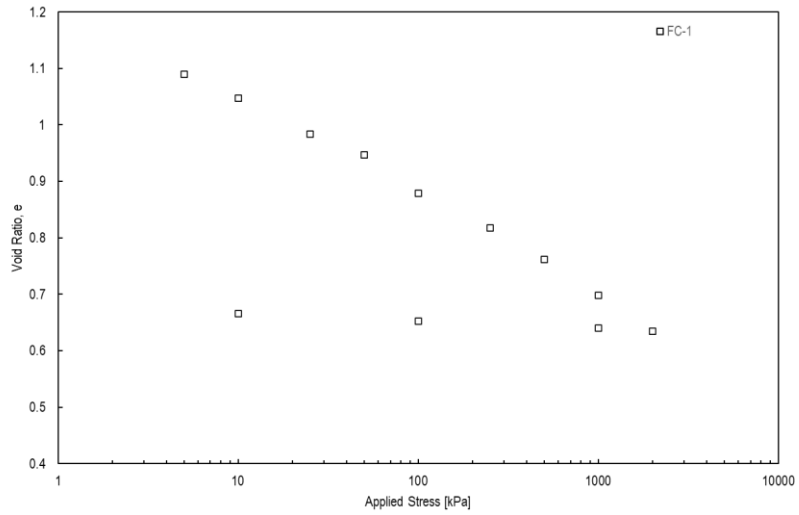

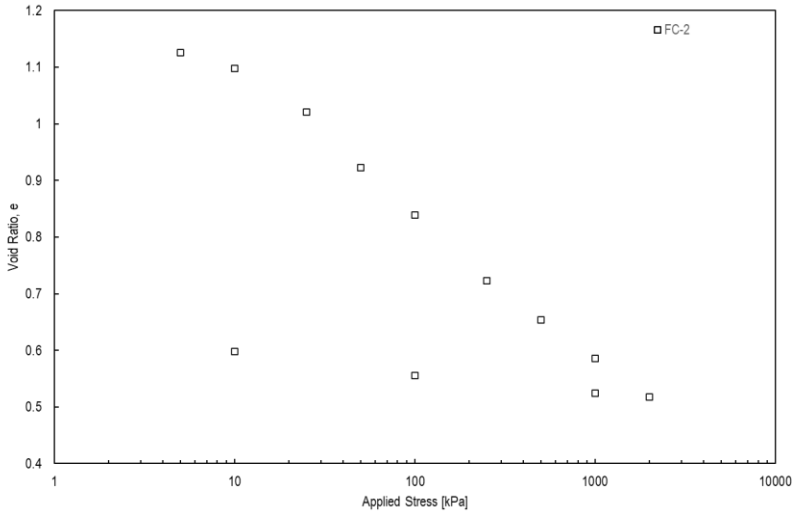

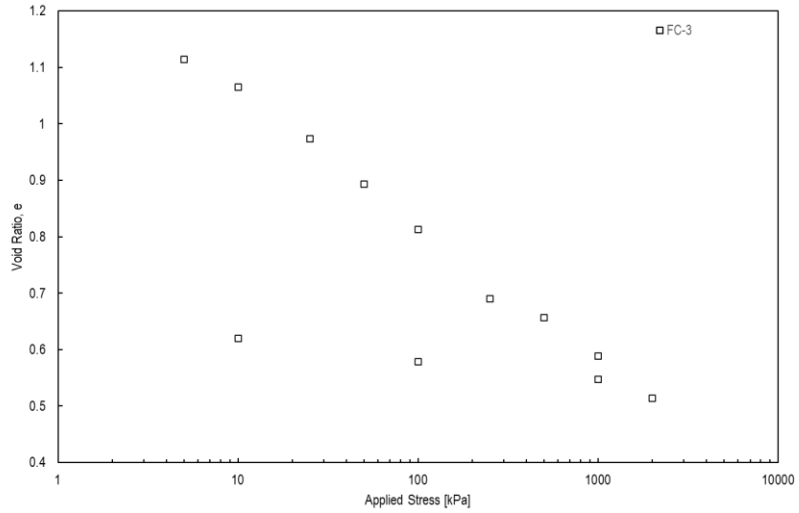

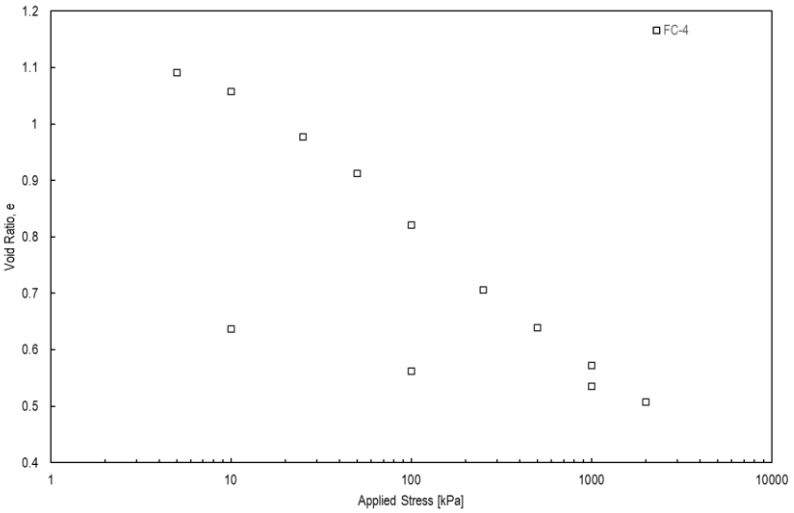

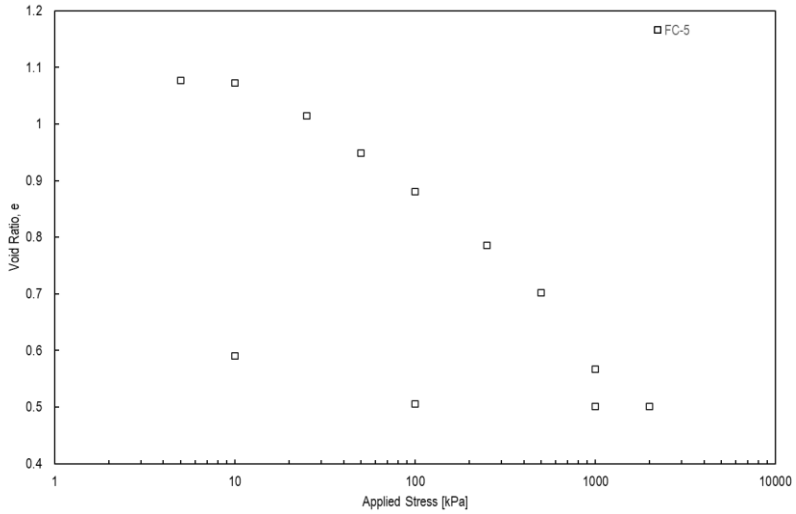
FC-5
Void Ratio, e
Applied Stress [kPa]
1.2
1.1
1
0.9
0.8
0.7
0.6
0.5
0.4
1
10
100
1000
10000

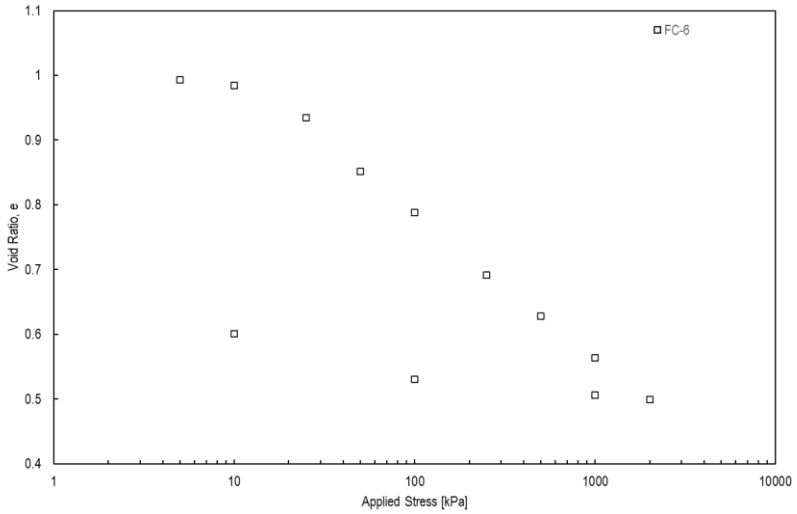
FC-6
Void Ratio, e
Applied Stress [kPa]
1.1
1
0.9
0.8
0.7
0.6
0.5
0.4
1
10
100
1000
10000

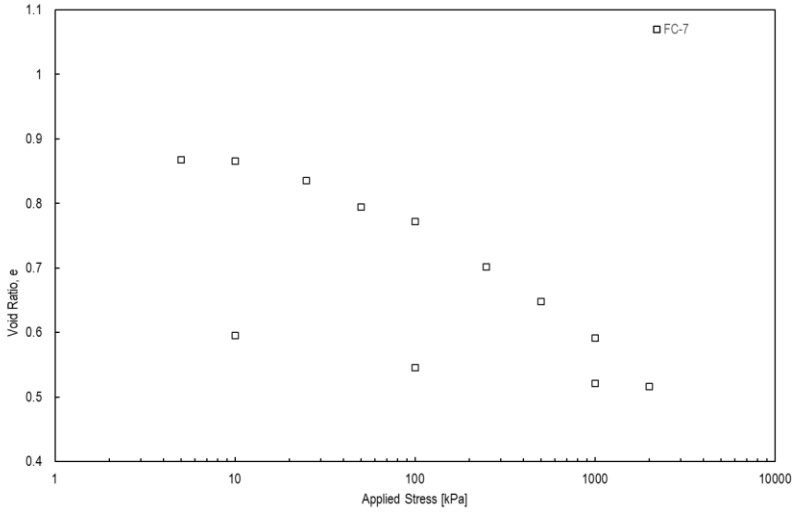
FC-7
Void Ratio, e
Applied Stress [kPa]
1.1
1
0.9
0.8
0.7
0.6
0.5
0.4
1
10
100
1000
10000

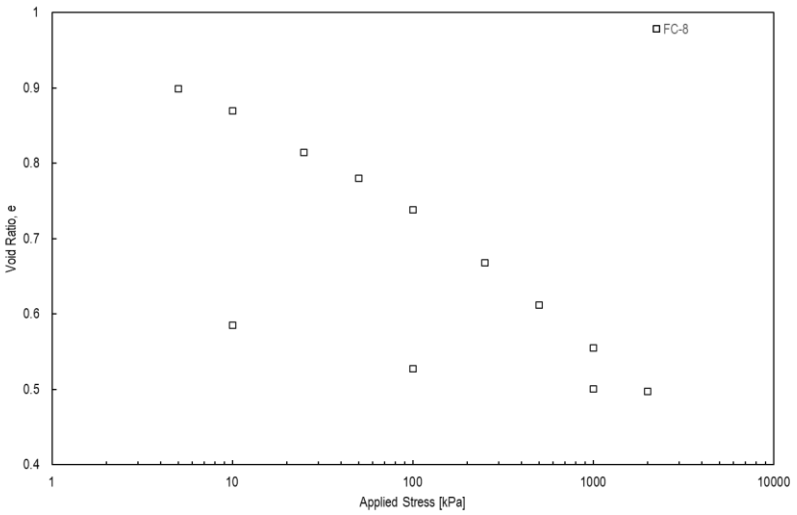
FC-8
Void Ratio, e
Applied Stress [kPa]
1
0.9
0.8
0.7
0.6
0.5
0.4
1
10
100
1000
10000

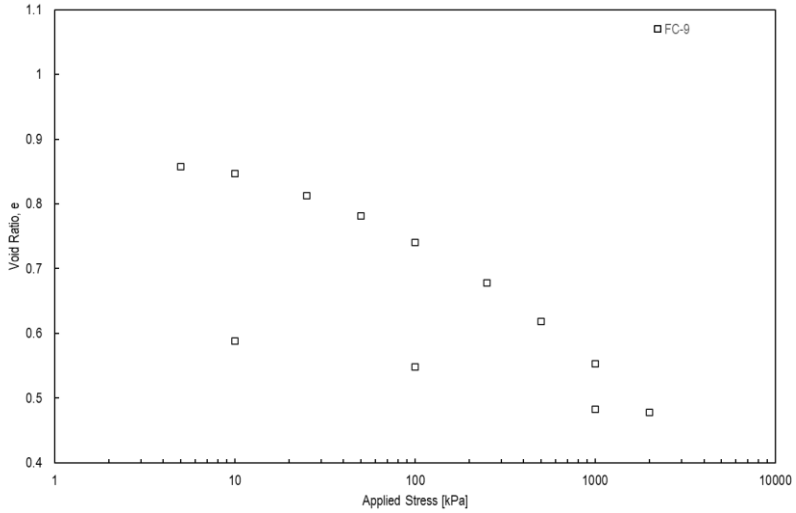
FC-9
Void Ratio, e
Applied Stress [kPa]
1.1
1
0.9
0.8
0.7
0.6
0.5
0.4
1
10
100
1000
10000

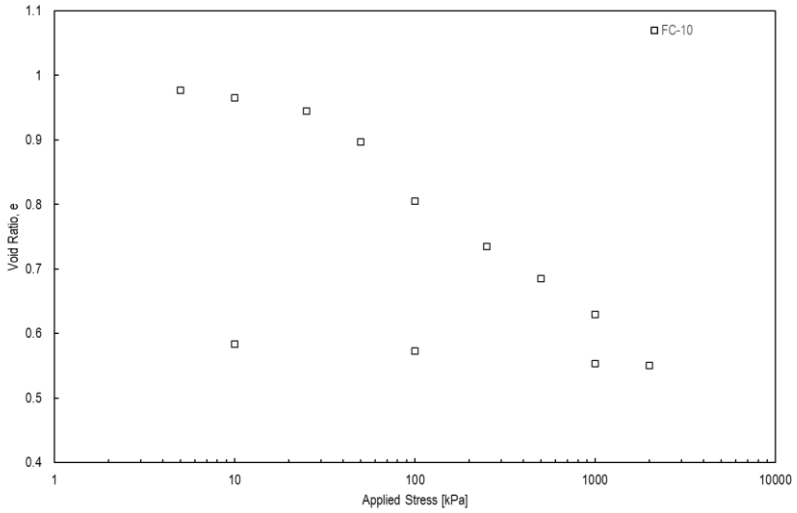
FC-10
Void Ratio, e
Applied Stress [kPa]
1.1
1
0.9
0.8
0.7
0.6
0.5
0.4
1
10
100
1000
10000

Compiled Consolidation Results

Sample	Initial Void Ratio, e_i	Final Void Ratio, e_f	Initial WC [%]	Final WC [%]	Precon. Pressure [kPa]	Compression Index, Cc	Recompression Index, Cr
PC-1	1.07	0.67	44%	22%	52	0.225	0.046
PC-2	1.06	0.60	45%	22%	60	0.237	0.056
PC-3	1.06	0.62	33%	22%	52	0.236	0.033
PC-4	0.99	0.64	32%	23%	40	0.240	0.056
PC-5	0.89	0.59	27%	23%	95	0.218	0.042
PC-6	0.90	0.60	27%	23%	150	0.236	0.044
PC-7	0.92	0.59	18%	22%	150	0.210	0.036
PC-8	0.90	0.59	18%	23%	150	0.236	0.065
PC-9	0.79	0.59	10%	22%	200	0.231	0.056
PC-10	0.89	0.58	8%	22%	280	0.259	0.036
FC-1	1.11	0.61	5%	25%	55	0.202	0.014
FC-2	1.19	0.62	5%	22%	25	0.227	0.032
FC-3	1.15	0.62	5%	22%	17	0.195	0.061
FC-4	1.14	0.63	5%	23%	45	0.221	0.065
FC-5	1.07	0.63	5%	21%	47	0.315	0.030
FC-6	0.99	0.62	5%	22%	40	0.213	0.039
FC-7	0.85	0.60	5%	22%	95	0.206	0.030
FC-8	0.84	0.63	5%	21%	90	0.189	0.032
FC-9	0.85	0.60	5%	21%	125	0.222	0.041
FC-10	0.96	0.61	5%	21%	55	0.205	0.013

APPENDIX C: Photographic Log

Photo 1. Homogenized tailings prior to testing

Photo 2. Atterberg limits testing

Photo 3. Atterberg limits testing

Photo 4. Atterberg limits testing

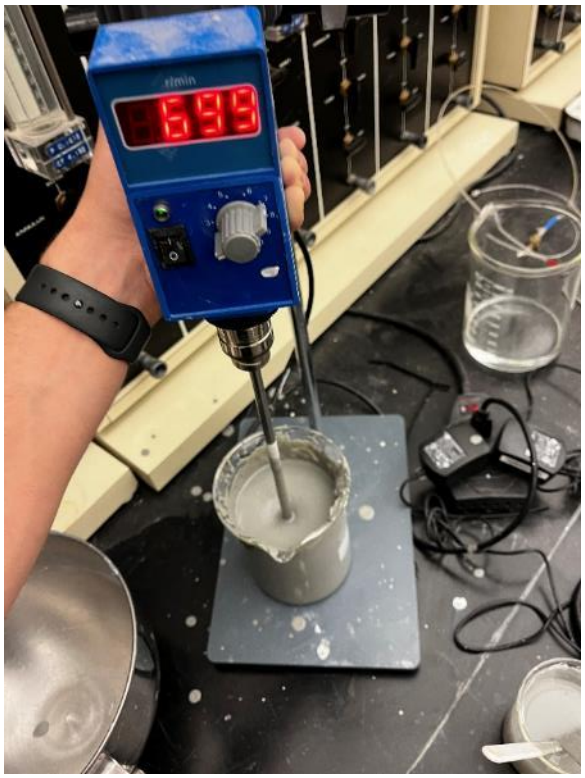

Photo 5. Mixing solids contents for mini vane shear

Photo 6. Mixing for mini vane shear

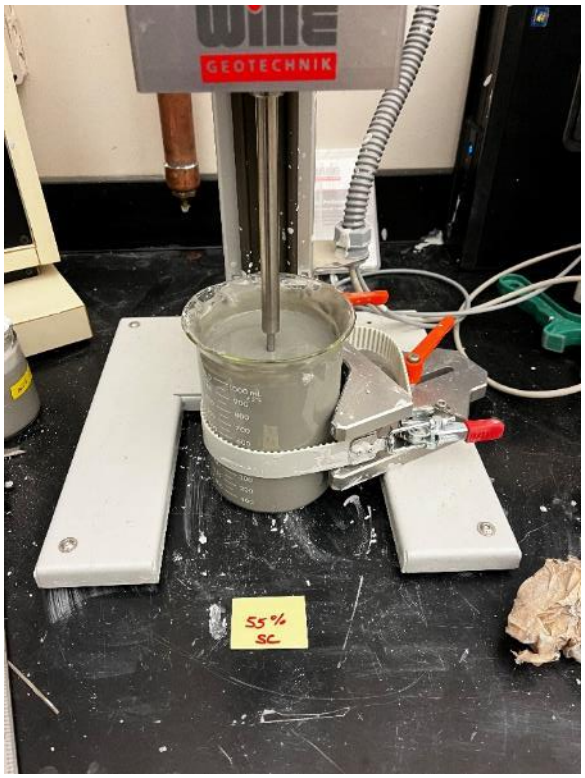

Photo 7. Mini vane shear at 55% SC

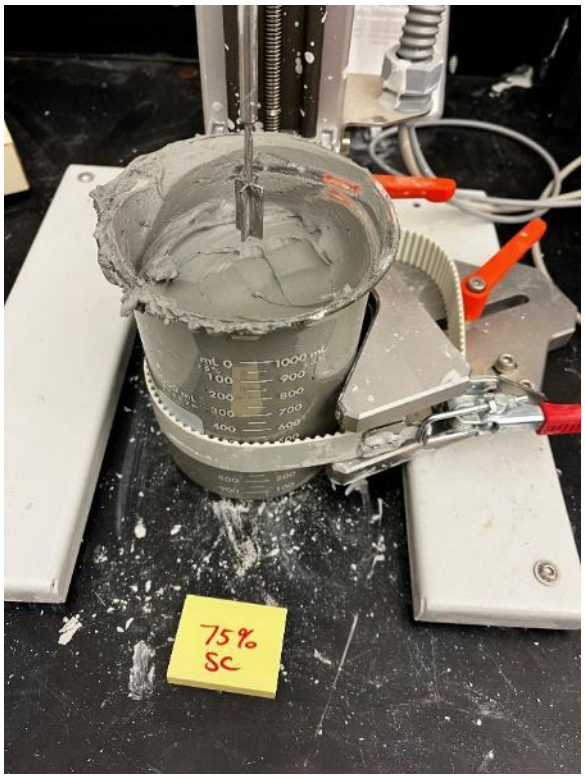

Photo 8. Mini vane shear at 75% SC

Photo 9. Zero effective stress void ratio test start

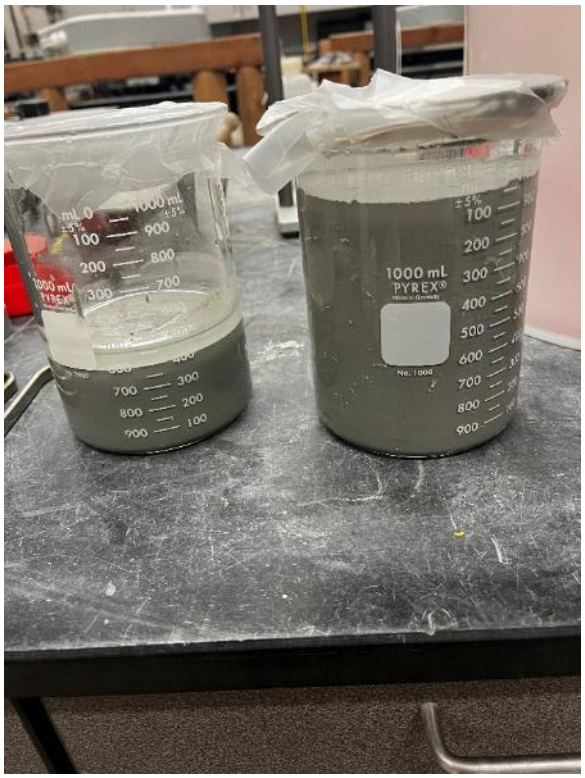

Photo 10. Zero effective stress void ratio finish

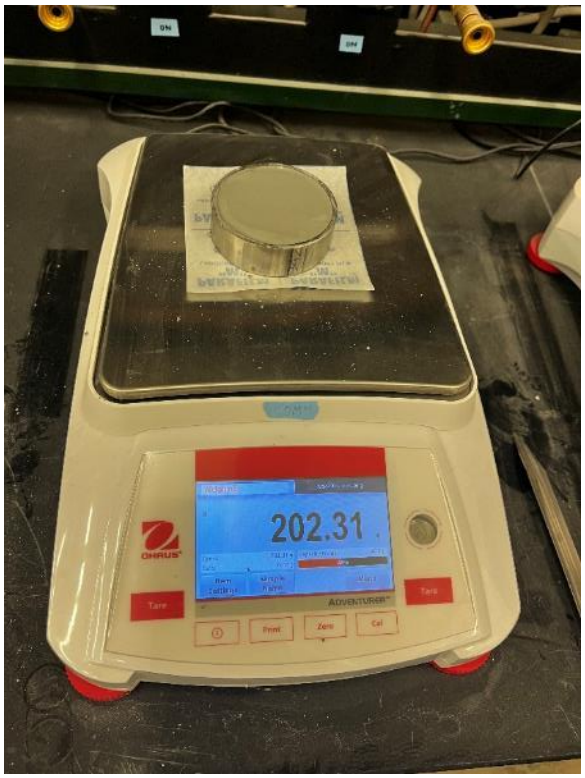

Photo 11. Shrinkage limit test sample

Photo 12. Shrinkage limit test sample

Photo 13. Thickened tailings preparation

Photo 14. Bucket B-1 initial placement

Photo 15. Bucket B-2 initial placement

Photo 16. Bucket B-3 initial placement

Photo 17. Bucket B-4 initial placement

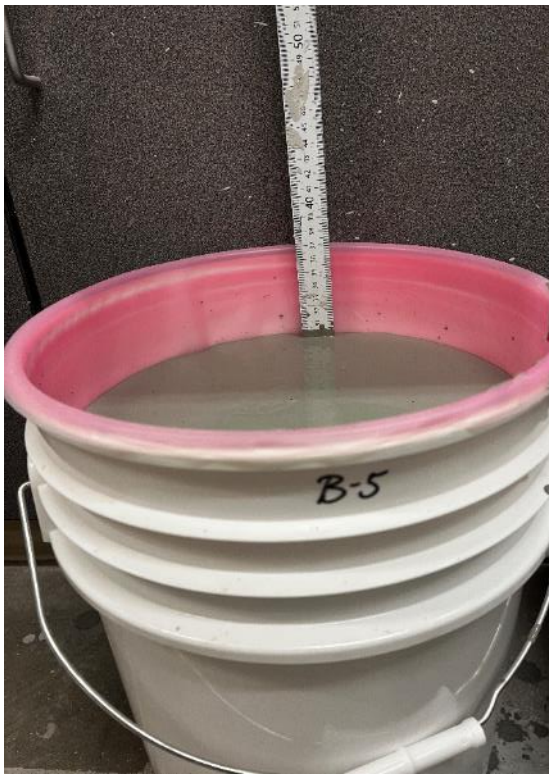

Photo 18. Bucket B-5 initial placement

Photo 19. Desiccation buckets after initial placement and during subsequent drying

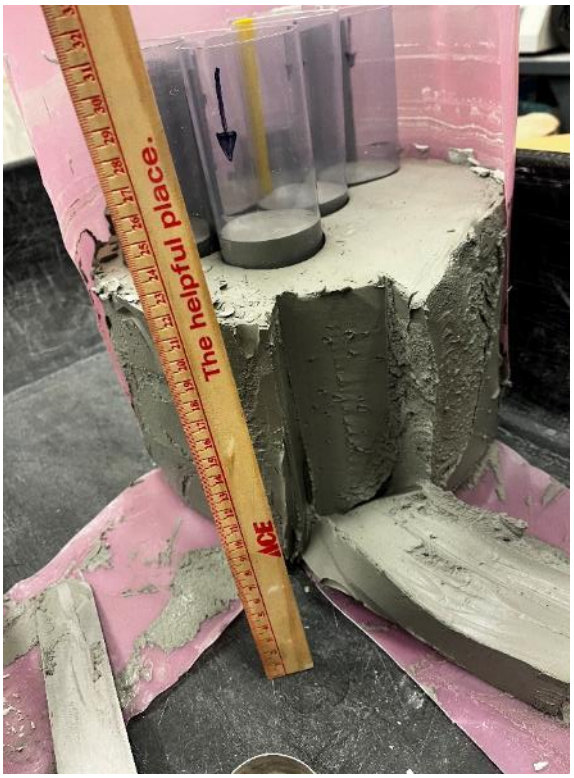

Photo 20. B-1 processing for sample testing

Photo 21. B-1 triaxial compression sample

Photo 22. Density samples processed from B-1

Photo 23. Moisture samples processed from B-1

Photo 24. PT-1 suspended in oversized mold

Photo 25. PT-1 placed on end platens

Photo 26. PT-1 as cell is filled with water

Photo 27. PT-1 post shear testing

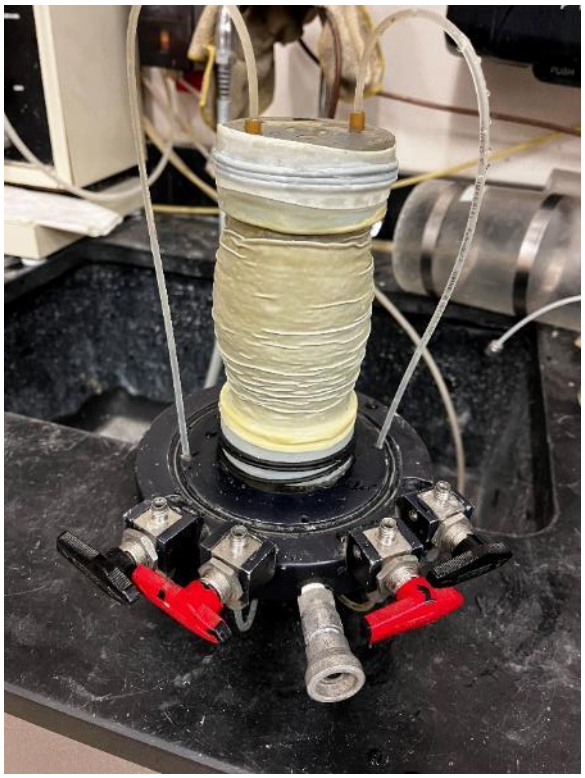

Photo 28. PT-2 post shear testing

Photo 29. B-2 at end of desiccation sequence

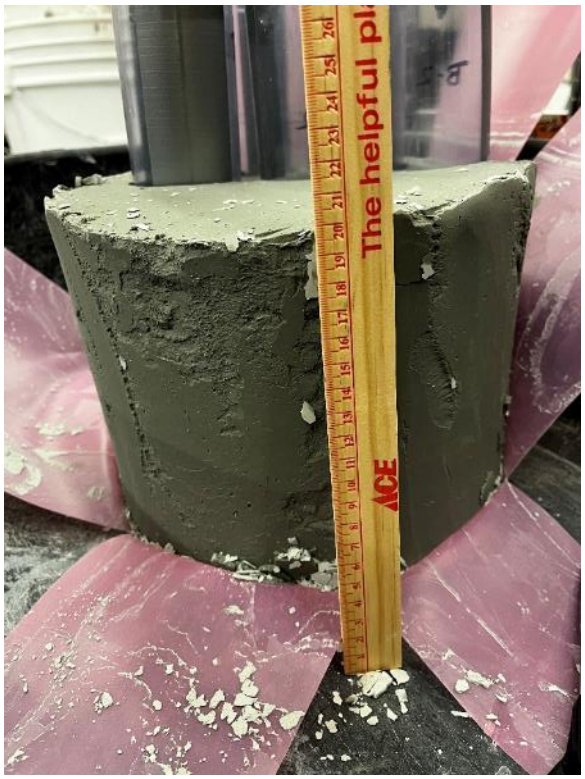

Photo 30. B-2 after removal of bucket and liner

Photo 31. B-2 outer edge removed to access samples for moisture density testing

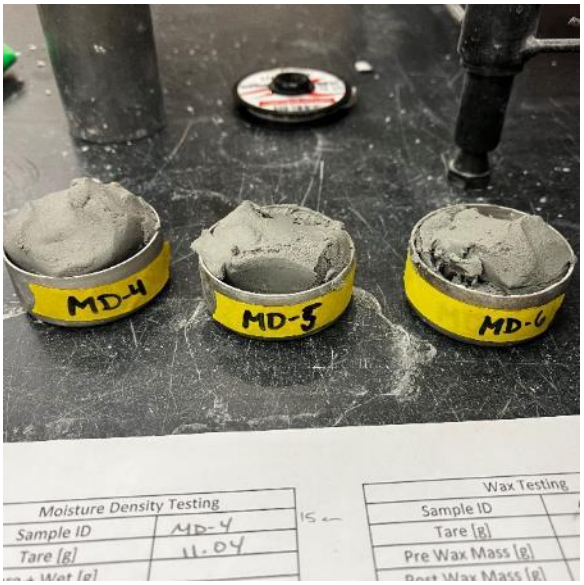

Photo 32. B-2 Moisture samples

Photo 33. B-2 consolidation sample prior to trim

Photo 34. B-2 consolidation test PC-3

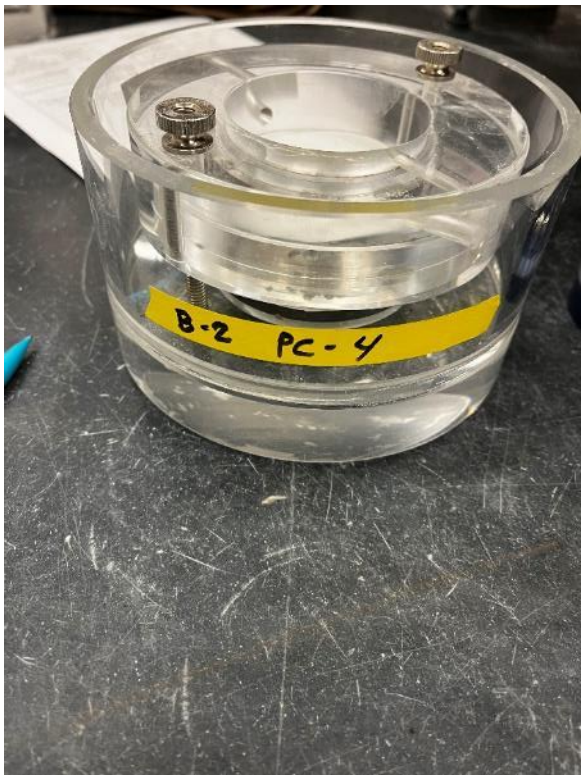

Photo 35. B-2 consolidation test PC-4

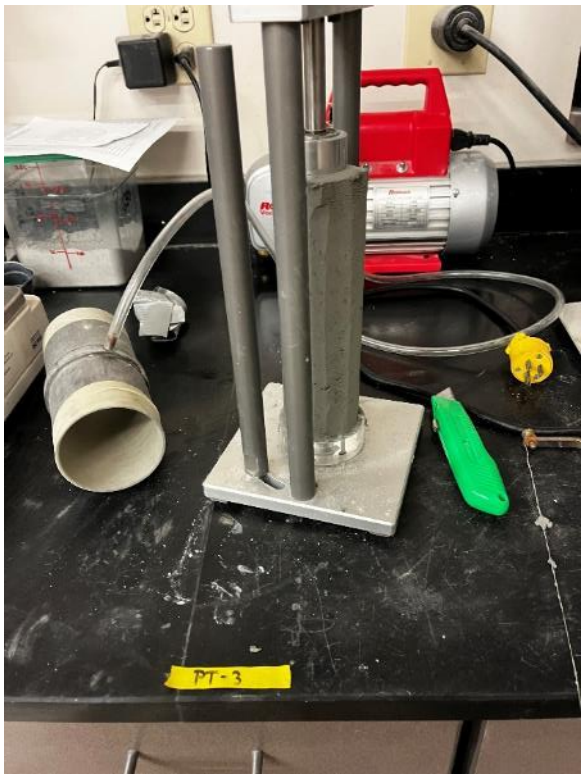

Photo 36. Trimming PT-3 for triaxial testing

Photo 37. Weight of PT-3 prior to testing

Photo 38. PT-3 oversized mold to apply membrane

Photo 39. PT-3 placement on end platens

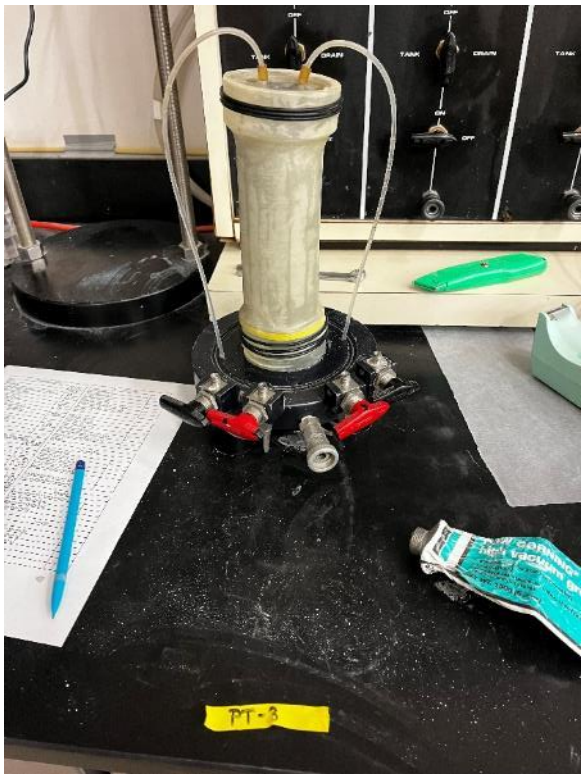

Photo 40. Set up of PT-3 on end platens

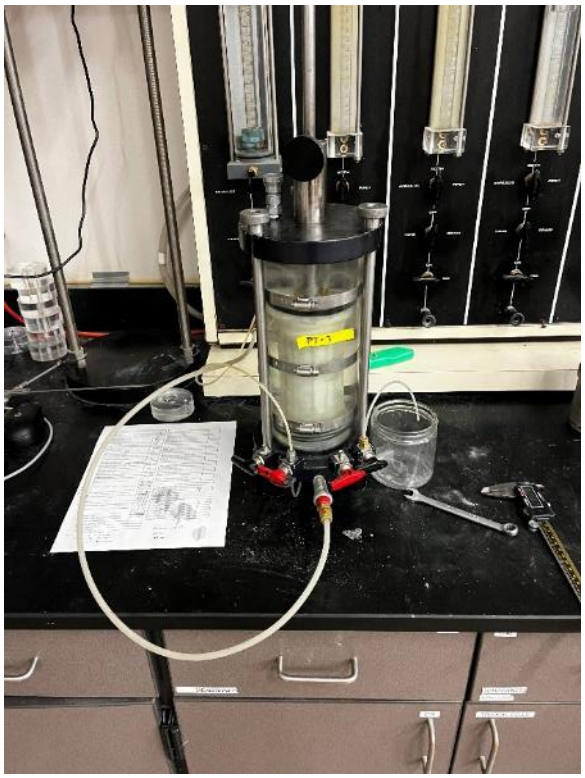

Photo 41. PT-3 after finish set up for testing

Photo 42. Weight of PT-4 prior to testing

Photo 43. PT-4 suspended in membrane

Photo 44. PT-4 suspended horizontally in mold

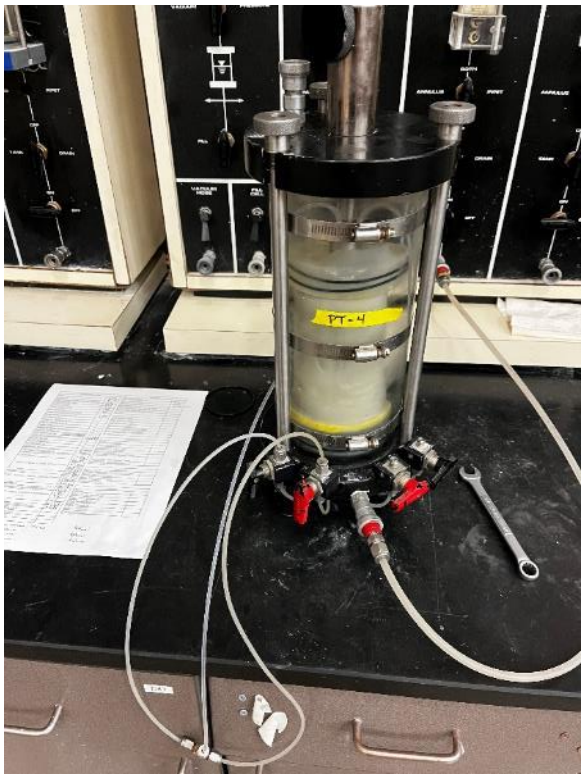

Photo 45. PT-4 after completion of setup

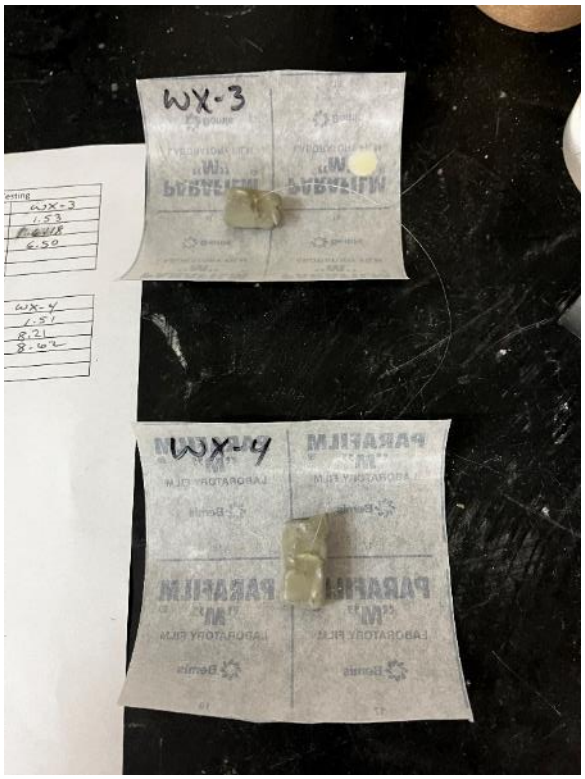

Photo 46. Density (wax) samples for B-2

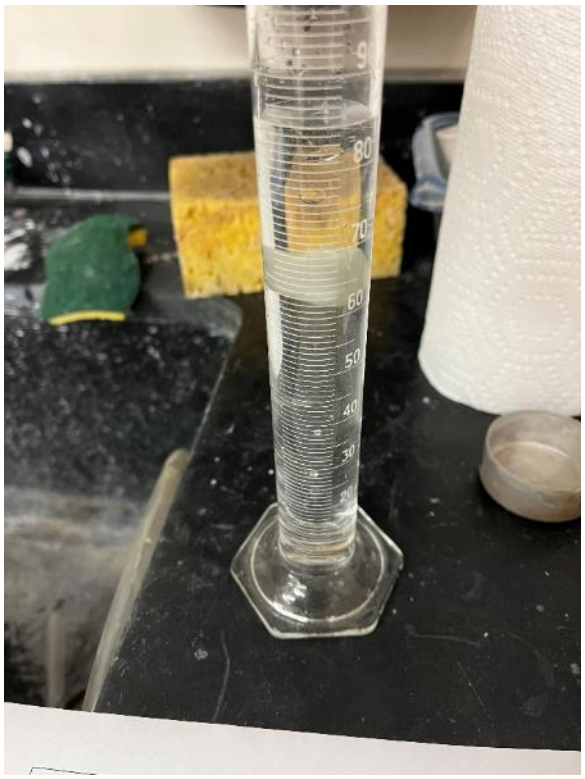

Photo 47. Density testing (submersion) for B-2

Photo 48. PT-3 post shear testing

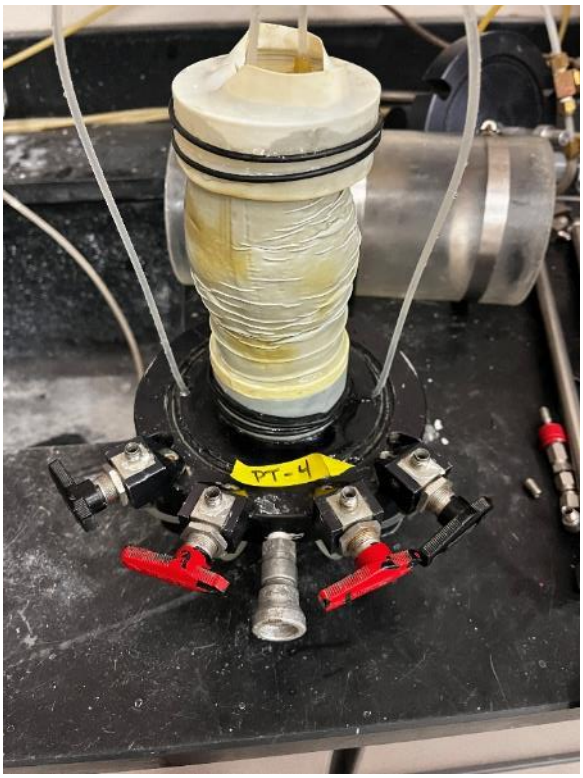

Photo 49. PT-4 post shear testing

Photo 50. B-3 at the end of desiccation sequence

Photo 51. B-3 at the end of desiccation sequence

Photo 52. B-3 after removal of bucket and liner

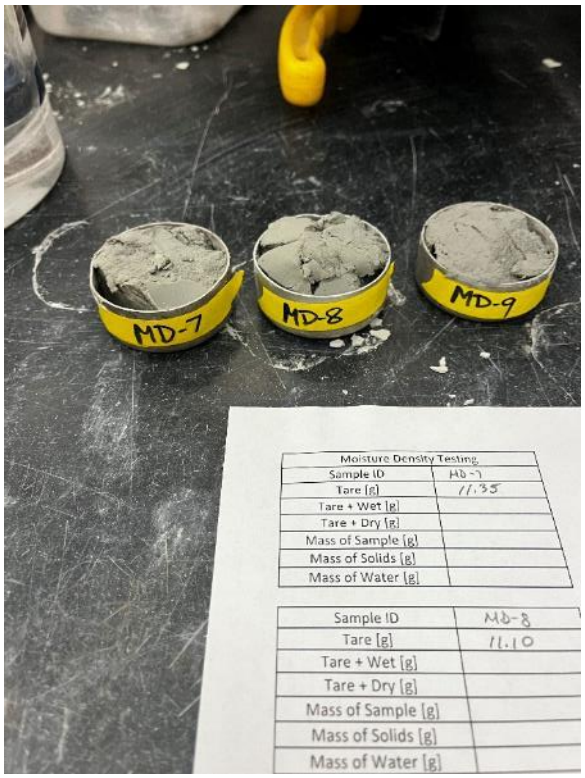

Photo 53. B-3 moisture samples

Photo 54. B-3 consolidation sample PC-5

Photo 55. B-3 consolidation sample PC-6

Photo 56. B-3 consolidation sample PC-5

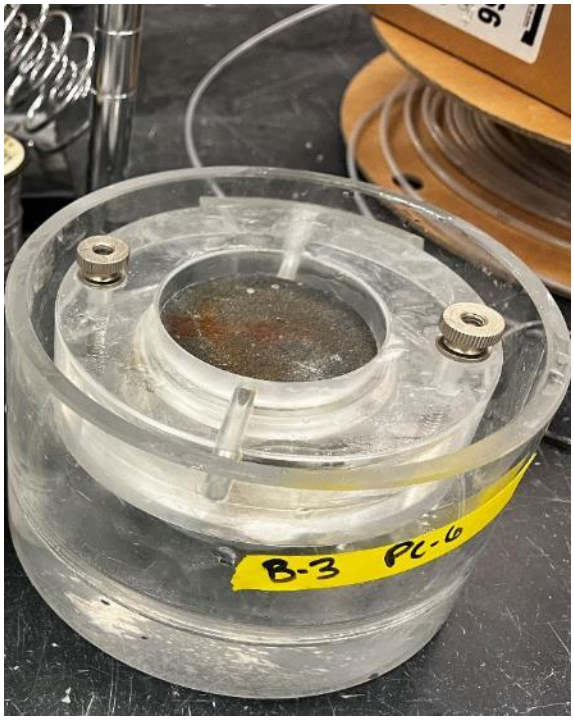

Photo 57. B-3 consolidation sample PC-6

Photo 58. PT-5 sample trimming for triaxial testing

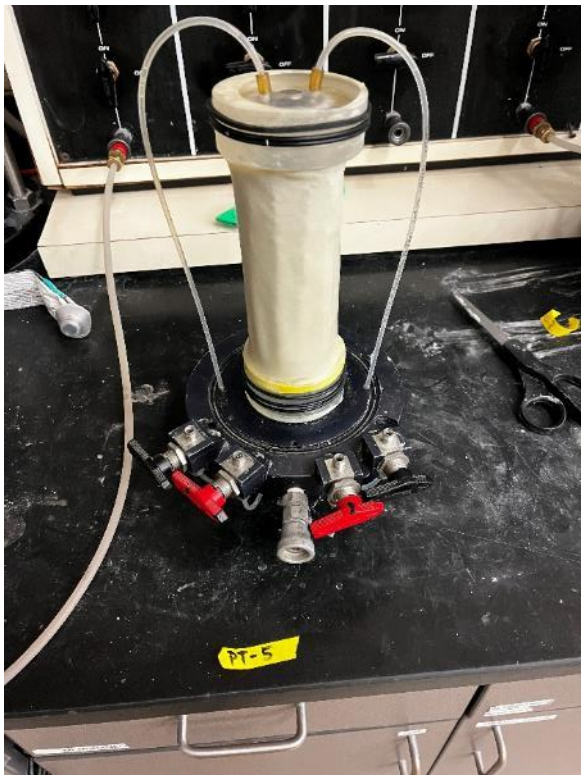

Photo 59. PT-5 after initial setup

Photo 60. PT-5 post shear testing

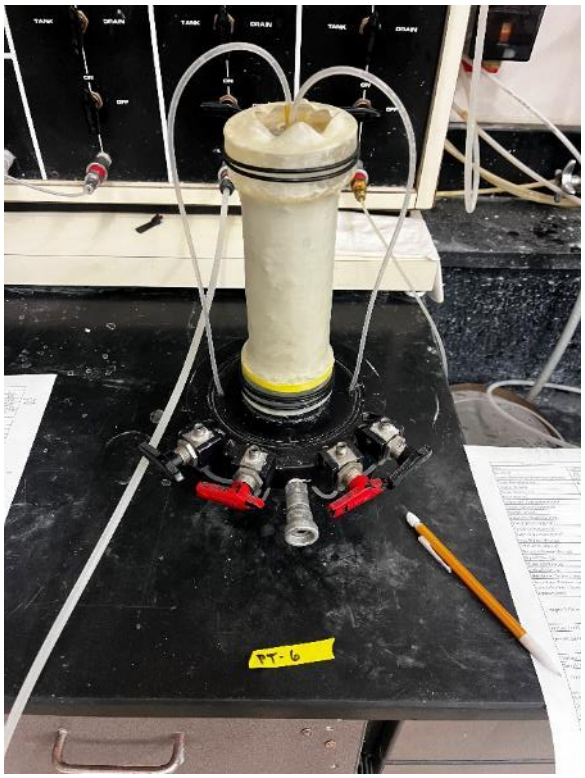

Photo 61. PT-6 after initial set up

Photo 62. PT-6 during shear testing

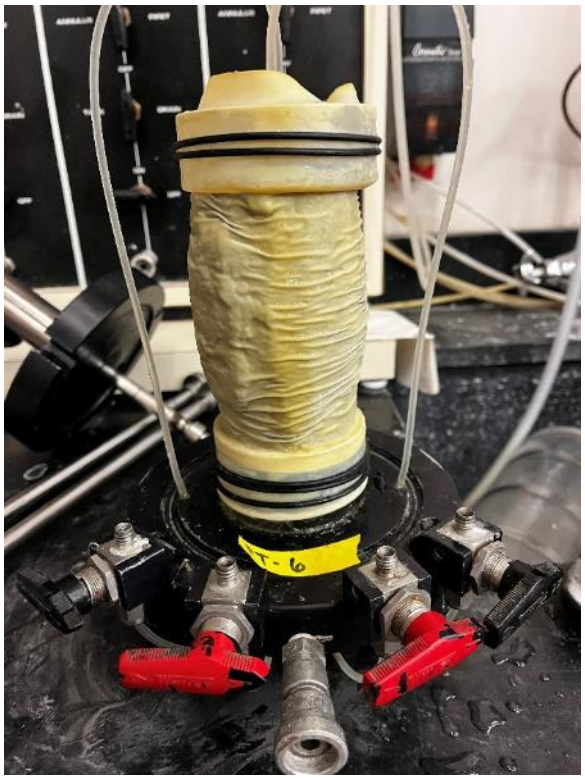

Photo 63. PT-6 post shear testing

Photo 64. B-4 after removal of bucket and liner

Photo 65. B-4 after removal of bucket and liner

Photo 66. B-4 moisture samples

Photo 67. B-4 consolidation sample PC-7

Photo 68. PT-7 during sample trimming

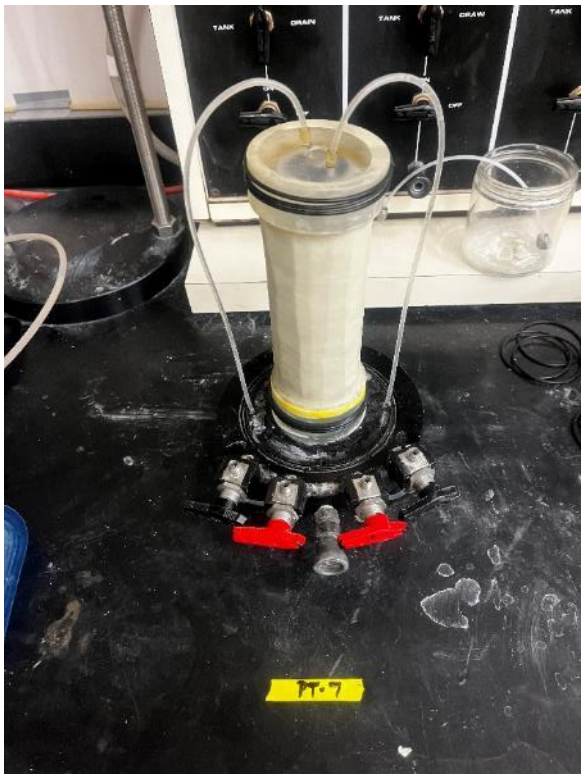

Photo 68. PT-7 after placement on end platens

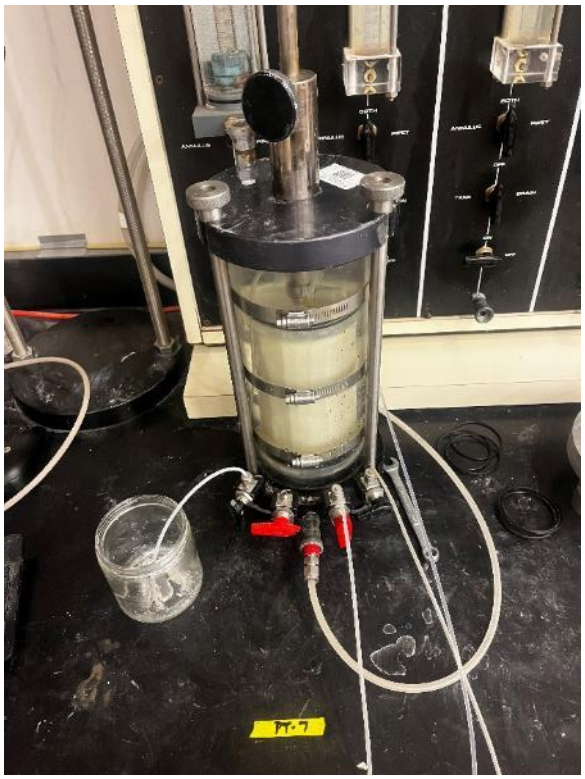

Photo 69. PT-7 after initial set up

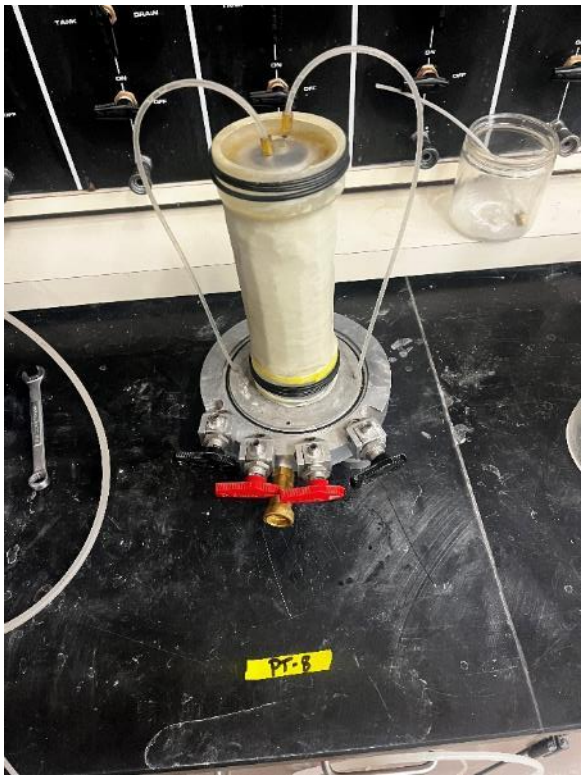

Photo 70. PT-8 after placement on end platens

Photo 71. PT-7 post shear testing

Photo 72. PT-8 post shear testing

Photo 73. B-5 after removal from bucket and liner

Photo 74. B-5 after removal from bucket and liner

Photo 75. PT-9 post shear testing

Photo 76. PT-9 post shear testing

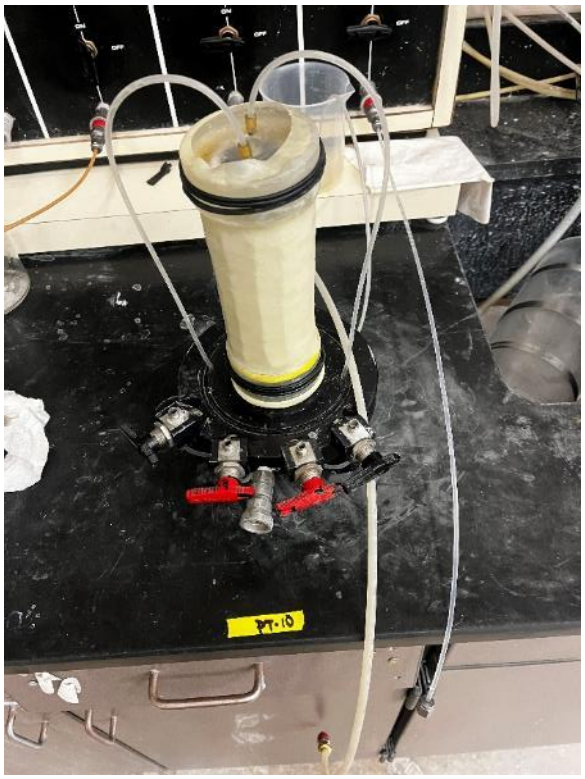

Photo 77. PT-10 after placement on end platens

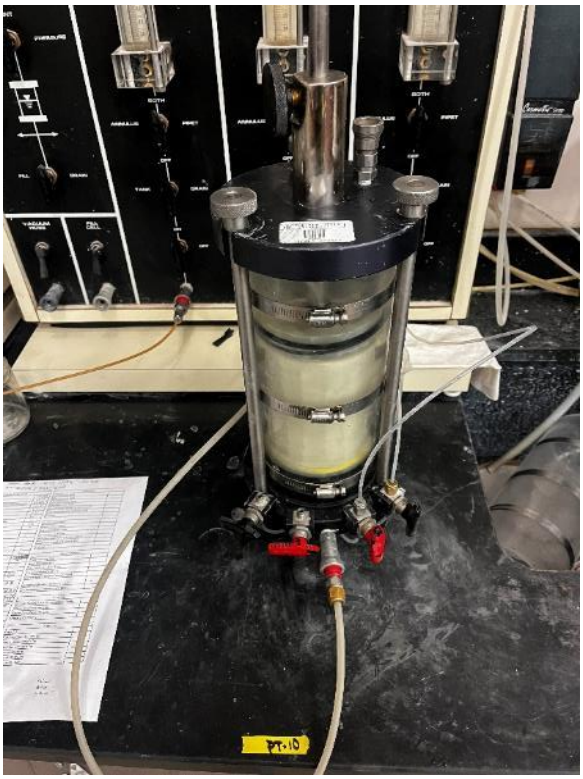

Photo 78. PT-10 after initial set up

Photo 80. Typical triaxial sample set up and equipment for each desiccation bucket

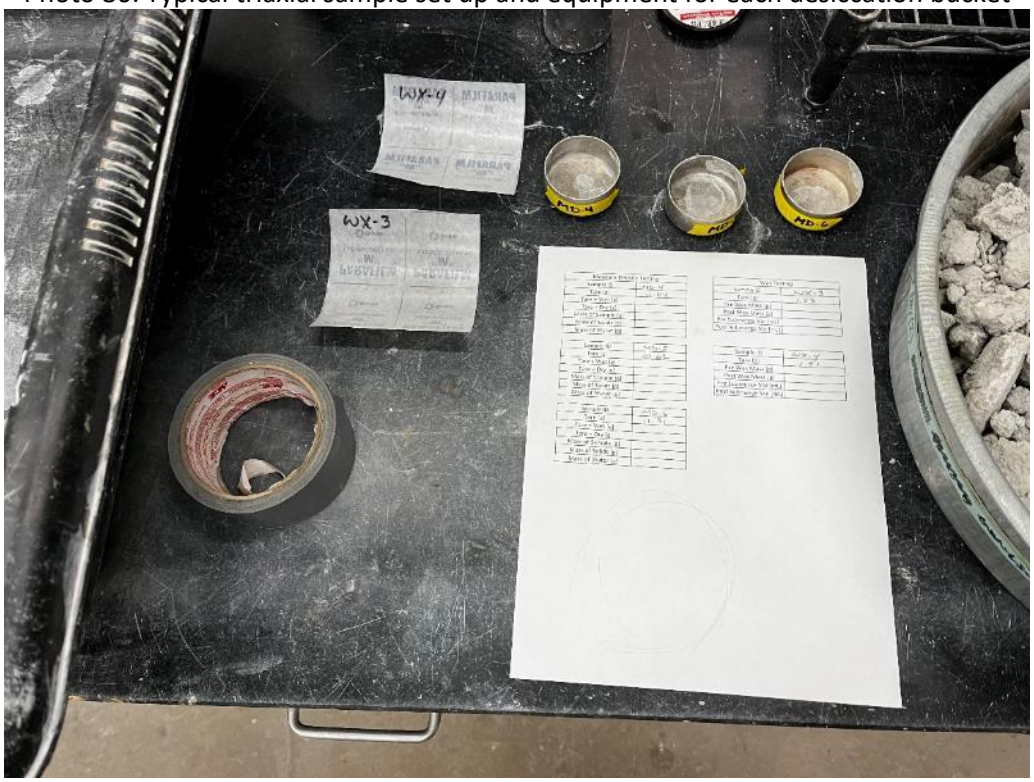

Photo 81. Typical moisture density sample set up and equipment for each desiccation bucket

Photo 82. Typical consolidation sample set up and equipment for each desiccation bucket

Photo 83. Triaxial equipment, cells, samples, pressure panels, and GeoJac for triaxial testing